

# **Efficient Maximum Power Point Tracking Techniques for a Grid-connected Photovoltaic System using Artificial Intelligence**



By

**Sadeq Duair Aneed Al-Majidi**

Power System Research Group

Department of Electronic and Computer Engineering

College of Engineering, Design and Physical Sciences

Brunel University London

United Kingdom

This thesis is submitted in partial fulfilment for the degree of  
Doctor of Philosophy (PhD) in Electrical Power Engineering

September 2020

*To my family*

*Parents...*

*Brothers...*

*Sisters ...*

*My wife...*

*and Children...*

*I introduce this effort*

*. . .*

# Abstract

The maximum power point tracking (MPPT) technique is considered a crucial part in photovoltaic (PV) system design for maximising the output power of a PV array and improving the stability and reliability of the PV system. This research focuses on developing common MPPT techniques, including: perturb and observe (P&O), fuzzy logic control (FLC), an adaptive neural-fuzzy inference system (ANFIS) and an artificial neural network (ANN) for a grid-connected PV system, with the best of them being identified.

Whilst several techniques have been designed, the P&O algorithm is widely used for MPPT due to its low cost and simple implementation. However, the main drawbacks of this method are a slow tracking speed, high oscillation and a drift problem associated with changing irradiance rapidly. Hence, a modified P&O-MPPT based on the Pythagorean theorem and a constant voltage algorithm is proposed to address those issues by developing variable step size and early step decision for the conventional P&O algorithm, respectively. Unlikely, these modifications do not avoid the drift problem nor eliminate the oscillation completely.

The FLC is a commonly deployed technique that achieves vastly improved performance for the MPPT technique in terms of response speed and low fluctuation. However, the key issues of the conventional FLC-MPPT are the drift problem and complex implementation, when compared with the P&O-MPPT. Hence, the MPPT technique based on the FLC and P&O algorithm is proposed to address these challenges. This technique incorporates the advantages of the P&O-MPPT to account for slow and fast changes in solar irradiance as well as reduced processing time for FLC-MPPT to address complex engineering problems when the number of rules of membership functions are fewer. As a result, the proposed technique achieves average tracking efficiencies of around 99.6% under the EN50530 standard test.

The ANFIS technique and the ANN technique are used to predict the maximum power point of a PV array, using experimental training data, instead of the rules of membership functions. To improve the accuracy of those techniques, a curve fitting technique and the Particle Swarm Optimisation algorithm are utilised, respectively. These optimisations are classified into two strategies: adjusting the tuning of the ANFIS model as well as determining the right topology and the initial weights of the ANN model. As a result, the training errors of those models are minimised. Hence, the ANFIS technique achieves average tracking efficiencies of greater than 99.3% under a semi-cloudy day test, while the ANN technique delivers average tracking efficiencies of more than 99.67% and 99.30% on sunny and cloudy day tests, respectively.

# **Declaration**

I declare that this thesis is my own work and is submitted for the first time to the Post-Graduate Research Office of Brunel University London. The study was originated, composed and reviewed by myself and my supervisors. All the information derived from other works has been acknowledged and referenced.

**Sadeq Duair Aneed Al-Majidi**

September 2020

# Acknowledgements

Firstly, I would like to express my appreciation and gratitude to the Iraqi Minister of Higher Education and Scientific Research (MOHESR), Missan University and the Iraqi Cultural Attaché-London for sponsorship and funding of my PhD study and managing the student affairs.

I would like to thank my supervisor, Professor Hamed S. Al-Raweshidy, for his advice and guidance during the PhD period. I am so thankful to my second supervisor Maysam F. Abbod for his support, encouragement and valuable assistance.

My thanks go also to my colleagues in the Power System Research Group and Department of Electronic and Computer Engineering at the College of Engineering, Design and Physical Sciences, who have been supportive throughout my PhD journey.

I would like to acknowledge the great attitude of all the staff members that I have interacted with at Brunel University London.

Finally, to my parents, brothers, sisters, wife and my children, I would like to thank you for being beside me as a source of care, love, encouragement and motivation, which has filled me with patience and commitment.

# Contents

Abstract.....	III
Declaration.....	IV
Acknowledgements.....	V
Contents .....	VI
LIST OF FIGURES .....	X
LIST OF TABLES.....	XIII
LIST OF SYMBOLS.....	XIV
LIST OF ABBREVIATIONS.....	XVI
Chapter 1.....	1
Introduction.....	1
1.1 Background .....	1
1.2 Motivations.....	3
1.3 Aim and Objectives .....	4
1.4 Thesis Contributions .....	5
1.5 Thesis Organisation.....	6
1.6 List of Publications.....	8
1.6.1 Journal publications.....	8
1.6.2 Conference publications .....	8
Chapter 2.....	9
Photovoltaic Energy.....	9
2.1 History of Photovoltaic Energy.....	9
2.2 Types of Photovoltaic cells .....	12
2.2.1 Monocrystalline silicon .....	12
2.2.2 Polycrystalline silicon.....	12
2.2.3 Amorphous silicon.....	12
2.3 Challenges of Photovoltaic Technology .....	13

2.3.1 Efficiency of the PV Cell.....	13
2.3.2 Stability of PV generation .....	13
2.3.3 Partial shading condition .....	14
2.3.4 Mismatch of PV load.....	14
2.3.5 Lifespan of an installed PV module .....	14
2.4 Maximum Power Point Tracking Techniques.....	14
2.5 Overview of the various MPPT methods .....	18
2.6- Summary .....	19
Chapter 3.....	22
Modelling and Control of PV Systems .....	22
3.1 Modelling of a PV Cell .....	22
3.2 Structure of a PV System .....	25
3.2.1 The Configuration of a PV Array .....	25
3.2.2 Topologies of PV systems .....	26
3.3 DC-DC Boost Converter.....	27
3.4 Control Scheme of a PV System.....	30
3.5 P&O Algorithm.....	32
3.6 Modified P&O-MPPT .....	34
3.7 Simulation Results.....	37
3.8 Summary .....	39
Chapter 4.....	43
Proposed MPPT Based on Fuzzy Logic Control .....	43
4.1 Introduction .....	43
4.2 Fuzzy Logic Control.....	45
4.2.1 Fuzzification .....	46
4.2.2 Fuzzy Rules .....	47
4.2.3 Defuzzification .....	47

4.3 Conventional FLC-MPPT .....	47
4.4 Proposed Method.....	51
4.5 Simulation Results.....	54
4.6 The EN 50530 Standard Test of MPPT Efficiency .....	60
4.7 Summary .....	63
Chapter 5 .....	65
Design of an Efficient MPPT based on ANFIS .....	65
5.1 Related Works .....	65
5.2 ANFIS Technique.....	70
5.3 ANFIS-MPPT Controller .....	71
5.4 Methodology of Collected Data .....	72
5.5 Curve Fitting Technique.....	74
5.6 Tuning of Proposed ANFIS Network.....	76
5.7 Results and Discussion.....	80
5.8 Real Measurement Test.....	84
5.9 Summary .....	88
Chapter 6.....	89
An optimised Neural Network for Predicting the MPP .....	89
6.1 State of the Art .....	89
6.2 Optimised ANN-MPPT Method .....	91
6.3 ANN Algorithm.....	92
6.3.1 Hidden Layer Size .....	93
6.3.2 Initial Training Weights.....	94
6.4 PSO Algorithm.....	94
6.5 Training of ANN Model.....	96
6.5.1 PSO-ANN algorithm - selected as the best topology of an ANN network .....	96
6.5.2 PSO-ANN algorithm - determining the initial weights of the ANN model .....	97

6.6 Results and Discussion.....	100
6.7 Experimental Measurement Tests .....	103
6.8 Overview of the Proposed Methods.....	107
6.9 Summary .....	108
Chapter 7.....	110
Conclusions and Future Work .....	110
7.1 Conclusions .....	110
7.2 Future Work .....	112
Bibliography .....	114
Appendix A.....	129
Experimental Data Sample .....	129
Appendix B.....	131
Data sheet of Sharp NU-S5E3E 185 PV module.....	131
Appendix C.....	133
PSO-ANN Algorithm (S-Function) .....	133
Appendix D.....	135
Modified P&O Algorithm (S-Function) .....	135
Appendix E .....	137
The Simulink model of a grid-connected PV system .....	137
Appendix F.....	138
The graphical rules of a FLC model .....	138
Appendix G.....	139
The linguistic rules of an ANFIS model.....	139
Appendix H.....	140
Neural Network Training Regression .....	140

## LIST OF FIGURES

Figure 1.1. The global growth of PV power installation capacity in GW .....	2
Figure 1.2. I–V characteristic of a PV array .....	4
Figure 2.1. The historical development of PV energy .....	10
Figure 2.2. Historical decrease in the price of a PV cell.....	11
Figure 2.3. Types of PV technologies.....	13
Figure 2.4. Common types of MPPT methods for PV systems.....	21
Figure 3.1. The structure of a PV cell.....	22
Figure 3. 2. The equivalent circuit of a PV cell.....	23
Figure 3.3. P–V curve of a PV array.....	25
Figure 3.4. The configuration of a PV array .....	25
Figure 3.5. Topologies of PV systems.....	26
Figure 3.6. The circuit diagram of a DC-DC boost converter .....	29
Figure 3.7. The state conditions of a DC-DC boost converter.....	29
Figure 3.8. The waveform of a DC-DC boost converter .....	30
Figure 3.9. The control scheme of the PV system .....	31
Figure 3.10. The waveform of an MPPT controller.....	31
Figure 3.11. The flowchart of the conventional P&O algorithm.....	33
Figure 3.12. P-V curve for a rapid irradiance change.....	34
Figure 3.13. P-V curve of the PV module illustrating the VSS.....	35
Figure 3.14. The flowchart of the modified P&O-MPPT method.....	37
Figure 3.15. The general diagram of a grid-connected PV system.....	39
Figure 3. 16. The input irradiance under constant conditions.....	40
Figure 3.17. The output power of a PV array without MPPT versus with MPPT .....	40
Figure 3.18. The input of input solar irradiance with varying conditions .....	40
Figure 3.19. PV array output for the modified VS conventional P&O method under .....	41
Figure 3.20. The DC voltage of a grid-connected PV system .....	42
Figure 4.1. The general diagram of a grid-connected PV system based on the FLC-MPPT...	45
Figure 4.2. General diagram of fuzzy logic system.....	46
Figure 4.3. Various types of defined membership functions (a) monotonic (b) trapezoidal (d) triangular (c) Gaussian.....	46
Figure 4.4. The defined membership functions of a conventional FLC-MPPT .....	49
Figure 4.5. A 3D surface between input1 (e) and input2 ( $\Delta e$ ) verse output ( $\Delta D$ ). .....	50

Figure 4.6. P-V curve for a rapid irradiance change.....	50
Figure 4.7. The designed membership functions of the proposal .....	53
Figure 4.8. A 3D surface between input1 ( $dp/dv$ ) and input2 ( $dp/p$ ) verse output ( $\Delta D$ ). .....	54
Figure 4.9. The input solar irradiance based on a rapid changing condition .....	56
Figure 4.10. PV array system for the proposed method versus conventional P&O under rapidly changing weather conditions .....	57
Figure 4.11. PV array system for the proposed method versus conventional FL under rapidly changing weather conditions.....	58
Figure 4.12. Grid-connected PV system using the proposed MPPT method .....	59
Figure 4.13. Triangular waveforms of irradiance for the EN50530 standard test of MPPT efficiency.....	61
Figure 4.14. The PV power for the EN50530 standard test of MPPT efficiency .....	62
Figure 4.15. The average efficiency of power tracking under the EN50530 standard test.....	63
Figure 5.1. The studied PV array installed at Brunel University London, UK.....	69
Figure 5.2. A block diagram of the ANFIS model. ....	71
Figure 5.3. The diagram of a PV system using an ANFIS-MPPT.....	72
Figure 5.4. The general diagram of a collected data system.....	73
Figure 5.5. The fitting curve of (a) PV power - irradiance level, (b) PV power - temperature operation. ....	76
Figure 5.6. Training data error versus epochs for the ANFIS model. ....	78
Figure 5.7. The defined membership function for (a) irradiance, and (b) temperature. ....	79
Figure 5.8. A 3D surface between inputs irradiance and temperature verse PV power. ....	79
Figure 5.9. PV array system for the ANFIS method versus P&O and FLC methods under a fixed irradiation condition.....	82
Figure 5.10. PV array system for the optimal ANFIS versus conventional ANFIS, conventional P&O and conventional FLC methods under a rapid change in weather conditions.....	83
Figure 5.11. Real measurement test of one day of: (a) irradiance, and (b) temperature.....	85
Figure 5.12. MPPT power for: (a) P&O versus the optimal ANFIS, (b) FLC versus the optimal ANFIS and (c) conventional ANFIS versus the optimal ANFIS. ....	86
Figure 5.13. The average efficiency of the generated power of PV array under the real measurement test.....	87
Figure 6.1. General diagram of a stand-alone PV system using an ANN-MPPT method.....	91
Figure 6.2. Block diagram of an ANN system.....	93

Figure 6.3. The Flowchart of a PSO algorithm.....	95
Figure 6.4. Schematic diagram of the training methodology.....	96
Figure 6.5. The search history of the PSO-ANN algorithm. ....	99
Figure 6.6. The best validation performance of (a) the conventional ANN and (b) the optimised ANN. ....	99
Figure 6.7. The irradiance level of weather conditions. ....	101
Figure 6.8. PV array system for the proposed method versus the P&O, FLC and ANN methods under theoretical climate conditions.....	102
Figure 6.9. Experimental measurement tests for a sunny and a cloudy day.....	104
Figure 6.10. MPPT predicting power on a sunny day using the proposed method versus....	105
Figure 6.11. MPPT power prediction on a cloudy day using the proposed method versus...	106
Figure 6.12. The average efficiency of the predicting power for the conventional P&O, FLC and ANN as well as the proposed method.....	107
Figure E.1. The Simulink model of a grid-connected PV system based on MATLAB simulation.....	137
Figure F.1. The graphical rules of a FLC model.....	138
Figure G.1. The linguistic rules of an ANFIS model.....	139
Figure H.1. The training regression of an ANN model .....	140

## LIST OF TABLES

Table 2.1. An overview of the main features of the most popular MPPT methods.....	20
Table 3.1. Parameters of the Simulink PV module.....	24
Table 3.2 The probabilities of direction for a P&O algorithm .....	32
Table 4.1. The fuzzy rules that are used in the conventional FLC-MPPT.....	50
Table 4.2. The fuzzy rules that are used in the proposed method.....	52
Table 4.3. A comparison of the properties of the proposed method, conventional P&O and conventional FLC.....	56
Table 4.4. A comparison of the output energies of the proposed method, conventional P&O and conventional FLC.....	56
Table 4.5. A Comparative study regarding the average efficiency for the proposed method and the conventional FLC and P&O-MPPT techniques. ....	61
Table 5.1. PV module characteristics. ....	69
Table 5.2. Simulation ANFIS model based on optimized data VS total data.....	78
Table 5.3. Mean Square Error (MSE) for different input membership functions.....	78
Table 5.4. A comparison of the properties of the ANFIC, P&O and FLC-MPPT. ....	81
Table 5.5. Comparative study regarding the average efficiency for the optimal ANFIS, conventional ANFIS, conventional FLC and P&O-MPPT techniques. ....	85
Table 6.1. The main steps of the first proposed algorithm to find the optimised topology of the ANN.....	97
Table 6.2. The major steps of the second proposed algorithm to find the initial weights of the ANN.....	98
Table 6.3. The rudimentary statistical analysis of the proposed algorithm. ....	100
Table 6.4. A comparative study covering the main properties of the conventional ANN, FLC and P&O-MPPT method as well as the optimised ANN-MPPT. ....	101
Table 6.5. Comparative study regarding the hourly average efficiency for the proposed method and the conventional ANN, FLC and P&O-MPPT techniques. ....	104
Table A.1 The data sample which collected from experimental PV test.....	129

## LIST OF SYMBOLS

$b_j$	The bias of the ANN model
$C$	The Capacitor
$c_1$ and $c_2$	The cognitive coefficient factors of PSO
$D$	The Duty ratio
$D_m$	The Duty ratio at the MPP of PV array
$f_s$	The switching frequency
$G$	The Solar irradiance
$G_{bi}$	The global best position of PSO algorithm
$I_C$	The Capacitor current
$I_d$	The current of PV diode
$i_L$	The Inductor current
$I_{PV}$	The photovoltaic output current
$I_{MPP}$	The PV Current at maximum power point
$I_L$	The output current generator of PV cell
$I_{SC}$	The short circuit current of PV cell
$I_{ph}$	The current generator from the solar cell
$I_{PV}$	The Output current of the PV cell
$I_{sh}$	The shunt circuit current of PV cell
$I_{SC}$	The short circuit current of PV cell
$I_0$	The saturation current of the PV diode
$k$	The Boltzmann's constant
$Ka$	The temperature coefficient
$L$	The inductor
$P_m$	The maximum output power
$P_{PV}$	The module output power
$P_{bi}$	The best fitness values of PSO algorithm
$P_{out}$	The actual output power of the PV array
$P_{max}$	The theoretical maximum power of PV array
$P_{ref}$	The predicting power of ANN model
$P_{act}$	The PV's actual power of PV array
$q$	The electrical charge

$R_{SC}$	The Series resistance of PV cell
$R_{sh}$	The Shunt resistance of PV cell
$R_m$	The resistive load at Pm
$r_1$ and $r_2$	The random velocity values of PSO
$T$	The temperature
$T_j(i)$	The target output
$V$	The speed velocity of PSO
$V_d$	The Voltage across the PV diode
$V_{pv}$	The output PV voltage
$V_i$	The input voltage
$V_m$	The PV voltage at maximum power point
$V_o$	The output voltage
$N$	The PV diode factor
$Y_j(i)$	The real output
$w_{ij}$	The connection weights of ANN model
$W_i$	The firing strength of FLC
$\Delta D$	The historical duty cycle changes during one sample
$\Delta P$	The historical power change during one sample
$\Delta V$	The historical voltage changes during one sample
$\Delta G$	The historical irradiance changes during one sample
$\Delta V_o$	The ripple output voltage of DC-DC converter
$\Delta i_L$	The ripple output current of DC-DC converter
$\eta_{MPPT}$	The tracking efficiency of MPPT

## LIST OF ABBREVIATIONS

AC	Alternative Current
AI	Artificial Intelligence
ANN	Artificial Neural Network
ANFIS	Adaptive Neuro-Fuzzy Inference System
BP	Back Propagation algorithm
BJT	Bipolar Junction Transistor
C	Constant
CV	Constant Voltage
COG	Centre of Gravity
DC	Direct Current
E	Error
FOCV	Fraction Open Circuit Voltage
FIS	Fuzzy Interface System
FL	Fuzzy Logic
FLC	Fuzzy Logic Controller
HC	Hill Climbing
GUI	Graphical User Interface
IC	Incremental Conductance
IGBT	Insulated Gate Bipolar Transistor
I-V	PV Current Vs Voltage
MOSFET	Metal Oxide Semiconductor Field Effect Transistor
MFs	Membership Functions
MPP	Maximum Power Point
MPPT	Maximum Power Point Tracking
MSE	Mean Square Error
OC	Open Circuit
PI	Proportional – Integral
P&O	Perturb and Observe
PSO	Particle Swarm Optimization
PV	Photovoltaic
P-V	PV Power Vs Voltage

PWM	Pulse Width Modulation
S	Signal of DC-DC converter
SC	Short Circuit
SCADA	Supervisory Control and Data Acquisition
SEPIC	Single Ended Primary Inductor Converter
STC	Standard Test Condition
LAN	Local Area Network
GA	Genetic Algorithm
GSA	Gravitational Search Algorithm
VSS	Variable Step Size

# Chapter 1

## Introduction

In this chapter, the background, motivations, aim and objectives of this thesis are introduced. Section 1.1 covers the background of photovoltaic (PV) energy, while Section 1.2 discusses the motivations of this research. In Section 1.3, the aim and objectives are explained. Section 1.4 presents the contributions of this thesis, which is followed by its structure in Section 1.5. Finally, the publications stemming from this research are provided in Section 1.6.

## 1.1 Background

In recent years, the global demand for energy has increased dramatically due to population growth. In addition, the phenomenon of global warming has intensified owing to the CO<sub>2</sub> emissions from fossil fuels. Nowadays, the major global production of electrical energy is met from fossil fuels, constituting about 80% [1]. This percentage is expected to generate about 40.4 Gt CO<sub>2</sub> by 2030 [2]. To solve the issue of lack of energy in future years and to minimise the side effects of burning fossil fuels, many studies have called for the use of renewable energies. Hence, developing renewable energies have been become a worthy research topic in the last decade. The Renewable Energy Instruction of the European Union has set a goal of energy generation over 32% of total production from renewable energies by 2030, with the added aim of this reaching 100% by 2050 [3].

Solar PV systems, wind turbines and hydropower are the main renewable energy resources, coming from sunlight, wind and fast running water, respectively. [4]. A solar PV system is considered to be one of the most attractive renewable energy resources due to its provision of sustainable, clean and safe energy [5]–[7]. In addition, it can be installed almost anywhere with different capacities and the operating cost of this resource is low [8], [9]. On top of that, several studies refer that the surface of earth receiving power radiation from the sun about  $1.8 \cdot 10^{11}$

MW, which is considered much more than the total global demand for electrical power [10]. In recent years, the worldwide installed capacity of a PV system has risen sharply, as show in Figure 1.1 [11]–[13]. This is because various countries, such as China and India, have connected large PV plants with a utility grid. Moreover, some countries, for example, the USA and UK, have encouraged their citizens to install grid-connected PV systems on the rooves of their houses. Furthermore, the average installed cost of this PV system has dropped dramatically.

The leader of installed PV systems for several years during the latter part of 20th century was the USA. In 1996, Its total PV generation reached more than 77 MW. After this date, Japan took this position until 2004 and in that year, the installed capacity of PV systems in Japan become 1132 MW. Then, Germany turned into the world's leader of generated PV electricity during next 10 years, achieving PV production of about 40 GW in 2016. In 2015, China astonished other countries when it took this position from Germany and in 2017, it became the first country to generated 100 GW from PV systems alone [14]. By the end of 2018, the global installation of PV systems exceeded 500 GW.

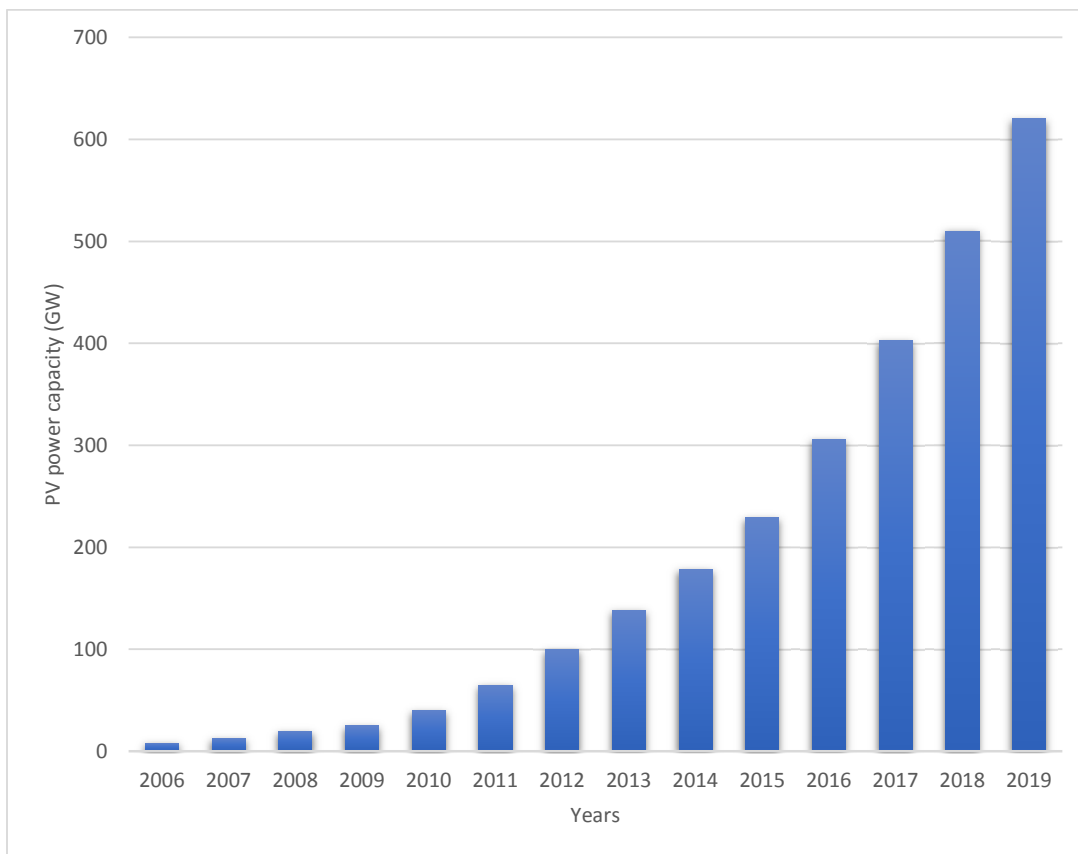


**Figure 1.1. The global growth of PV power installation capacity in GW [11-13]**

The generation of this PV installation contributed about 3% of global electrical energy consumption. In Italy, Greece, Germany, and Chile, the PV sources supplied about 8% of their annual domestic consumption, where that in Honduras was the largest contributor at about 14%. In Australia and USA, PV production reached 7% and 4% of their electrical energy consumption, respectively, while the PV production in China and India closed to 2.55% [15]. According to the International Energy Agency (IEA), global energy production from PV resources will reach 16% of global electricity by the 2050s [16].

### 1.2 Motivations

In general, there are two types of a PV system: grid-connected and stand-alone PV systems. This work focuses on the first type, which has been widely installed around the world due to its lower cost [3,8]. The grid-connected PV system refers to PV generation that is connected to the grid. The system consists of a PV array, power conversion system and grid connection equipment. Unlike the stand-alone PV system, it generally does not contain a storage unit (battery) as this is still very expensive. Hence, the power generation from this system feeds directly to the consumer when the weather conditions surrounding the PV array is right. Despite the impressive global growth of the grid-connected PV system capacity in recent years owing to the advantages and properties of the PV system, as mentioned in Section 1.1, the efficiency, stability and reliability remain major factors when seeking to introduce this resource to the market [17]–[19].

The output power from a PV system mostly depends on irradiance and temperature, i.e. weather conditions, as shown in Figure 1.2, which illustrates the current-voltage (I-V) characteristic of a PV array. This indicates that the PV power generation increases when the input irradiance increases, conversely, it decreases at a high operating temperature [20] [21]. On this chart, there is a unique point, which represents the maximum power point (MPP), and the location of this point shifts according to the climate conditions. To track this point continuously, the PV controller has been designed, the tracking efficiency of which is calculated based on the ratio of the theoretical maximum power and the actual maximum power of a PV module.

The oscillation of the PV output power owing to the variation of weather conditions is considered a major challenge for the PV system when it is connected with a grid [3]. In particular, the stability of the power system can be affected when weather conditions are highly variable, especially for a large-scale PV plant. Hence, designing a control system for hybrid

power generation is essential for adjusting the PV power when it is connected with the utility grid [22].

A failure in the equipment of a PV system may happen similar to any other electrical device due accidental events. The most common such failure for the PV system is when there are rapidly changing in weather conditions, resulting in a large change in the DC voltage of a PV array. In this case, the PV power conversion system may be damaged and/or the lifespan of the PV array can degrade quickly due to a hot-spot on the PV array [23]. To address these issues, control systems have been designed to enhance the average tracking efficiency, improve the stability and manage the power flow of a PV generation under different weather conditions [24]. Whilst several techniques have been used to design this control system, maximum power point tracking (MPPT) based on artificial intelligent techniques is considered the most efficient for a nonlinear system, such as the PV system.

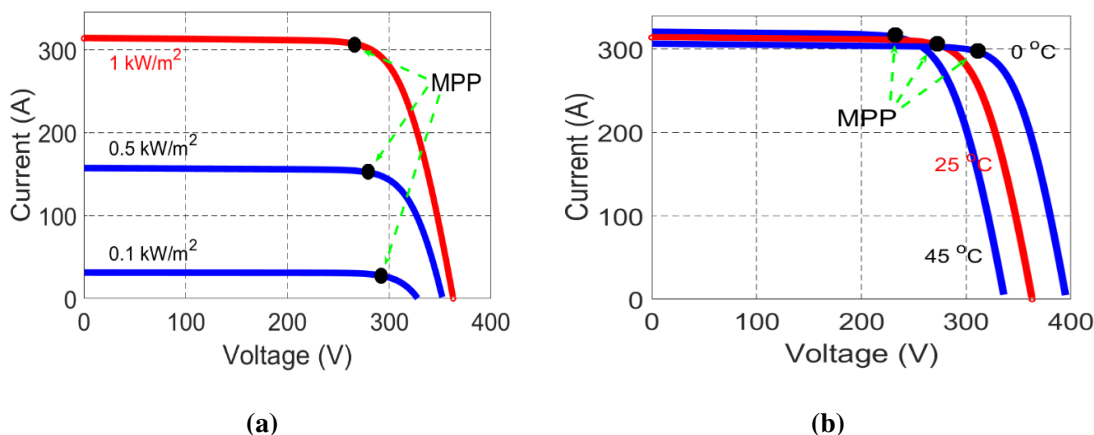


**Figure 1.2. I–V characteristic of a PV array under: a) various values of irradiance at a temperature of 25 °C; b) various values of temperature at an irradiance of 1000 W/m<sup>2</sup>**

### 1.3 Aim and Objectives

Higher tracking efficiency, optimal output power and reliable operation load are important features for consumers and investors, if they are to be attracted to installing PV systems [25]–[27]. The most effective way to improve the average tracking efficiency, enhance the stability and increase the reliability of PV system generation is to employ the MPPT technique with a PV power conversion system [28]–[31]. Basically, The MPPT technique is a power control system that feeds an appropriate duty cycle ( $D$ ) to the PV power conversion system (DC-DC converter) based on the output and/or input of the PV module to capture maximum power

production continuously, thereby achieving maximum power and delivering stable voltage under varying weather conditions. In general, there are several issues that are key when aiming to design the best MPPT technique for a PV system, including cost, efficiency, loss of energy, tracking time, level of oscillation, accurate tracking MPP and type of implementation [32] [33]. Taking these into account, many types of MPPT methods have been developed for PV systems, which can be divided into two types: classical methods, and artificial intelligence methods. The main aim of this research is to propose common MPPT techniques based on an artificial intelligence for a grid-connected PV system and then, to select the best of them.

The main objectives of this thesis are as follows:

1. The modelling of a grid-connected PV system designed using a MALAB environment to assess the functionality of a PV module. This PV system consists of a PV array, DC–DC boost converter with MPPT controller, DC-AC inverter and a utility grid;
2. The MPPT technique is tested and examined to demonstrate its greater effectiveness for the PV system when compared with the performance of one without a MPPT controller;
3. Various MPPT methods are compared based on their common features to help MPPT designers select the most suitable method for a PV operating system for their applications;
4. A micro-grid PV system being installed at Brunel University London, Uxbridge, UK, to collect a large and real training dataset of a PV array, which is an essential part in the designing of several MPPT methods;
5. The EN 50530 standard test and experimental measurement tests are used to calculate the average tracking efficiency of the proposed MPPT methods under various atmospheric conditions and to assess their performance during different states.

### **1.4 Thesis Contributions**

The major contributions of this research are as follows:

1. A modified Perturb and Observe (P&O)-MPPT controller based on a Pythagorean theorem and Constant Voltage technique is presented to solve the main issues of a conventional P&O-MPPT by developing variable step size and early step decision for the conventional P&O algorithm.

2. A novel MPPT technique based on fuzzy logic control (FLC) and the P&O algorithm is proposed to incorporate the advantages of the P&O-MPPT to account for slow and fast changes in solar irradiance and reduced processing time for the FLC-MPPT to address complex engineering problems when the number of membership functions are fewer.
3. An Adaptive Neural-Fuzzy Inference System (ANFIS) based on a large experimental training data is designed to avoid the ANFIS model from experiencing a high training error. These data were collected throughout the whole of 2018 from experimental tests of a PV array installed at Brunel University London, Uxbridge, United Kingdom, and then analysed using a fitting curve technique to optimise the tuning of the ANFIS model.
4. A feedforward Artificial Neural Network ANN technique using experimental data is developed for predicting a maximum power point of PV arrays. In order to improve the ANN model accuracy, the particle swarm optimisation algorithm is utilised to find the best topology and to calculate the optimum initial weights of the ANN model. Hence, the dilemma between computational time and the best-fitting regression of the ANN model is addressed, as well as the mean squared error being minimised.

### 1.5 Thesis Organisation

This thesis consists of seven chapters and it is organised as follows.

- ❖ **Chapter 1** presents the general statement of this research. It covers the background of PV technology, followed by research motivations, aims and objectives and thesis contributions. Finally, a list of publications from the work in this thesis is provided.
- ❖ **Chapter 2** introduces a brief review of historical PV energy, followed by types of PV cells and the main challenges of PV technology. Then, the principle work of the MPPT technique and literature survey of common MPPT methods are provided. Finally, these are compared and classified based on their popular features.
- ❖ **Chapter 3** covers the modelling, structure, controller of the PV system. It proposes the modelling of a PV cell, followed by a structure for a PV array. Then, topologies of PV systems are introduced, and the DC-DC boost converter is presented. The control scheme of PV system is covered, followed by the principle work along with the schematic diagrams of the conventional P&O and modified P&O algorithms. A MATLAB-SIMULINK model

for a grid-connected PV system is designed. Finally, the simulation results are provided and discussed.

- ❖ **Chapter 4** designs a novel maximum power point tracking technique based on fuzzy logic control for a grid-connected PV system. A literature review on the modified FLC technique for a PV-MPPT system is presented and fuzzy logic control is explained. The advantages and disadvantages of the FLC-MPPT are discussed, followed by the designed membership functions of this novel FLC controller based on a modified P&O algorithm. The P&O-MPPT, FLC-MPPT and proposed method are simulated, being then compared, according to their common features. Finally, the EN 50530 standard test is used to calculate the efficiency of the proposed method under varying weather conditions.
- ❖ **Chapter 5** proposes an efficient maximum power point tracking technique based on the ANFIS method using a real large photovoltaic system dataset. Related works of used ANFIS-MPPT for PV systems are presented. The principle work of the ANFIS technique is introduced, following by a schematic diagram of the ANFIS-MPPT controller. The methodologies of the collected and optimised data as well as the tuning of the proposed ANFIS model are explained. The P&O-MPPT, FLC-MPPT and the proposed ANFIS method are simulated, being then compared, according to their popular features. Finally, a real measurement test of a semi-cloudy day is used to calculate the average efficiency of the proposed method under varying climatic conditions.
- ❖ **Chapter 6** utilities an optimised feedforward Artificial Neural Network technique based on particle swarm optimisation using experimental data for predicting the maximum power point of a photovoltaic array. A state-of-the-art ANN-MPPT for PV systems is advanced. The principles of the feedforward ANN technique and PSO algorithm are covered, following by a schematic diagram of ANN-MPPT controller being presented. The training of the proposed ANN model is designed, followed by the results being provided. Then, experimental data of sunny and cloudy days are used to determine the average efficiency of this proposed method under varying atmospheric conditions. Finally, comparative analysis regarding the main properties of the proposed methods in this thesis is presented.
- ❖ **Chapter 7** contains the conclusions of this research, with proposed directions for future work.

## 1.6 List of Publications

Six scientific papers have been published from this research comprising three journal and three conference papers.

### 1.6.1 Journal publications

1. S. D. Al-Majidi, M. F. Abbod, and H. S. Al-Raweshidy, "A novel maximum power point tracking technique based on fuzzy logic for photovoltaic systems," *International Journal of Hydrogen Energy*, vol.43, no.31, pp.14158-14171, 2018.
2. S. D. Al-Majidi, M. F. Abbod, and H. S. Al-Raweshidy, "Design of an Efficient Maximum Power Point Tracker Based on ANFIS Using an Experimental Photovoltaic System Data," *Electronics*, vol. 8, no. 8, pp.858, 2019.
3. S. D. Al-Majidi, M. F. Abbod, and H. S. Al-Raweshidy, "A Particle Swarm Optimisation-trained Feedforward Neural Network for Predicting the Maximum Power Point of a Photovoltaic Array" *Engineering Applications of Artificial Intelligence*, vol. 92, no. June, pp. 103688, 2020.

### 1.6.2 Conference publications

1. S. D. Al-Majidi, M. F. Abbod, and H. S. Al-Raweshidy. "A Modified P&O-MPPT based on Pythagorean Theorem and CV-MPPT for PV Systems" *53<sup>rd</sup> International Universities Power Engineering Conference (UPEC)*, Glasgow, UK, 2018.
2. S. D. Al-Majidi, M. F. Abbod, and H. S. Al-Raweshidy. "Design of an Intelligent ANN-MPPT Controller using Real Photovoltaic System Data" *54<sup>th</sup> International Universities Power Engineering Conference (UPEC)*, Bucharest, Romania, 2019.
3. S. D. Al-Majidi, M. F. Abbod, and H. S. Al-Raweshidy. "Maximum Power Point Tracking Technique based on Neural-Fuzzy approach for a Stand-alone PV System" *55<sup>th</sup> International Universities Power Engineering Conference (UPEC)*, Torino, Italy 2020.

## Chapter 2

### Photovoltaic Energy

This chapter presents the history, types and challenges of PV energy. Despite the conversion efficiency of PV technology having been enhanced recently, it still faces several issues in relation to its application system, such as mismatching of the maximum power point and loss of stability and reliability. The most effective method to address those problems is to employ an MPPT controller. The chapter is organised as follows: Section 2.1 briefly reviews the history of PV energy; Section 2.2 presents the various types of PV cells; Section 2.3 covers the main challenges of PV technology; the most common methods of MPPT techniques are covered in Section 2.4; an overview of the various MPPT methods based on their common features is provided in Section 2.5; and finally, Section 2.6 contains the chapter summary.

#### 2.1 History of Photovoltaic Energy

In 1839, Becquerel noticed the phenomenon of the photon-voltage effect when he was studying the effect of light on electrolytic cells [34]. Later, in 1877, Adams and Day also noticed this phenomenon on solid Selenium. Subsequently, in 1883, Fritz proposed the first PV cell with very low conversion efficiency of about 1%. However, researchers took a long time to design the modern PV module, which was produced in 1954 at Bell Laboratories [35]. The conversion efficiency of this module was about 6-10% [36]. Using PV energy was limited to the aerospace and military industries due to its high cost. In the 1960s, several types of PV module were developed based on compound semiconductors such as, polycrystalline Si (pc-Si) and thin-film [20]. Those types had an enhanced efficiency of about 15%, high production capacity and structural integration. As a result, the capital installing cost for large-scale PV system generation had been reduced. These properties of the new PV system as well as the oil crisis, which happened in the 1970s, encouraged investment in this energy resource [37].

Accordingly, several universities were installed with PV system, such as Delaware University and built University in the United States. The conversion efficiency of this PV module was 17% [35]. The 1980s was the first time when a large-scale PV plant of more than MW in an industrial purpose was installed, with a conversion efficiency of about 20%. Whilst the first PV system for domestic purposes was produced in the 1990s due to the recommendation of programmes investing in PV resources. By this time, the conversion efficiency of a PV cell had increased up to 30% [38]. In 2000, researchers designed a new PV cell based on two junctions with conversion efficiency of more than 33%. Ten years later, they further developed this new PV cell based on multi-junctions, with a conversion efficiency greater than 42%. In 2012, researchers at the National Renewable Energy Laboratory (NREL) managed to get this multi-junction PV cell to reach a conversion efficiency of greater than 44% [39], [40].

Several kinds of PV cells have been developed recently, such as monocrystalline, thin-film pc-silicon, thin-film amorphous, thin-film chalcogenide, and the concentrated PV cell [41]. They are used for various applications, such as a water-pump systems, high-way signals, lighting streets, roadside emergency telephones, surveillance cameras, stand-alone PV systems and grid-connected PV systems [42]. Figure 2.1 presents the major historical developments of PV technology regarding its conversion efficiency based on several research endeavours [36-40].

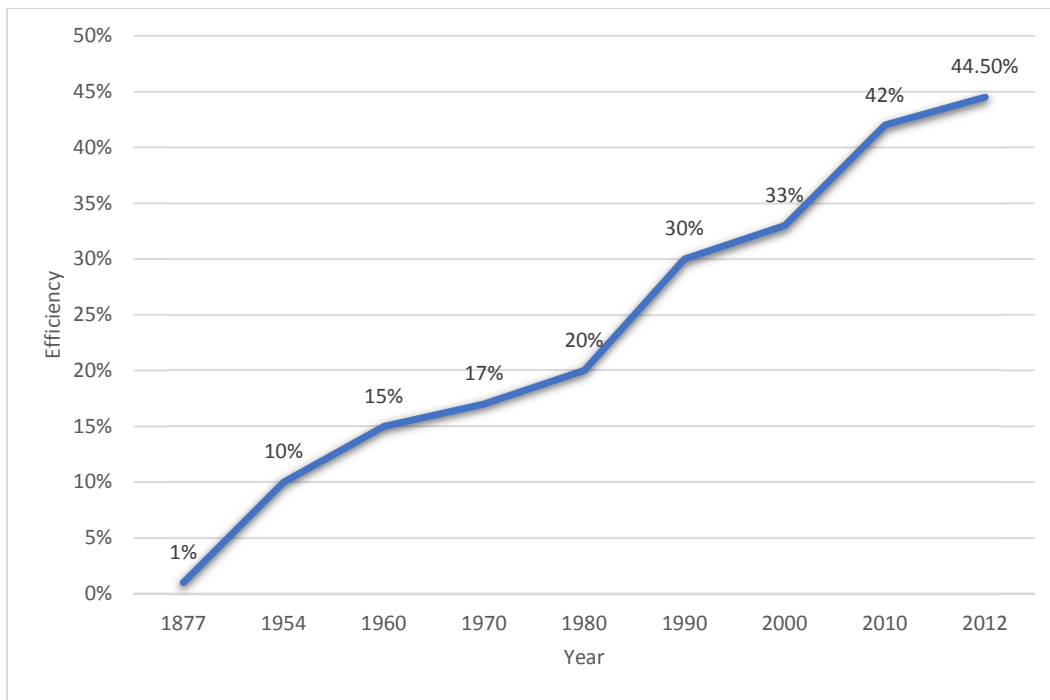


**Figure 2.1. The historical development of PV energy [36-40]**

Moreover, the price of this technology has decreased dramatically, as shown in Figure 2.2 [43], where it can be seen that the average cost of a solar PV cell has decreased from \$76.67/W in 1977 to \$0.74/W in 2013.

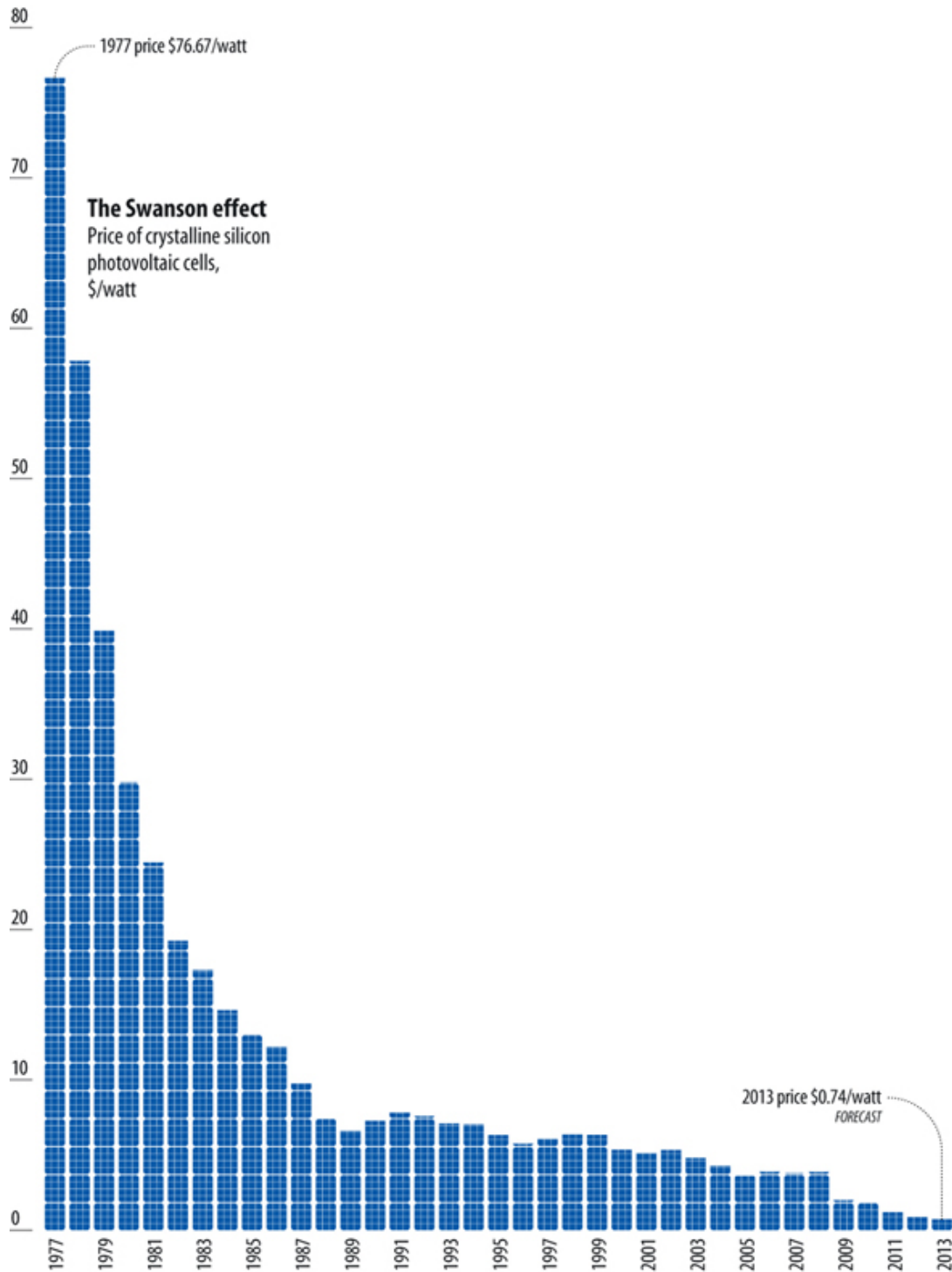


Figure 2.2. Historical decrease in the price of a PV cell [43]

## **2.2 Types of Photovoltaic cells**

In general, there are three main commercial technologies for manufacturing PV cells, including monocrystalline silicon, polycrystalline silicon and amorphous silicon, as shown in Figure 2.3 [5],[7],[9].

### **2.2.1 Monocrystalline silicon**

Monocrystalline silicon technology is considered the highest efficiency PV cell, with a conversion efficiency of about 17 to 22%. This PV cell is made from extremely pure silicon and its manufacture requires a separate single cylindrical crystal of silicon to produce monocrystalline silicon using a floating zone technology. This technology is highly intensive and expensive, which makes this type of PV cell most costly when compared with other PV technologies. Therefore, this type is suitable for a higher producing consumption situation.

### **2.2.2 Polycrystalline silicon**

As inferred above, polycrystalline silicon technology delivers a cheaper PV cell than that of monocrystalline silicon. However, its conversion efficiency is lower, at only about 12 to 16%. It is made from an ingot of melted and recrystallised silicon. The manufacturing process of this type of PV cell requires cutting this ingot into very thin wafers according to the grain boundaries and then, being assembled. The gaps among this grain boundaries are what cause a lower conversion efficiency. However, given this manufacturing process's lower cost, it is more suitable for a lower producing consumption situation.

### **2.2.3 Amorphous silicon**

Amorphous silicon technology has the lowest cost and lowest conversion efficiency of around 6 to 10%. It is made from a thin wafer of silicon and the manufacturing process of this type of PV cell is divided into two steps. Firstly, it is deposited on a carrier material based on a several stage process to produce an amorphous silicon film and secondly, it is sandwiched between glass plates to manufacture a sample PV module. The main disadvantages of this PV cell are that it requires a large installing surface, it has the lowest lifespan and it has the lowest conversion efficiency when compared with the other technologies. Hence, it is more appropriate for a small power consumption situation.



**Figure 2.3. Types of PV technologies**

## **2.3 Challenges of Photovoltaic Technology**

### **2.3.1 Efficiency of the PV Cell**

The output power of a PV cell changes according to the weather conditions surrounding the PV cell [44], [45]. Basically, the generating power of the PV array increases as the irradiance increases owing to high numbers of photon-voltage hitting the electron-hole of the cell, thus resulting in increased PV output current. Conversely, this decreases at a high operating temperature, because the open circuit voltage of PV cell will drop as temperature increases due to the extension of the band gap of the PV semiconductor. During this time, the movement of PV electrons becomes less valent when input irradiation is absorbed, resulting in a decreasing loss of energy. However, there is unique operation point for the PV cell, which is called the maximum power point (MPP) and this point shifts according to the weather conditions.

### **2.3.2 Stability of PV generation**

The fluctuation of PV output power due to passing clouds is considered a major issue for designing a grid-connected PV system [3], [46]. Several issues can affect the operation of the PV system, such as a voltage rise and voltage oscillation. That is, the stability and reliability of PV power generation can be severely affected when atmospheric conditions are highly variant, especially regarding large-scale PV generation. This issue is not very common in conventional power systems, so controlling the flow of energy throughout a hybrid power system to adjust the PV generation for the utility grid is essential.

### **2.3.3 Partial shading condition**

In normal conditions, a PV array exhibits a single unique maximum power point (MPP) in relation to the input solar irradiance and temperature operation [47]. However, the PV array will generate several MPPs when there is a shading, which can be caused by trees or dust, i.e. on part of the PV array. This is because each PV module will produce its MPP [48] and as a result, several PV power values will be generated in same time. Hence, the global PV power generation will be decreasing. In this case, a hotspot on the PV module may occur owing to a large change in PV voltage when the operation point shafts rapidly, thus leading to damage in the PV system.

### **2.3.4 Mismatch of PV load**

The voltage operation of a PV array also depends upon the value of the load [49], [50]. When the output power generation of a PV array is lower or higher than the power load, the PV voltage operation will drop or rise to a new operating point and consequently, the efficiency of PV generation will drop. In addition, the equipment of a grid-connected PV system may be damaged in case of a large-scale PV plant when it disconnects due to the fault.

### **2.3.5 Lifespan of an installed PV module**

Most PV manufacturing companies assert that the lifespan of PV module is typically 20-years with its production being at least 80% of the rated power [51]. However, several studies have indicated that the weather operating conditions of an installed PV system play an important role in degrading its lifespan by about 0.2% per year [52]. This is due to large changes in PV voltage that accrue when the weather conditions change rapidly.

## **2.4 Maximum Power Point Tracking Techniques**

The maximum power point tracking (MPPT) technique is an essential part of the PV system design for tracking the MPP of a PV array, which enhances the stability and reliability of the PV system when it is connected to a grid [53]–[55]. In addition, it addresses the problem of a partial shading condition and the challenge of a matching of PV load. Consequently, it contributes to conserving the lifespan of an installed PV Module. In general, tracking efficiency, cost, energy loss and type of implementation are the key issues when aiming to design a MPPT method for a PV system [56]. Taking these into account, several common types of MPPT techniques have been proposed for PV systems, which can be divided into two types:

conventional techniques, such as constant voltage (CV) [57], fraction open circuit voltage (FOCV) [33], Perturb and Observe (P&O) [58] and incremental conductance (IC) [59]; and artificial intelligence techniques (AI), for example, fuzzy logic controller (FLC) [60], artificial neural network (ANN) [61], adaptive neuro-fuzzy inference system (ANFIS) [16] and particle swarm optimisation (PSO) [47].

The CV method is the simplest MPPT algorithm for a PV system, because it does not require an input sensor to determine the MPP [57]. This algorithm assumes that the PV panel variations, such as irradiance and temperature of weather conditions, are insignificant, and that the constant reference voltage ( $V_{ref.}$ ) is adequate for achieving performance close to the MPP, as given in Eq. (2.1):

$$V_{ref.} = k \times V_{oc} \quad (2.1)$$

where,  $V_{oc}$  is the open circuit voltage of a PV array and  $k$  is a constant value between 0.71 and 0.78, which is adjusted according to the characteristics and the weather conditions for an installed PV array. Hence, the operating point of the PV array is assumed to be near to the MPP by regulating the PV voltage to match with a fixed reference voltage. However, it is necessary to collect climatic installing data to establish the fixed voltage reference, as this may change from one location to another. The main advantage of this technique is that it has a high speed for reaching the steady state case, particularly in low and diffused radiation conditions [62]. However, it only calculates the MPP approximately.

Another simple method for the MPPT controller is FOCV control. This method tracks the MPP of the PV module based on a linear proportional relationship between the operating voltage of the installed PV module at MPP and its open circuit voltage, which is calculated according to the datasheet of this installed PV module, as shown in Eq. (2.1). The constant ( $k$ ) in Eq. (2.1) is changed and adjusted continuously according to the weather conditions of the installed PV array. This method is more accurate in finding the MPP under varying weather conditions than the CV method. However, it also only calculates the MPP approximately.

The P&O-MPPT can be used to determine the MPP accurately. The principle work of this algorithm is calculating the PV power by using the sensed values of the voltage and current of the PV module. These are then compared with the previous power and voltage, with the direction of the algorithm to adjust the duty cycle of the power converter accordingly. It is a widely used method for PV-MPPT due to its simple implementation and low cost [63]. However, it faces many issues, such as a slow tracking speed, high fluctuation around the MPP,

and a drift issue associated with fast changing irradiation [64]. As a result, the PV array achieves a low tracking efficiency, especially on cloudy days [23]. The IC-MPPT was designed to overcome the limitations of the P&O algorithm by using the incremental conductance of the PV array. The principle work of this algorithm depends on researching the optimised operating point based on the fact of derivative power-voltage characterises of the PV array ( $\frac{dP}{dV}$ ), as given in Eqs. (2.2) and (2.3):

$$\frac{dP}{dV} > 0 \quad \text{left of MPP} \quad (2.2)$$

$$\frac{dP}{dV} < 0 \quad \text{right of MPP} \quad (2.3)$$

If  $\frac{dP}{dV}$  has a positive value, the optimised operation point is on the left of the MPP, otherwise, it is on the right. The major advantage of this algorithm is that it has a high ability to reach the MPP point under a rapid change of environmental conditions [59]. However, instability and measurement noise are big problems facing the operating work of the PV system due to the use of a derivative operation in this algorithm [65], [66]. In addition, these are classified as complex and costly control circuits when compared with the P&O method. Hence, several modulations based on the power-voltage curve of a PV array have been proposed to address the issues of the classical MPPT methods by an adaptive algorithm or variable step size for those conventional methods, such as in [67]–[74]. Whilst those modifications enhance the performance of the classical MPPT methods, they are considered as being insufficient solutions, because these modifications do not eliminate the issues of classical MPPT methods completely. In addition, they do not achieve a high efficiency under a rapid change in weather conditions. Consequently, AI methods based on MPPT have been introduced to address these problems. These methods do not require complex mathematics and accurate parameters when managing the system [75].

In particular, the FLC-MPPT is one of the most powerful controllers for a PV system owing to its faster tracking speed and lesser oscillation around the MPP point, when compared with classical MPPT methods [76]. Furthermore, it does not require training data, unlike the ANFIS and ANN methods, because it deals with imprecise and noisy input information based on a mathematical model, thus resulting in its operating for different types of PV array with the same MPPT proposal. However, its implementation is complex by comparison with the classical MPPT methods. In addition, it suffers from the drift issue associated with a change in the solar irradiation and operating temperature [77]. This is because it heavily depends on the good

knowledge of a PV system to design an optimal MPPT controller, which results in incorrect fuzzy rules and inaccurate membership functions of the FLC system. To address those issues, many modifications have been presented for an adaptive and optimised defined membership function of the traditional FLC-MPPT using several optimisation methods. For example, a genetic algorithm, the PSO algorithm or the M5P model tree, as evidenced in [78]–[85]. Whilst these proposals avoid the drift problem during changing irradiance, their hardware implementations become more complex.

Recently, an MPPT with ANN technique was used to solve the issue of conventional FLC-MPPT, which provides a heuristic output function using numerical quantifying data and therefore, it does not require good knowledge of the PV parameters to design an optimised MPPT controller [76]. Hence, the ANN-MPPT method has a faster tracking speed for transient state and lesser oscillation around the MPP point at steady state conditions when compared with FLC-MPPT. In addition, it is more accurate for addressing the MPP in rapidly changing atmospheric conditions. As a result, it achieves higher efficiency than the conventional FLC-MPPT method. However, slow training and black box work as well as the training strategy of the ANN model are key weaknesses of the ANN system [86]. To solve these limitations, several modifications have been proposed to enhance the performance of the ANN model using various types of optimisation strategies, such as in [61], [75], [87]–[92]. The methodologies of these strategies can be divided into three cases: selecting the effective training data, finding the best topology of an ANN model and calculating the parameters of the ANN algorithm. However, the training error of this technique is a high value.

The ANFIS method offers the most powerful intelligence technique for PV systems, because it is integrated into the ANN and FLC system. It is an adapted neural network technique based on a fuzzy inference system. The MPPT technique based on ANFIS also has a faster response, less oscillation and is more accurate for addressing the MPP under different weather conditions. However, getting accurate training data and optimised tuning of the ANFIS model are big challenges when designing an efficient ANFIS-MPPT controller [93]. Several proposals have been made recently using theoretical and experimental training data [16], [54], [94]–[101]. Whilst the proposed ANFIS-MPPT controllers based on the experimental training data achieve higher performance when compared with the proposed ANFIS-MPPT controllers based on the theoretical training data, the rules of the ANFIS model have not been optimised, thus resulting in a high training error.

The last MPPT method for PV application is the PSO algorithm. The principle idea of this algorithm is that it tries to find an optimised duty cycle, where each value has a degree of possibility for a candidate solution. Hence, it does not require training data or prior data to design the MPPT controller based on the PSO algorithm. This method is more efficient when the PV array is under partial shaded conditions. However, it has a long tracking time, medium oscillation and highly complex implementation when compared with the other intelligent MPPT methods. To address these issues, the dynamic of the PSO algorithm has been enhanced recently by addressing its optimal parameters [47],[54],[80]. However, this method does not work properly under a rapid change in weather conditions, because it requires a longer time to find the optimised duty cycle.

In those previous studies, the researchers had developed various MPPT controllers for PV systems based on different techniques and then, several optimisations were proposed to enhance them. However, most of those proposals did not address the complex implementation challenge when they tried to improve their performance further. In this thesis, common MPPT methods, including: the P&O algorithm, FLC technique, ANFIS model and an ANN technique are proposed to increase the tracking efficiency, improve the stability and enhance the reliability of a grid-connected PV system, particularly under a rapid change in weather conditions, without adding a step control unit. Figure 2.4 classifies the main commonly used types of MPPT methods for PV systems.

### **2.5 Overview of the various MPPT methods**

To summarise, the most common MPPT methods, Table 2.1 reports a comparative overview of the main properties of the conventional CV, FOCV, P&O, IC, FLC, ANN, ANFIS and PSO-MPPT techniques used in PV systems. The properties include type of implantation, level of cost, required training data and prior training after their implementation stage. Moreover, do they have a fast or slow tracking speed for a transient state and high or low oscillation around the MPP at steady state conditions? Finally, can they calculate the MPP accurately or approximately under different weather conditions? As a result, are they achieving a high or low efficiency under various state conditions? Regarding to this comparison, the MPPT methods based on AI techniques have more complexity, cost more and are difficult to implement. However, they have higher tracking efficiency, faster tracking speed and less oscillation than the classical MPPT methods.

## **2.6- Summary**

In this Chapter, a general overview of PV energy based on MPPT techniques has been presented. A brief historical view about the developing PV technology has been provided. The types of PV cells and the main challenges of PV technology have been presented. A literature review of the most popular MPPT method for a PV system has been presented. The advantages and disadvantages of each MPPT method have been provided. The conventional CV, FOCV, P&O, IC FLC, ANN, ANFIS and PSO-MPPT methods have been compared regarding their popular features. Basically, whilst AI techniques based on MPPT have more complexity, cost more and are more difficult to implement, they have higher tracking efficiency, faster tracking speed and less oscillation than the conventional MPPT methods.

**Table 2.1. An overview of the main features of the most popular MPPT methods.**

<b>MPPT Method</b>	<b>implementation</b>	<b>Cost</b>	<b>Required data</b>	<b>Prior training</b>	<b>Tracking speed</b>	<b>Oscillation</b>	<b>Calculating MPP</b>	<b>Tracking Efficiency</b>
<b>CV</b>	Simple	Inexpensive	Yes	Yes	Fast	Low	Approximate	Low
<b>FOCV</b>	Simple	Inexpensive	Yes	Yes	Fast	Low	Approximate	Low
<b>P&amp;O</b>	Simple	Inexpensive	No	No	Slow	High	Accurate	Low
<b>IC</b>	Complex	Inexpensive	No	No	Slow	Medium	Accurate	Low
<b>FLC</b>	Complex	Expensive	No	Yes	Fast	Medium	Accurate	Medium
<b>ANN</b>	Complex	Expensive	Yes	Yes	Fast	Low	Accurate	High
<b>ANFIS</b>	Complex	Expensive	Yes	Yes	Fast	Low	Accurate	High
<b>PSO</b>	Complex	Expensive	No	No	Slow	Medium	Accurate	High

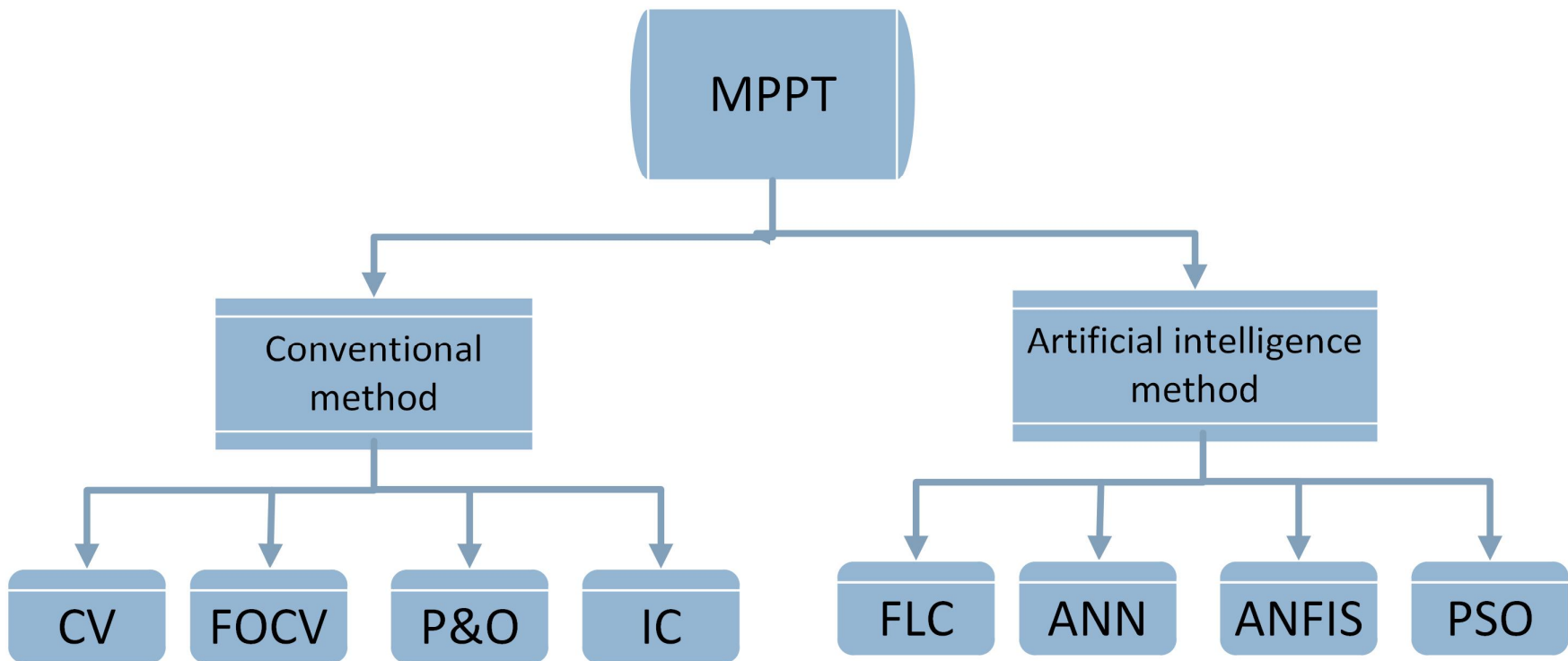


**Figure 2.4. Common types of MPPT methods for PV systems**

# Chapter 3

## Modelling and Control of PV Systems

This Chapter presents the modelling, structure and controller of a PV system. A grid-connected PV system is designed based on an MPPT controller to provide proof of the efficacy of the principle work and features of the MPPT method. The Chapter is organised as follows. Section 3.1 proposes the modelling of a PV cell and Section 3.2 explains the structure of a PV system. The DC-DC boost converter and the control scheme of the PV System are covered in Sections 3.3 and 3.4, respectively. The conventional P&O and modified P&O algorithms are discussed in Sections 3.5 and 3.6, respectively. In Section 3.7, the simulation results of a MATLAB-SIMULINK model for a grid-connected PV system are provided. Finally, Section 3.8 contains the chapter summary.

### 3.1 Modelling of a PV Cell

The fundamental element of photovoltaic system is the solar PV cell, the structure of which is illustrated in Figure 3.1.

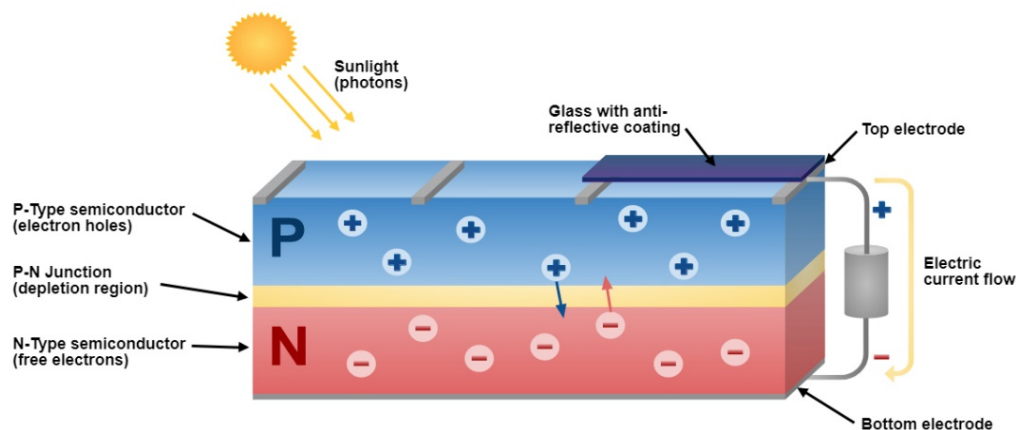


Figure 3.1. The structure of a PV cell

It is a semiconductor with added boron and phosphorus atoms to form a p-n junction with two layers using a high-temperature. These two layers consist of positive and negative ions, which pertain to the P-holes and N-electrons, respectively. Then, a top electrode and bottom electrode are added for an electric current flow. Finally, it is covered in glass with an anti-reflective coating. The principle work of this cell is that it converts the lighting into electrical energy based on the photo-voltage effect phenomenon [102]. In a typical solar cell, the resistances are not included, but they are implanted and connected with the PV diode in a practical case, as shown in Figure 3.2.

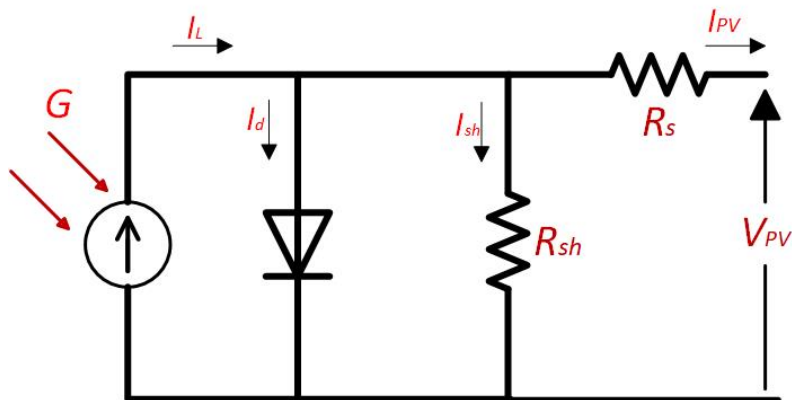


Figure 3. 2. The equivalent circuit of a PV cell

This is due to factors of the magnitude of resistance of the PV semiconductor and non-optimum PN junction diode, resulting in the implementing of series and shunt resistance, respectively. Kirchoff's law, as given in Eq. (3.1), can find the current generator from the solar cell [103], [104]:

$$I_{PV} = I_L - I_d - I_{sh} \quad (3.1)$$

where,  $I_L$  is the current generator which is given in Eq. (3.2) as:

$$I_L = G\{I_{SC}[1 + ka(T - T_{STC})]\} \quad (3.2)$$

where,  $G$  is the solar irradiation,  $T$  is the ambient temperature of the climate conditions,  $I_{SC}$  is the short circuit current of the PV cell,  $ka$  is the temperature coefficient,  $T_{STC}$  is the temperature operation of the PV cell under standard test conditions (STC), and  $I_d$  is the current of the PV diode, which is given by Shockley's Eq. (3.3):

$$I_d = I_0 \left\{ \exp\left(\frac{qV_d}{nkT}\right) - 1 \right\} \quad (3.3)$$

where,  $I_o$  is the saturation current of the PV diode,  $V_d$  is the voltage across the PV diode,  $q$  is the electrical charge ( $1.69 \times 10^{-19}$  C),  $k$  is the Boltzmann constant ( $1.38 \times 10^{-23}$  J/K), and  $n$  is the PV diode factor. Now, the universal equation that describes the current-voltage (I-V) characteristic chart of the PV cell is given by Eq. (3.4):

$$I_{PV} = I_L - I_o \left[ \exp \left( \frac{q(V_{PV} + I R_S)}{nkT} \right) - 1 \right] - \left[ \frac{V_{PV} + I R_S}{R_{Sh}} \right] \quad (3.4)$$

where,  $I_{PV}$  is the PV output current, and  $V_{PV}$  is the PV output voltage. To simulate the current-voltage characteristics (I-V) in a MATLAB environment, Eqs. (3.1) - (3.4) are used. The parameters of the PV module used in this research are shown in Table 3.1[49]. This PV module is connected as 66 parallel strings and 5 series panels to present the wanted PV array. As shown in Figure 3.3, there are unique points on the power-voltage (P-V) curve of the PV array, which are recognised as the maximum power points (MPPs) and the location of those points shifts according to the irradiation and temperature of the climate conditions: the maximum available power of the PV array increases as solar irradiation increases, conversely a PV generator better for low temperature operation than increased one [105].

**Table 3.1. Parameters of the Simulink PV module**

<b>Characteristics</b>	<b>Value</b>
Cell number	96
Open circuit voltage	64.2 V
Maximum power voltage	54.7 V
Short circuit current	5.96 A
Maximum power current	5.58 A
Maximum power point	305 W
Diode ideality factor	0.944
Temperature Coefficient ( $I_{sc}$ )	+0.061%/ $^{\circ}C$
Temperature Coefficient ( $V_{oc}$ )	-0.272 V/ $^{\circ}C$

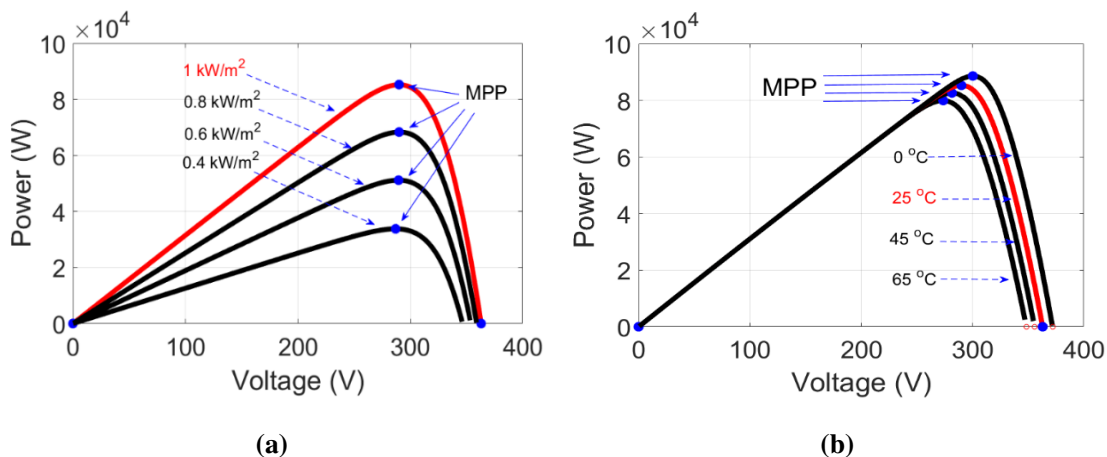


Figure 3.3. P–V curve of a PV array under: a) various values of irradiance at a temperature of 25 °C; b) various values of temperature at an irradiance of 1000 W/m<sup>2</sup>

### 3.2 Structure of a PV System

#### 3.2.1 The Configuration of a PV Array

The fundamental element of a photovoltaic system is a solar cell. Several solar PV cells are connected in parallel and series to obtain the desired current and voltage for a solar panel(module), Then, many solar panels are connected in series and/or parallel to give different configurations of a PV array, as shown in Figure 3.4 [106].



Figure 3.4. The configuration of a PV array [106]

### 3.2.2 Topologies of PV systems

To improve the stability, reliability and quality of the output of PV generation, a power conversion system is employed [107]. There are two types for PV power conversion system: single and double stage. These types of PV power conversion system are classified into four topologies: centralised approach, string approach, multi-string approach, and AC-module approach, as shown in Figure 3.5 [108]. Whilst the single stage-power conversion system is lower in cost due to its fewer part count, it suffers from several drawbacks, such as hot-spots during various weather and partial shading conditions of the PV array, increased probability of leakage current through the parasitic capacitance between the PV array and the ground system, high harmonic injection and voltage rise when it connects with the grid and reduced safety [60], [109], [110].

These issues occur in grid-connected PV system due to a large change in the DC voltage of the PV array, especially when the weather conditions surrounding the PV array are changing rapidly. To address them, the first stage is used to boost the MPP voltage and track the maximum power, whilst the second, converts this DC power into high quality AC power. Hence, a DC-DC converter and DC-AC inverter have been designed and connected with generating PV arrays for interfacing with the grid, as explained in the topology of the multi-string approach [111].

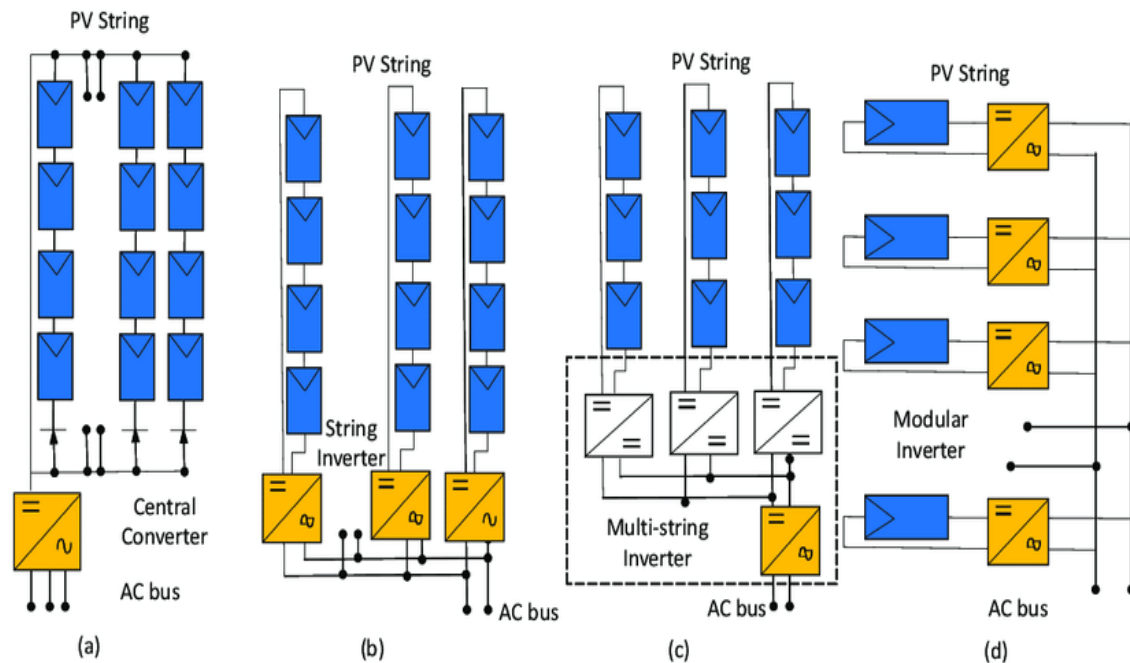


Figure 3.5. Topologies of PV systems [108]

### 3.3 DC-DC Boost Converter

Whilst several DC-DC converters have been designed, such as boost, buck and chuk converters, the boost converter is widely used for the PV generated system due to its high efficiency [112]. This is because the DC-DC boost converter provides and regulates a higher output voltage than the input voltage with a low output current. In this case, the loss power will be low according to a loss power equation. As shown in Figure 3.6, the heart of the DC-DC boost converter is a transistor, which regulates the amplified processing by a controller. The Metal Oxide Semiconductor Field Effect Transistor (MOSFET), Bipolar Junction Transistor (BJT) and Insulated Gate Bipolar Transistor (IGBT) are common transistors used in a DC-DC converter. However, the MOSFET transistor is usually used for designing the DC-DC boost converter due to its ability to work under a heavy load and higher frequency condition [113]. [114], whilst also having lower power losses.

The principle work of this converter is divided into two states, as shown in Figure 3.7. First, when the MOSFET is switched ON, the current flows through an inductor ( $L$ ) in a reverse direction and the inductor stores the energy by generating a magnetic field. The current change in the inductor  $I_L$  during time period ( $t$ ) is given by Eq. (3.5):

$$\frac{\Delta I_L}{\Delta t} = \frac{V_i}{L} \quad (3.5)$$

where,  $V_i$  is the input voltage. At the end of the ON-state, the changing value of  $I_L$  increases and thus, is given by Eq. (3.6):

$$\Delta I_{L_{on}} = \frac{1}{L} \int_0^{DT} V_i dt = \frac{DT}{L} V_i \quad (3.6)$$

In state two, when the MOSFET transistor is switched OFF, the energy stored and main source will be in series, which leads to a higher output voltage. The inductor voltage in this state is given by Eq. (3.7):

$$V_o - V_i = L \frac{dI_L}{dt} \quad (3.7)$$

where,  $V_o$  is the output voltage. The inductor current is changing linearly as long as the MOSFET switch remains opened. The rating change of the  $I_L$  when the MOSFET is switched OFF is given by Eq. (3.8):

$$\Delta I_{L_{off}} = \int_{DT}^T \frac{(V_i - V_o)dt}{L} = \frac{(V_i - V_o)(1 - D)}{L} \quad (3.8)$$

To support the steady-state mode of the DC-DC convertor, the total rating value of the inductor current must be equal to zero, as given in Eq. (3.9).

$$\Delta I_{L_{on}} + \Delta I_{L_{off}} = 0 \quad (3.9)$$

Now, substituting Eq. (3.6) and Eq. (3.8) into Eq. (3.9) gives:

$$\frac{V_i D T}{L} + \frac{(V_i - V_o)(1 - D) T}{L} = 0 \quad (3.10)$$

This can be written as Eq. (3.11):

$$-V_i D = (V_i - V_o)(1 - D) \quad (3.11)$$

Now, the voltage gain of the circuit is given as in Eq. (3.12):

$$G_n = \frac{V_o}{V_i} = \frac{1}{(1 - D)} \quad (3.12)$$

Eq. (3.13) is used to determine the value of the inductor:

$$L = \frac{V_i D_{max}}{\Delta i_L f_s} \quad (3.13)$$

where,  $\Delta i_L$  is the ripple input current factor,  $f_s$  is the switching frequency and  $D_{max}$  is the duty cycle of the MPPT controller at the maximum power output of the PV source. While the input capacitor ( $C_1$ ) and the output capacitor ( $C_2$ ) are calculated based on Eqs. (3.14) and Eq. (3.15), respectively:

$$C_1 = \frac{D_{max}}{8L\Delta V_i f_s^2} \quad (3.14)$$

$$C_2 = \frac{D_{max}}{R\Delta V_o f_s} \quad (3.15)$$

where,  $\Delta V_i$  and  $\Delta V_o$  are the ripple input and output voltage factors, respectively, whilst  $R$  is the output resistance. Finally, the diode boost converter is selected regarding to its reverse rating current. This value should allow the input current to flow from the PV array to the load at the OFF-state. Hence, the forward current diode of the DC-DC converter should be equalled to the maximum current load of PV system. Figure 3.8. presents the waveform of a DC-DC boost converter under different states. As can be seen, the current of the inductor starts to increase from minimum to maximum value at the ON-state, otherwise, it begins to decrease from maximum to minimum value at the OFF-state.

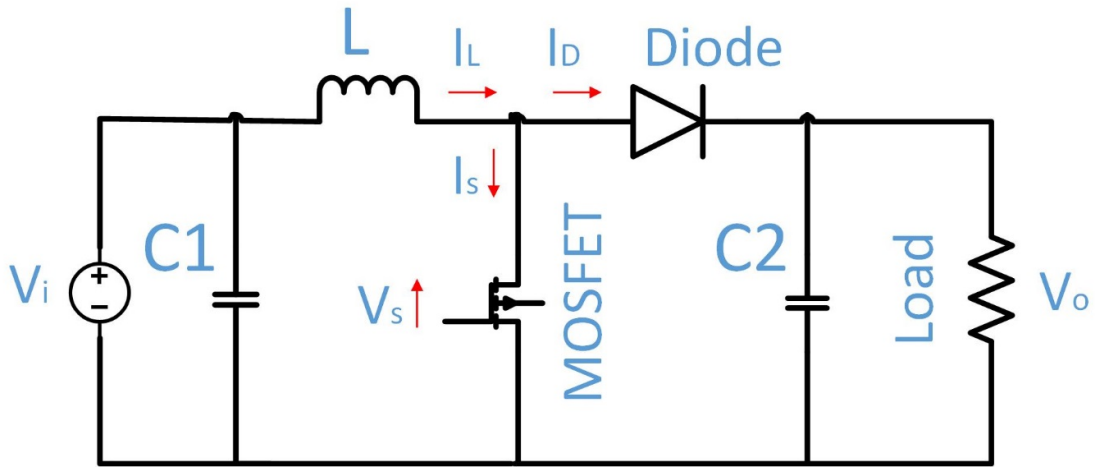


Figure 3.6. The circuit diagram of a DC-DC boost converter

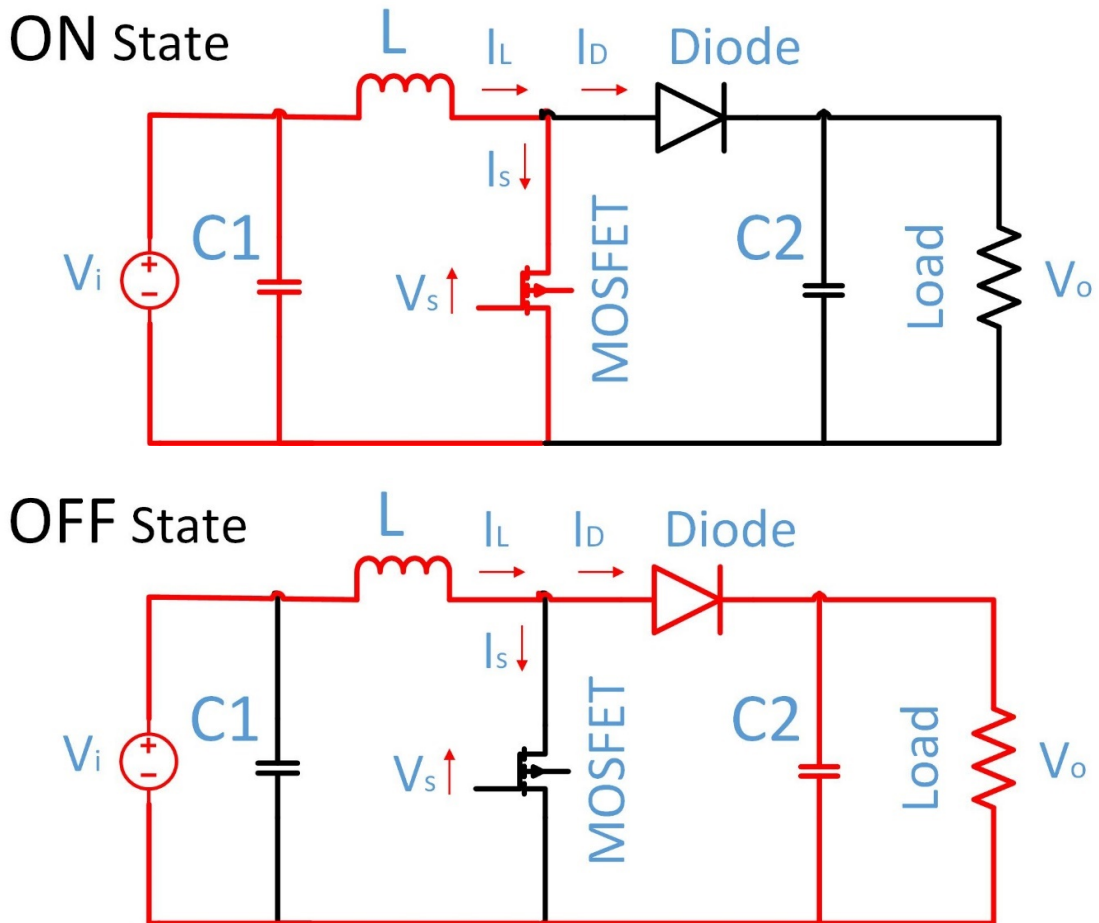


Figure 3.7. The state conditions of a DC-DC boost converter

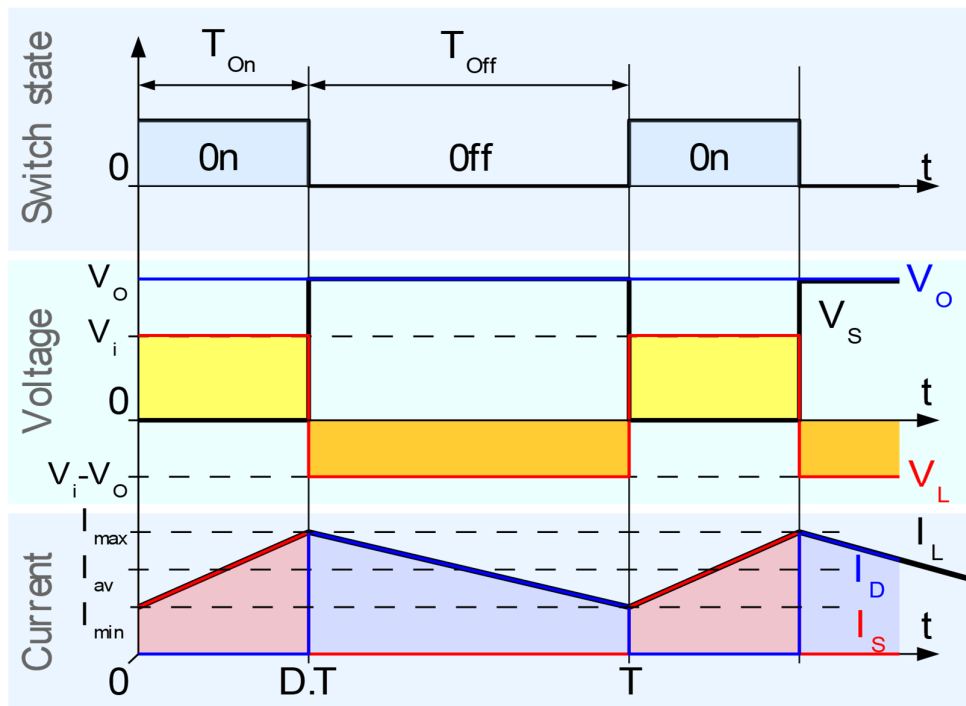


Figure 3.8. The waveform of a DC-DC boost converter [115]

### 3.4 Control Scheme of a PV System

As shown in Figure 3.3, there is a unique point on the P-V curve of a PV array recognised as the MPP, with its location shifting according to weather conditions. To track the MPP continuously, the MPPT technique is employed with the PV power conversion system and connected between the PV array and the load or grid. The principle work of this technique is that it feeds the appropriate duty cycle ( $D$ ) based on the output of the PV array in the form of the current and voltage and/or the inputs of solar irradiance and temperature to adjust the operation work of a PV power conversion system, thus resulting in high tracking power. This duty cycle is converted to a signal by pulse width modulation (PWM), as shown in Figure 3.9.

The PWM circuit compares the duty cycle signal with a sawtooth counter signal to generate the PWM pulse. If the sawtooth signal is less than the duty cycle signal, the output PWM signal is in the ON-state ( $T_{on}$ ), otherwise it is in the OFF-state ( $T_{off}$ ), as shown in Figure 3.10. This process is repeating so as to adjust the operating work of the PV array under varying weather conditions. The optimal duty cycle depends on the location of the operational MPP on the P-V curve. When the operating point is to the right, then the  $D$  will be increasing until it reaches to the MPP, otherwise it will be decreasing. To implement the MPPT algorithms, a microcontroller system is used. As mentioned in Chapter one, this power controller has several

advantages for a PV system, including: enhancing the efficiency of the PV array; improving the stability of PV generation; and increasing the reliability of the PV system [3] [116]. Whilst several techniques have been developed, the Perturb and Observe (P&O) algorithm is widely used for MPPT due to its low cost and simple implementation. However, the main drawbacks of this method are a long converging time, high oscillation around the maximum power point, and a drift problem associated with rapidly changing irradiance. In this chapter, a conventional P&O and modified P&O-MPPTs are proposed to model the PV system.

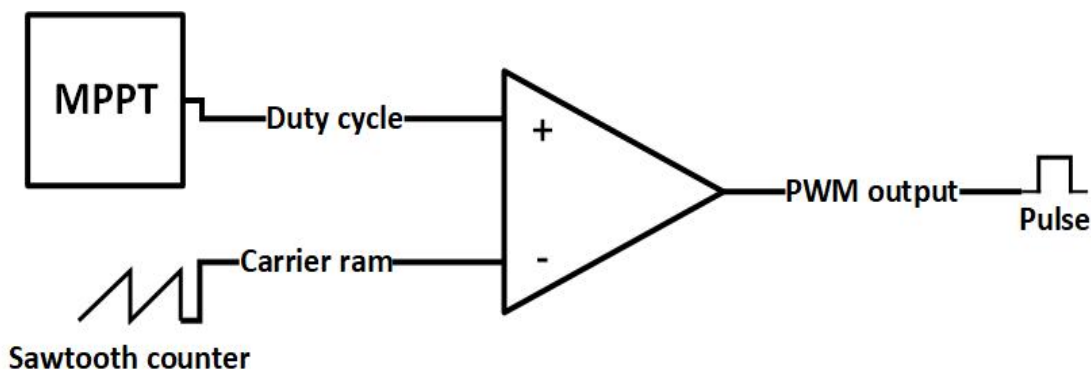


Figure 3.9. The control scheme of the PV system

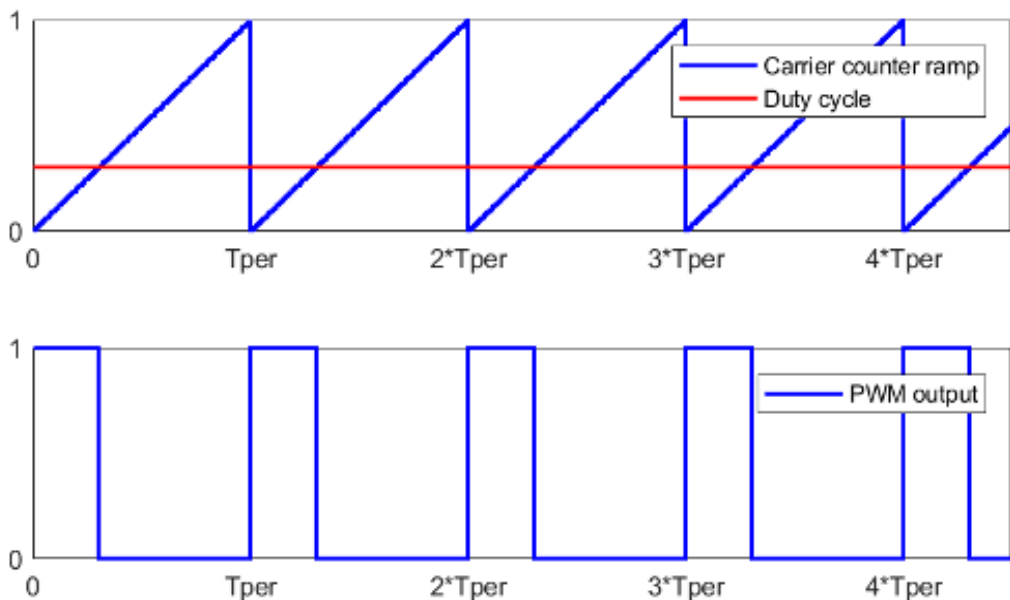


Figure 3.10. The waveform of an MPPT controller

### 3.5 P&O Algorithm

The P&O algorithm is widely used for PV-MPPT techniques due to its low cost and simple implementation. As shown in Figure 3.11, the principle work of this method depends on calculating the PV power by using the sensed values of the voltage and current PV array. Then, these are compared with the previous power to address the direction of the P&O algorithm and subsequently, updating the duty cycle ( $D$ ) of the DC-DC converter, according to Eq. (3.16):

$$D(k + 1) = D(k) \pm \Delta D \tag{3.16}$$

where,  $D(k+1)$  and  $D(k)$  are the next and previous perturbations of  $D$ , respectively and  $\Delta D$  is the incremental step size of the reference  $D$ . Basically, the operating point of the P&O algorithm moves in the same direction when the voltage and power of the PV array increase due to increasing  $D$ ; otherwise it moves in the opposite direction. The process is continued until it reaches to the MPP and then, oscillates around it. The total properties of the P&O direction are explained in Table 3.2. In general, there are three major issues facing P&O-MPPT operation: long converged time, high oscillation around the MPP and a drift problem associated with rapidly changing irradiance.

These issues are explained as follows. Clearly, a large  $\Delta D$  leads to a fast steady-state and large fluctuation after reaching the MPP. Conversely, a small  $\Delta D$  results to a slow steady state and smooth fluctuations. According to this conception, the size of  $\Delta D$  is crucial for adjusting the system operation. Another drawback is the loss of the right direction of the MPPT tracker when weather conditions alter rapidly. This phenomenon can happen, as shown in Figure 3.12, when point **A** (low point), which represents the MPP at a low solar irradiance level is oscillated between **B** and **B'** and then, moves to point **C** or **D** (high point) due to rapidly increasing irradiance. As a result, the right direction of algorithm moves far away from the new MPP, according to the principle properties direction of the conventional P&O algorithm, as shown in Table 1. In other hands, this phenomenon happens in case of the increasing irradiance only [117].

**Table 3.2 The probabilities of direction for a P&O algorithm**

$\Delta P$	$\Delta V$	Direction of Perturbation
+	+	+
+	-	-
-	+	-
-	-	+

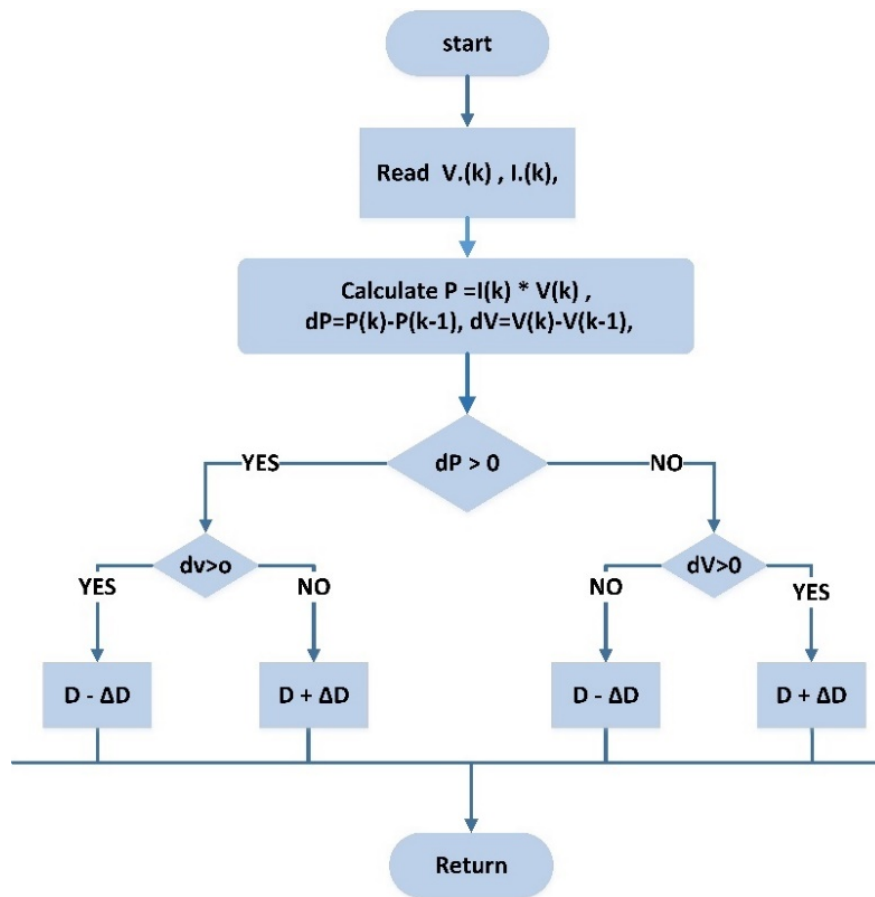
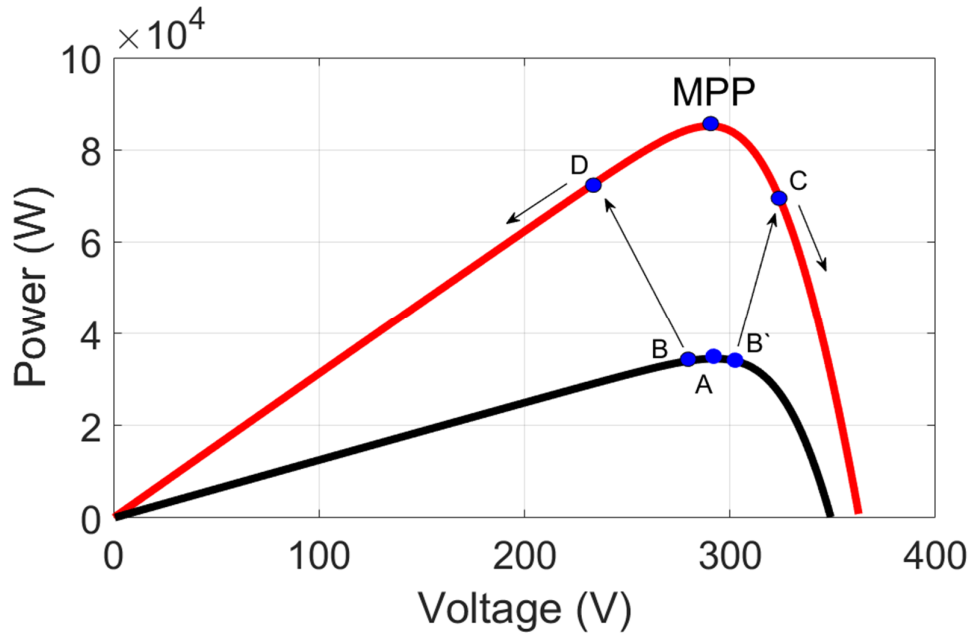


Figure 3.11. The flowchart of the conventional P&O algorithm [62]

To address those drawbacks, several modifications have been presented as state of the art. Among them, Yang and Zhao [118] suggested a variable step size (VSS) based on the power-voltage curve to adapt the P&O-MPPT tracker. Whilst this proposal reduces the oscillation around the MPP point and increases the speed of the MPPT tracker when the weather conditions change rapidly, the drift problem was not discussed. Similarly, Xiao and Dunford [68] adapted the conventional P&O-MPPT tracking based on the power-duty cycle curve in the form of a high robot to track the MPP. However, the drift problem is not eliminated completely when the solar irradiance changes suddenly. Sera et al. [119] added a new step for the P&O-MPPT algorithm based on the historical change in PV power ( $\Delta P$ ) to detect this deviation early, but this modification seems to be a non-optimal solution, because this threshold changes according to the weather conditions. Similarly, Killi and Samanta [69] added the historical change in the PV current ( $\Delta I$ ) as a step decision between the decision of positive historical change in power ( $\Delta P$ ) and positive historical change in voltage ( $\Delta V$ ). Whilst this modification

avoids the system drift problem, the proposal is not valid for the other side of the P&O algorithm, i.e. when the  $\Delta P$  and  $\Delta V$  exhibit negative historical changes. To solve the drift problem completely, Kollimalla et al. [120] designed the P&O-MPPT algorithm consisting of three stages to track all the properties for the diversion problem. However, the implementation of this is highly complex.



**Figure 3.12. P-V curve for a rapid irradiance change from A (low point) to D or C (high point), thus illustrating the drift problem**

### 3.6 Modified P&O-MPPT

The proposed modification is divided into two parts. The first involves developing a novel and simple VSS, which can improve tracking faster and reduce the oscillation around the MPP. This VSS is calculated according to Pythagorean theorem which proves that the square of the side opposite the right angle is equal to the sum of squares other two sides, as given in Eq. (3.17):

$$a^2 + b^2 = c^2 \tag{3.17}$$

where,  $c$  is the length of the hypotenuse and  $a$  and  $b$  are the lengths of the triangle's other two sides. This triangle is equal to the movement of  $\Delta P$  and  $\Delta V$  in P-V curve, as shown in Figure 3.13. This theorem is adopted to represent the VSS for P&O algorithm, as given in Eq. (3.18):

$$\Delta D_k = M \cdot \sqrt{\Delta P_k^2 + \Delta V_k^2} \quad (3.18)$$

where,  $\Delta P_k$  is the historical change in PV power,  $\Delta V_k$  is the historical change in PV voltage and  $M$  is a constant step size, which is adjusted according to the parameters of the PV system. The general tracking equation is now written as Eq. (3.19):

$$D_{k+1} = D_k \pm M \cdot \sqrt{\Delta P_k^2 + \Delta V_k^2} \quad (3.19)$$

This VSS is automatically tuned according to the operating point to enable a fast-tracking ability. If the operational point is far from the MPP, the historical change in PV power and voltage are large, but they become smaller when the operational point of PV system is at the MPP, as shown in Figure 3.13. Consequently, the proposed system increases the speed of the MPPT tracker when the weather conditions change rapidly and reduces the oscillation around the MPP at steady-state conditions.

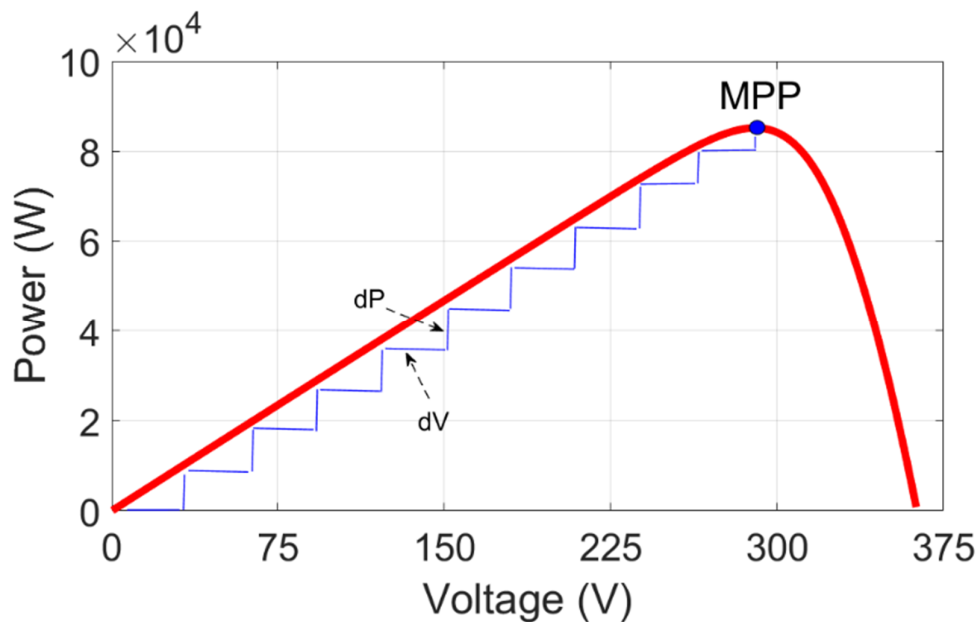


**Figure 3.13. P-V curve of the PV module illustrating the VSS**

The second part of this modification is adopted a new step decision for the conventional P&O algorithm to address the drift problem early. Basically, the drift problem happens when the solar irradiance on the PV array increases rapidly by at least  $10 \text{ W/m}^2/\text{s}$  [117]. The input of solar irradiance is divided into two types: slow change and fast change, as shown in Eqs. (3.20) and (3.21):

$$\Delta G < 10 \frac{W}{m^2} \quad \text{slow change} \quad (3.20)$$

$$\Delta G > 10 \frac{W}{m^2} \quad \text{fast change} \quad (3.21)$$

where,  $\Delta G$  is the historical change in the solar irradiance. The standard test condition of solar irradiance  $G_{STC}$  is  $1000 \text{ W/m}^2$ . Now, the following is obtained:

$$\frac{\Delta G}{G} < 0.01 \quad \text{slow change} \quad (3.22)$$

$$\frac{\Delta G}{G} > 0.01 \quad \text{fast change} \quad (3.23)$$

As proven in [71], the normalised change in power is equal to the normalised change in solar irradiance, as shown in Eq. (3.24):

$$\frac{\Delta P}{P} = \frac{\Delta G}{G} \quad (3.24)$$

Substituting Eqs. (3.22) and (3.23) into Eq. (3.24) gives:

$$\frac{\Delta P}{P} < 0.01 \quad \text{slow change} \quad (3.25)$$

$$\frac{\Delta P}{P} > 0.01 \quad \text{fast change} \quad (3.26)$$

where,  $\Delta P$  is the historical change in PV power and  $P$  is its previous iteration. If the value of  $P$  changes due to the changing irradiance, the value of  $\Delta P$  also changes in the same direction. Consequently, the value of  $\Delta P/P$  is almost constant during different environmental conditions. In addition, this value is positive when the operation point is on the drift issue state, otherwise it has a negative value. A constant value ( $C = 0.01$ ) is added in the start of the program to address the drift problem early, as shown in Figure 3.14, which illustrates the flow chart of the proposed algorithm. If  $\Delta P/P$  is less than  $C$ , it will recognise that the solar irradiance on the PV array is changing slowly and the P&O algorithm should be processed at this operating point, otherwise a constant voltage (CV) algorithm processes it.

The CV-MPPT assumes that the irradiance level and temperature operation variations on the PV array are insignificant, and the constant reference voltage approximates to the real MPP voltage [57]. The MPP voltage is calculated at nearly 78% of the open voltage ( $V_{oc}$ ) under varying weather conditions [121]. Hence, the  $V_{set}$  is applied as  $0.76 V_{oc}$  to enable the proposed algorithm to ascertain the side of operating point after the solar irradiance changes rapidly. If the PV voltage is higher than  $V_{set}$ , the operation point is on the right of the MPP, resulting in

decreasing the D reference, otherwise, the D reference is increasing and when operation point is close to MPP, the C becomes very tiny. Consequently, the control unit switches into the conventional P&O algorithm to establish the exact optimal MPP.

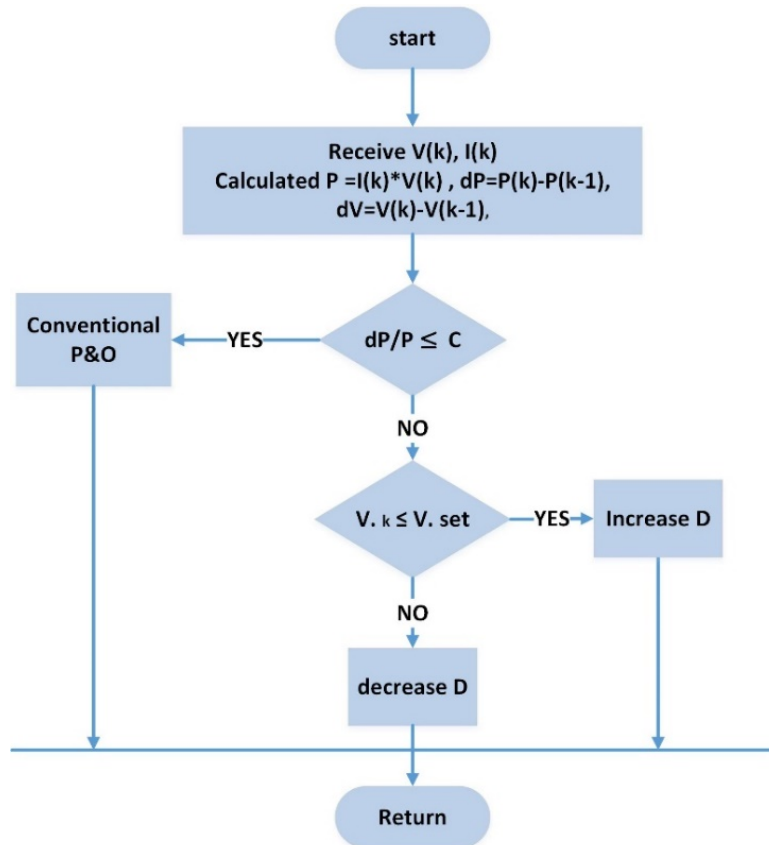


Figure 3.14. The flowchart of the modified P&O-MPPT method

### 3.7 Simulation Results

To test the performance of the MPPT method, a MATLAB-SIMULINK model for a grid-connected PV system was developed. This grid-connected PV system consists of a PV array, DC–DC boost converter with MPPT controller, DC-AC inverter and utility grid, as shown in Figure 3.15. The parameters of the PV array used in this simulation are 321 V open-circuit voltage, 273.5 V maximum power voltage, 393.3 A short-circuit current and 368.3 A maximum power current. Whilst the parameters of the DC-DC boost converter are a 5mH inductor, 100  $\mu$ F input capacitor and 24000  $\mu$ F output capacitor, which are calculated according to Eqs. (3.13), (3.14) and (3.15), respectively. The reverse current diode of the DC-DC converter is chosen at 400 A to allow for maximum output current of the PV array to flow from to the load at the OFF-state. The switching frequency of MOSTFET is selected at 5 kHz, with the updating

time of the MPPT controller being every  $500\mu\text{s}$ . The type of PV module used in this simulation is SunPower SPR-305-WHT and the main parameters of this are provided in Table 3.1. The DC-DC converter amplifies the PV voltage to 500 V DC, which is then converted to 260 V AC with the unity power factor in the DC-AC inverter. In the utility grid, this AC voltage relates to a 10 kV-medium voltage distribution network by a 260 V/15 kV-100 kVA transformer.

The simulations were configured under exactly the same parameters as for conventional P&O and modified P&O-MPPTs as well as without the MPPT state. The simulation was divided into two scenarios. First, the PV system with and without P&O-MPPT controller was simulated. As shown in Figure 3.16, the solar irradiance of weather conditions was kept at a constant value of  $1,000 \text{ W/m}^2$ . As shown in Figure 3.17, the output power of the PV system with the MPPT controller was higher than without MPPT controller, at about 100 kW and 80 kW, respectively. This is because the MPPT controller tracks the MPP of the PV array accurately.

In the second scenario, the modified P&O and conventional P&O algorithms were simulated. The input of solar irradiance used in this simulation decreased rapidly from 1,000 to  $400 \text{ W/m}^2$  from 0.5 to 1 s, and then increased rapidly from 400 to  $1,000 \text{ W/m}^2$  from 1.5 to 2 s, as shown in Figure 3.18. The temperature operation was kept at a constant value of  $25^\circ\text{C}$ . As shown in Figure 3.19, the tracking power of the conventional P&O-MPPT method ascertains the right direction of the input solar irradiance when it decreases. However, it loses it when the irradiance increases rapidly. However, the modified P&O-MPPT method avoids the drift problem under different changes (increasing and decreasing of the input of solar irradiance). As a result, it takes a shorter time to address the drift problem than with the conventional P&O method.

In addition, the PV voltage of the proposed method has a smooth oscillation around the MPP at steady-state conditions compared to the conventional P&O-MPPT due to its VSS, as shown in the zoomed in part of Figure 3.19(b). Consequently, the disputed power is higher in the conventional P&O-MPPT than with the modified P&O-MPPT. The resulting output power of the conventional P&O-MPPT and the proposed method at steady-state conditions are 100.722 kW and 100.724 kW, respectively, as shown in the zoomed in part of Figure 3.19(a). According to the simulation results, the modified P&O-MPPT method quickly tracks the MPP during weather condition changes and reduces the oscillation around the MPP under steady-state conditions. In addition, the output PV power is higher compared to the conventional P&O-MPPT. However, it does not avoid the drift problem completely when the weather conditions

vary rapidly. This is because the threshold of the early step decision, which is designed to address the drift problem, changes in regard to weather conditions.

To prove the effectiveness of the MPPT controller on the grid-connected PV system, the output of the DC-DC converter was simulated before and after the weather conditions changed. As shown in the zoomed in area in Figure 3.20 (a), the output voltage of the DC-DC boost converter for the conventional P&O-MPPT and modified P&O-MPPT methods are stable during the rapid decrease in weather conditions. However, it drifts away to the right of the MPP for the conventional P&O-MPPT controller when the weather conditions suddenly change, while the modified P&O-MPPT technique is almost stable, as shown in the zoomed in area in Figure 3.20(b). However, the grid-connected PV systems based on the conventional P&O and modified P&O algorithms deliver fluctuating DC voltage during rapidly changing weather conditions, because they do not avoid the drift problem completely.

### 3.8 Summary

In this chapter, the modelling and control of a PV system have been presented. To sum up, the modelling of a PV cell has been proposed, the main structure of a PV system has been explained and its control scheme described. The conventional P&O-MPPT and the modified P&O-MPPT have been discussed, with the simulation results being provided and compared. Generally, using the MPPT with a PV system is important for enhancing the tracking efficiency, stability, reliability and quality of the output system under different climatic conditions. The modified P&O-MPPT based on Pythagorean theorem and CV-MPPT has been shown to addresses the main issues of the conventional P&O algorithm. However, this modification does not avoid the drift problem or eliminate oscillation completely.

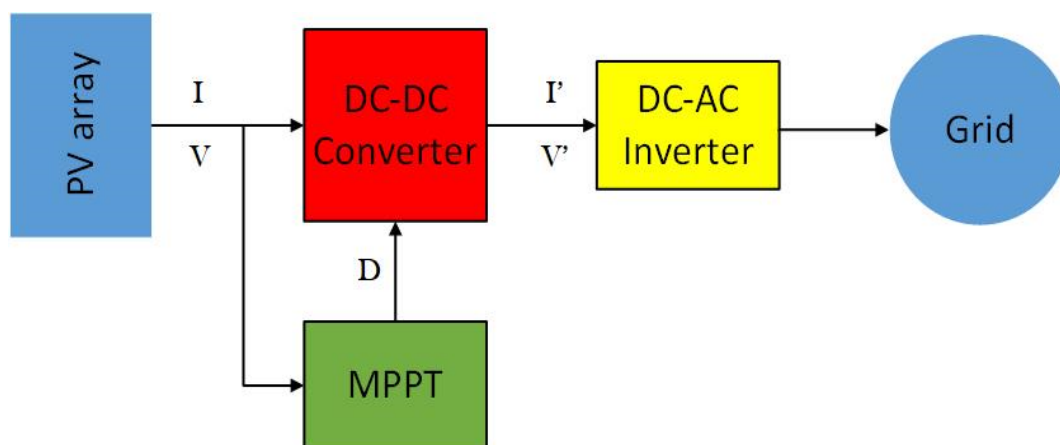


Figure 3.15. The general diagram of a grid-connected PV system

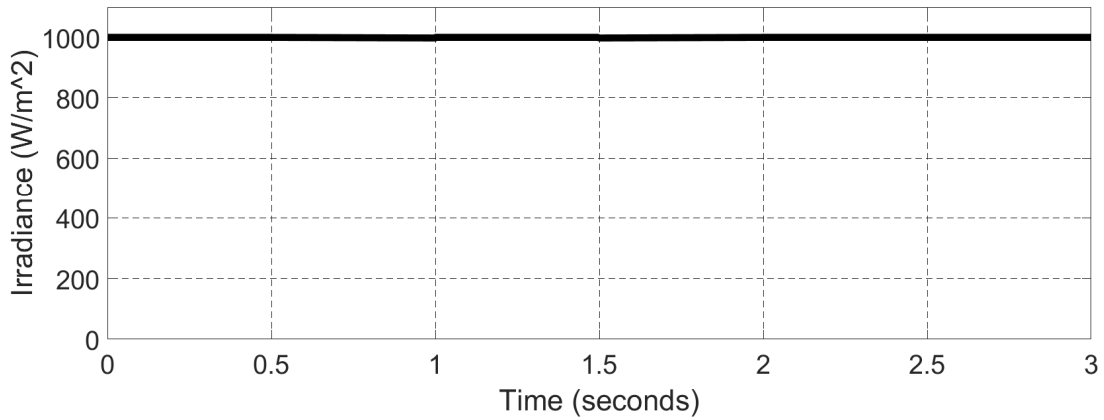


Figure 3.16. The input irradiance under constant conditions

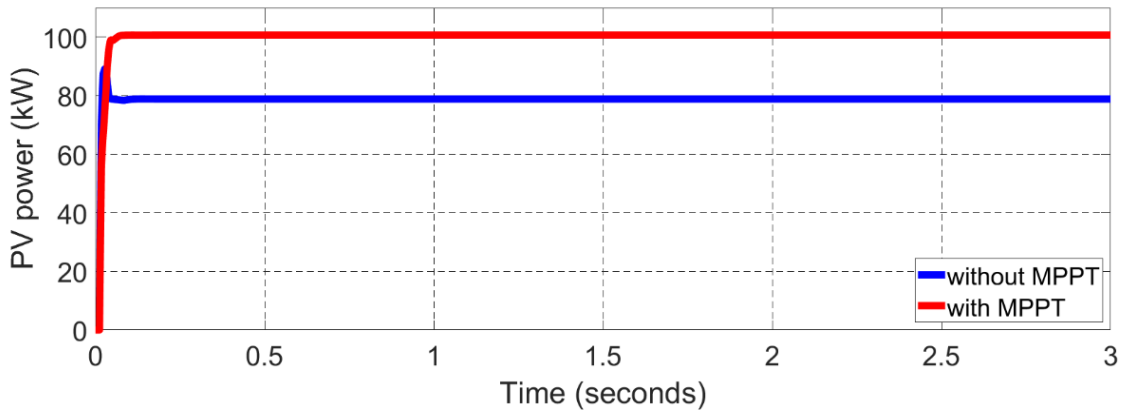


Figure 3.17. The output power of a PV array without MPPT versus with MPPT

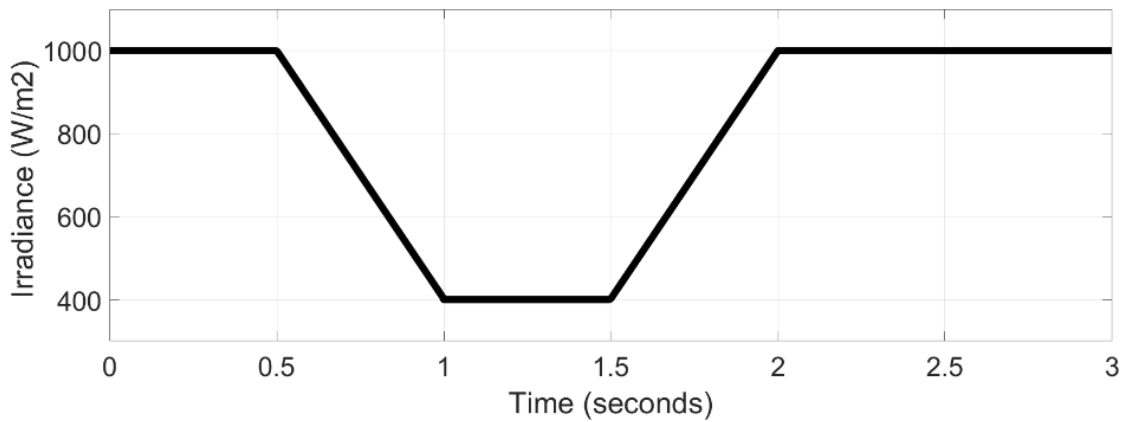
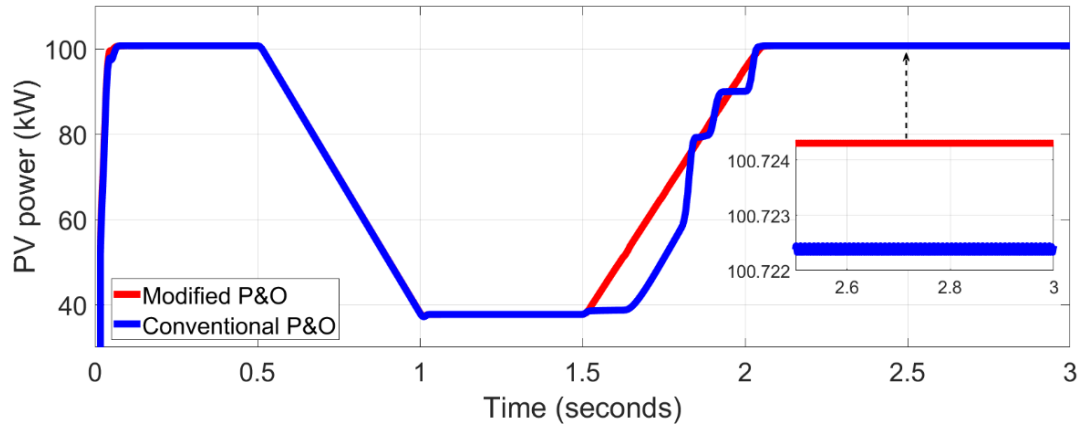
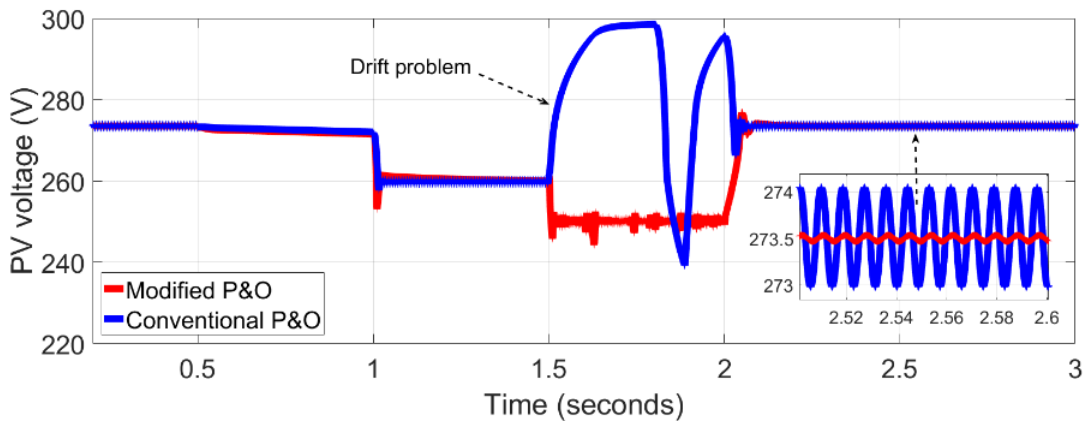


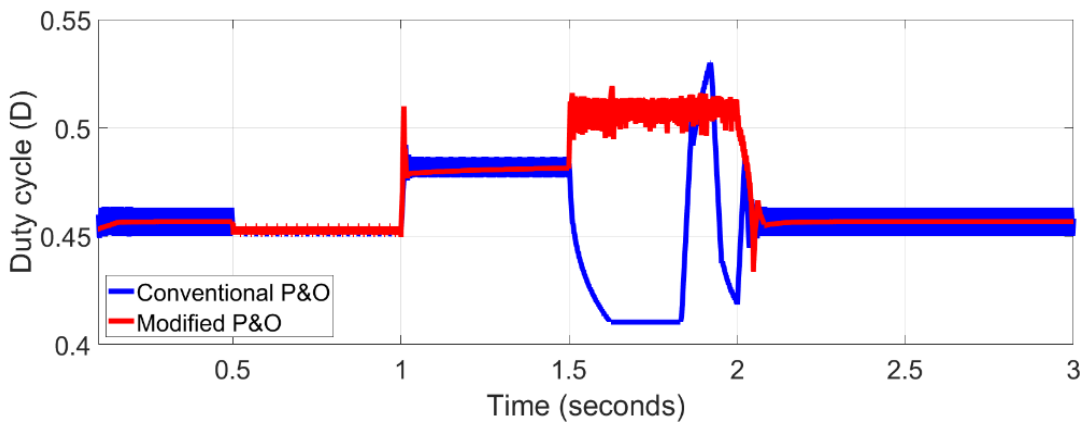
Figure 3.18. The input of input solar irradiance with varying conditions



(a)

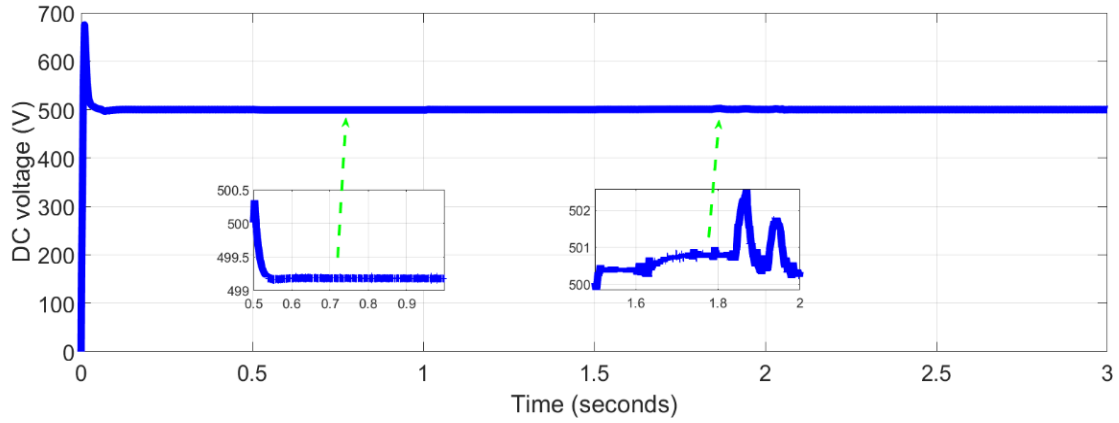


(b)

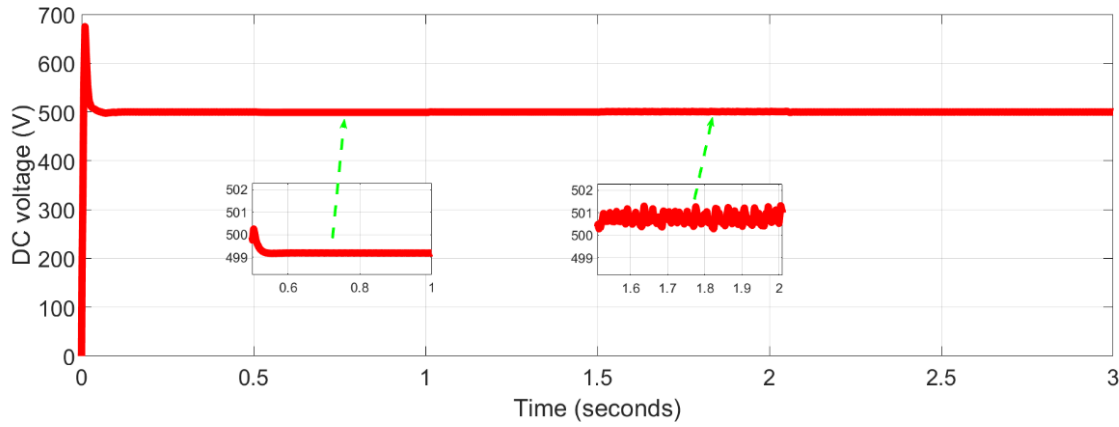


(c)

**Figure 3.19. PV array output for the modified VS conventional P&O method under a theoretically rapid change in solar irradiance: (a) power, (b) voltage, and (c) duty cycle**



(a)



(b)

**Figure 3.20. The DC voltage of a grid-connected PV system using (a) the conventional P&O-MPPT and (b) modified P&O-MP**

## Chapter 4

### Proposed MPPT Based on Fuzzy Logic Control

Fuzzy logic control (FLC) is common technique that achieves vastly improved performance for MPPT technique in terms of response speed and low fluctuation about the maximum power point. However, major issues of the conventional FLC-MPPT are a drift problem associated with changing irradiance and complex implementation when compared with the P&O-MPPT. In this Chapter, a proposed MPPT technique based on FLC and P&O algorithm is presented. The proposed method incorporates the advantages of the P&O-MPPT to account for slow and fast changes in solar irradiance and the reduced processing time for the FLC-MPPT to address complex engineering problems when the membership functions are few. To evaluate the performance, the P&O-MPPT, FLC-MPPT and the proposed method are simulated by a MATLAB-SIMULINK model for a grid-connected PV system. The EN50530 standard test is used to calculate the average tracking efficiency of the proposed method under varying weather conditions.

#### 4.1 Introduction

As mentioned in Chapter 2, the P&O-MPPT is a popular method for PV-MPPT owing to its low cost and simple implementation. However, it poses many challenges, such as a lower converging speed, high oscillation around a maximum power point MPP, and a drift problem associated with rapidly changing irradiance [63]. Several modifications have been introduced based on a Power–Voltage (P-V) curve, but they are considered as insufficient solutions for addressing all of these problems. Consequently, artificial intelligence techniques based on MPPT have been proposed to solve the significant problems of the classical MPPT methods [122]. In addition, these techniques do not need accurate parameters or complex mathematics when managing the system [55]. In particular, the FLC-MPPT technique is one of the most

powerful controllers for a PV system due to its high converging speed and low fluctuation around the MPP [76], [123]. Moreover, it does not require training data, thus resulting in its working for various types of PV module with the same MPPT design. However, the main disadvantages are the aforementioned drift problem associated with changing irradiance and complex implementation when compared with the classical MPPT methods[124], [125].

Several types of modifications have been proposed to address those issues. Among them, Soufi et al. [80] used a particle swarm optimisation (PSO) algorithm to adjust the duty cycle of the boost convertor in the right direction for conventional FLC-MPPT when the input solar irradiance changes rapidly. In [81], Guenounou et al. designed a gain controller based on the FLC approach for online adapting of the step size of conventional FLC-MPPT. In [126], Alajmi et al. developed a novel FLC-MPPT based on a hill climbing algorithm for a stand-alone PV system. Harrag and Messalti in [127] presented an improved maximum power point tracking technique using the Fuzzy-IC algorithm for a PV array and fuel cells. Kottas et al. [128] improved the conventional FLC-MPPT method by adding fuzzy cognitive networks. Whilst these proposals reduce the oscillations around the MPP and avoid the drift problem during changing irradiance, their hardware implementation becomes more complex due to an additional step control unit.

Hence, Obeidi et al. [82] used a genetic algorithm (GA) algorithm to optimise the designed membership functions of the conventional FLC-MPPT controller for which the fuzzy base had already been created. Similarity, Gupta and Garg [79] presented maximum power point tracking based on an asymmetrical fuzzy functions process to minimise the longer processing time of conventional FLC-MPPT. With the same idea, S. ali Blaifi et al. [83] presented maximum power point tracking by modelling the fuzzy logic algorithm using an M5P model tree. In [84], Subiyanto et al. used a Hopfield NN to tune the designed membership functions of FL-MPPT automatically, instead of adopting the trial-and-error approach. Similarity, Nabipour et al. [85] designed improved maximum power point tracking based on an indirect fuzzy for PV systems. The results in [79], [82]–[85] report that the optimised fuzzy controller achieved improved performances, fast responses with less oscillations as well as avoiding the drift problem. However, the implementation of all these methods is more complex than for the classical MPPT techniques.

In this Chapter, a proposed FLC-MPPT technique based on a modified P&O algorithm is designed. The proposed design takes into account two key issues. First, whilst the conventional

P&O-MPPT is a suitable method for the PV system under a slow change of irradiance, it faces significant challenges under a fast one. The second issue is that the complex engineering problems of a fuzzy system become diminished when the designed membership functions are few. The general diagram of a grid-connected PV system based on the FLC-MPPT is presented in Figure 4.1. The fuzzy rules of the proposed method are obtained from a modified P&O-MPPT algorithm. The proposed technique accurately tracks the maximum power point and avoids the drift problem under different states. Moreover, our simplified FLC-MPPT method, when applied to a grid-connected PV system, achieved efficiencies greater than 99.6% under the EN50530 standard test. The rest of this Chapter is organised as follows. Section 4.2 analyses the fuzzy logic control system. Section 4.3 discusses the principle work of the conventional FLC-MPPT method. In Section 4.4, the proposed method is presented, whilst the simulated results are provided and discussed in Section 4.5. The EN50530 standard test results for comparative analyses are provided in Section 4.6. Finally, Section 4.7 covers the summary of this Chapter.

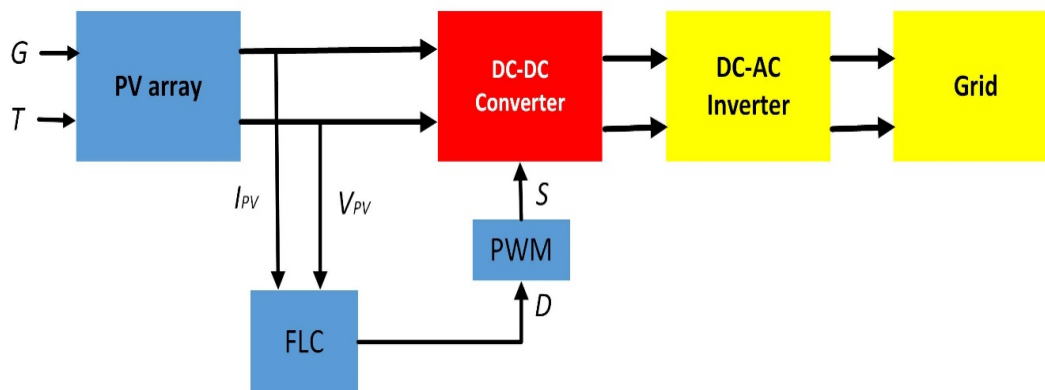


**Figure 4.1. The general diagram of a grid-connected PV system based on the FLC-MPPT.**

## 4.2 Fuzzy Logic Control

Fuzzy logic control is considered an important technique in industrial engineering application because it has a high ability to work with nonlinear system [129]. It deals with imprecise and noisy input information based on a mathematical model in order to imitate human-like decisions in control implementation [130]. This technique supports two types of fuzzy software system; Mamdani and Sugeno. In this Chapter, fuzzy Mamdani system is used because it has a higher ability to adapt a fuzzy rule application based on a human expert knowledge [131]. The main structure of FLC includes three stages: fuzzification, fuzzy rules

and defuzzification [132]. A general block diagram of the FLC technique is shown in Figure 4.2.

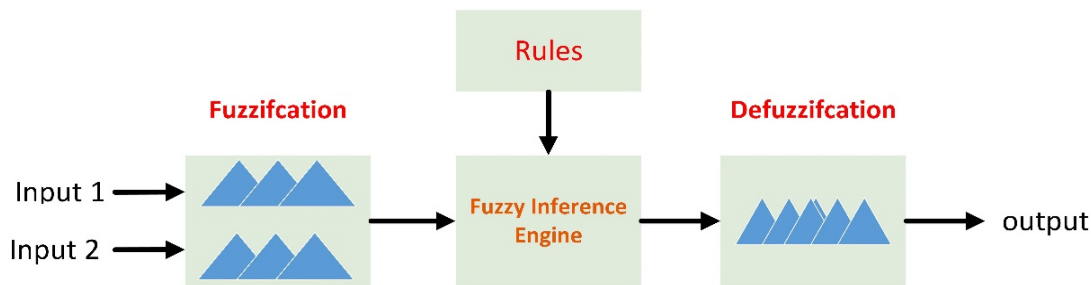


Figure 4.2. General diagram of fuzzy logic system.

### 4.2.1 Fuzzification

In fuzzification stage, the input variables are converted into linguistic variables based on many defined membership functions (MFs) such as a triangular, trapezoidal, Gaussian, bell-shaped, sigmoidal or (S-curve) with subset degree between 0 to 1, as shown in Figure 4.3. Each type has advantages and disadvantages. However, the trapezoidal MFs and triangular MFs are commonly used because they have a high dynamic variation in short processing time [133]. The quantity of those MFs is also an important aspect of the design as it determines the speed and accuracy of the FLC system [134].

If the system has more membership functions. The implementation problem becomes over complex, resulting in an accurate system but with an excessive processing time. In contrast, if the system has few membership functions, then it is too simple and whilst there is a faster processing system time and there is a high acceptable diversity of outcomes. As well as, selecting a discourse range of those MFs is an important feature to optimise this technique. The discourse range of the MFs is determined regarding to a limited operating work of application system.

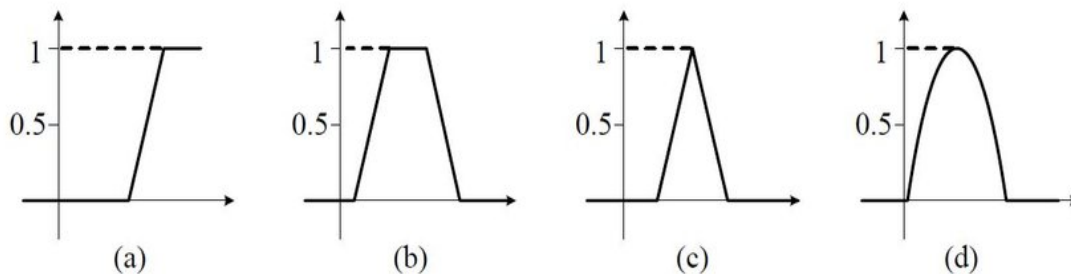


Figure 4.3. Various types of defined membership functions (a) monotonic (b) trapezoidal (d) triangular (c) Gaussian.

### 4.2.2 Fuzzy Rules

In fuzzy rule stage, these linguistics variables get manipulated, according to rules based on the “if–then” concept that are guided by the desired behaviour of the system. The operator who has familiar with the application system designs those fuzzy rules. After the fuzzy rules generate, The AND or OR fuzzy operators are used to adjust the subset degree of MFs. While the clipping technique is utilised to regulate the rule base with the accurate value of the rule antecedent.

### 4.2.3 Defuzzification

The last stage of the FLC is the reverse of fuzzification process which it converts the linguistic variables into numerical variables using the output of MFs. There are three defuzzification technique; Mean of maximum method, Height method and Centre of gravity method (COG). However, the latter method is the most common used because its defuzzified value is very smooth when compared with other methods [135]. The centroid defuzzification algorithm is applied to perform those functions based on the centred gravity of the defined membership functions. The output of this method is determined as shown in Eq. (4.1)

$$COG = \frac{\sum_i^n W_i C_i}{\sum_i^n W_i} \quad (4.1)$$

where  $W_i$  is the firing strength of the  $i^{\text{th}}$  rule and  $C_i$  is the centre value of the output membership functions.

### 4.3 Conventional FLC-MPPT

Nowadays, FLC based on an MPPT technique has become a popular method for PV systems [124]. Usually, the conventional FLC- MPPT has two inputs and one output, as shown in Eqs. (4.2) and (4.3) [136]:

$$e(k) = \frac{\Delta P}{\Delta V} = \frac{P_{(k)} - P_{(k-1)}}{V_{(k)} - V_{(k-1)}} \quad (4.2)$$

$$\Delta e = e_{(k)} - e_{(k-1)} \quad (4.3)$$

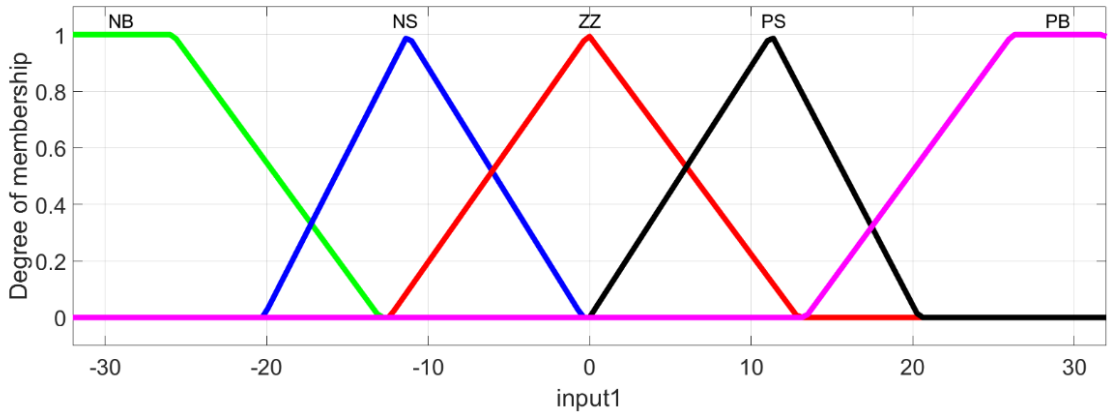
where  $e(k)$  is the change of slop P-V curve, and  $\Delta e$  is the change in its value of slop P-V curve. The output is the change of duty cycle  $\Delta D$ , which adjusts the performance of DC-DC converter as through Eq. (4.4) [55]:

$$D(k + 1) = D(k) + \Delta D \quad (4.4)$$

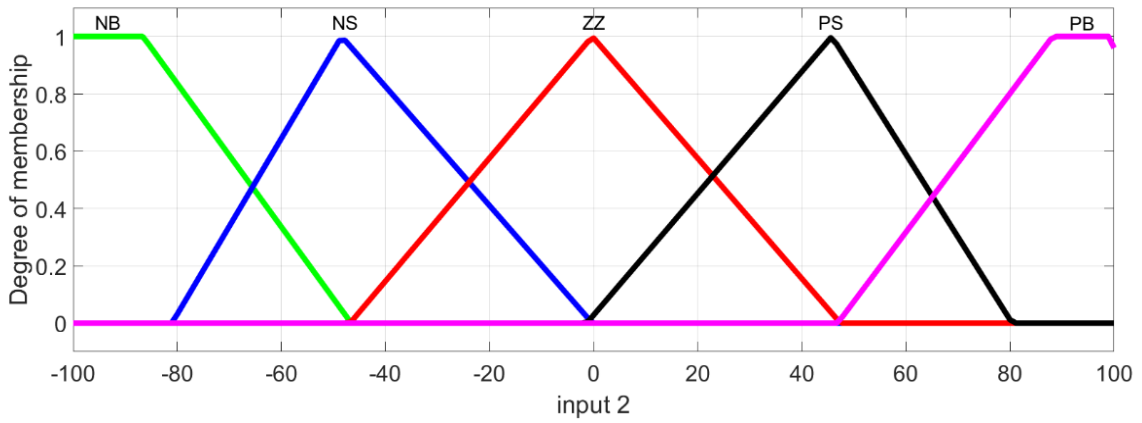
where  $D(k+1)$  and  $D(k)$  are the next and previous iteration for the duty cycle respectively, and  $\Delta D$  its incremental increase, which is the output of the fuzzy controller. The work of the conventional FLC-MPPT is to examine the first input, if this value is greater than zero the incremental change of the duty cycle increases until the MPP is reached, whereas if it is less than zero then the opposite occurs until the optimal value is reached. The second input is then used to reduce the oscillation in the duty cycle effectively. The quantity of membership functions of the conventional FLC-MPPT method is divided into five values: negative big (NB), negative small (NS), Z, Zero (ZZ), positive small (PS), and positive big (PB), as shown in Figure 4.4. For example, if the value of the error is NB and changing error also negative big PB, the predefined rules assign the next variable duty cycle as ZZ, with process continuing until the optimal MPP is reached. All the rules of the conventional FLC-MPPT algorithm as well as its 3D surface are provided in Table 4.1 and Figure 4.5, respectively.

In general, FLC-MPPT is considered one of the most efficient controllers for a PV system due to its smooth fluctuation, and high accuracy in reaching the MPP. In addition, as mentioned earlier, it does not require training data and thus works on different types of PV module the same MPPT design. In other words, it needs a comprehensive study about the PV system operation to design an accurate controller. Moreover, implementation of this method is complex compared with the classical MPPT methods.

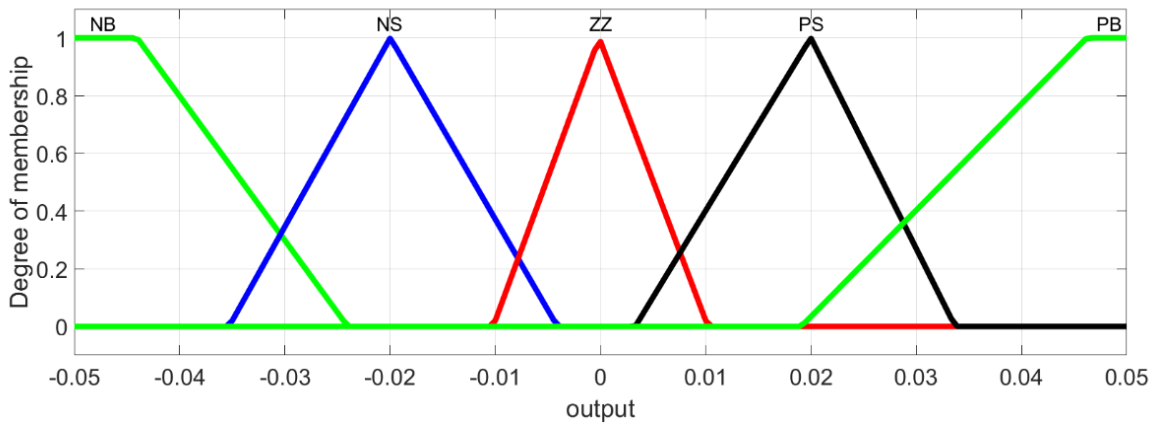
The main challenge of this method is the drift phenomenon which happens when weather conditions change, which Figure 4.6 explains it. If Point **A** (low point), which represents the MPP at a low solar irradiance level is moving to **B** (high point) due to a rapid increase in solar irradiance, the right direction of the fuzzy tracker is moving far away from the new MPP, according to the rule base of the conventional FLC-MPPT algorithm, as show in Table 4.1. To solve this issue. Many modifications have been proposed, such as an adaptive and optimised membership function of the conventional FLC-MPPT algorithm. However, in this case the implementation becomes much more complex.



(a)



(b)



(c)

Figure 4.4. The defined membership functions of a conventional FLC-MPPT: (a) input1 ( $e$ ); (b) input 2 ( $\Delta e$ ); and (c) output ( $\Delta D$ ).

**Table 4.1. The fuzzy rules that are used in the conventional FLC-MPPT.**

$\Delta e$	E				
	NB	NS	ZZ	PS	PB
NB	ZZ	ZZ	NB	NB	NB
NS	ZZ	ZZ	NS	NS	NS
ZZ	NS	ZZ	ZZ	ZZ	PS
PS	PS	PS	PS	ZZ	ZZ
PB	PB	PB	PB	ZZ	ZZ

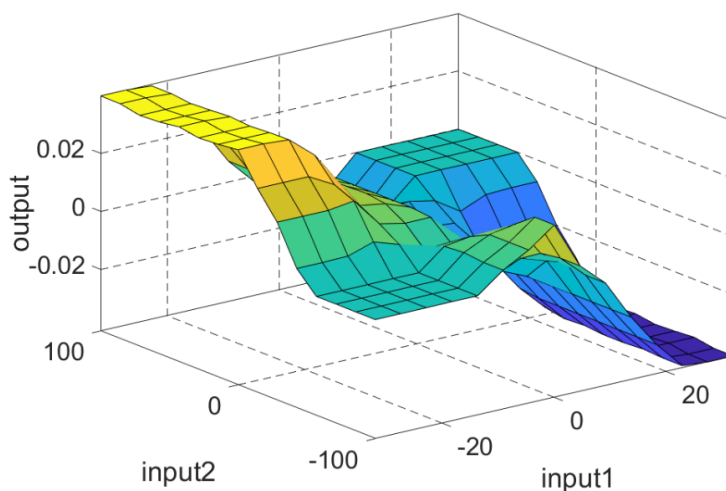


**Figure 4.5. A 3D surface between input1 (e) and input2 ( $\Delta e$ ) verse output ( $\Delta D$ ).**

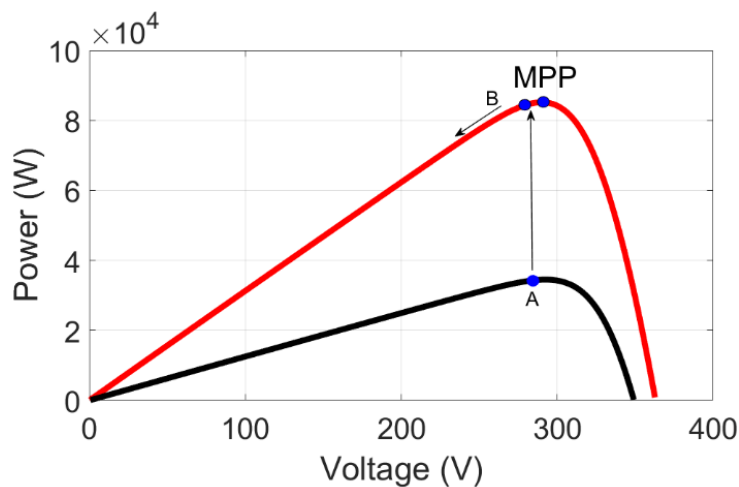


**Figure 4.6. P-V curve for a rapid irradiance change from A (low point) to B (high point), thus illustrating the drift problem in the FL-MPPT algorithm.**

#### 4.4 Proposed Method

The proposed method is designed to incorporate the advantages of the FLC-MPPT method and P&O-MPPT algorithm, whilst eliminating their drawbacks. As mentioned in Chapter 3, the P&O algorithm is a suitable method for a PV-MPPT system when solar irradiance changes slowly from 1 to 10 W/m<sup>2</sup>/s. However, this method is flawed when the changing irradiance is quicker than this. Therefore, the normalised change in the applying solar irradiance regarding to the normalised change in the output power of PV array is classified into two major types: fast change and slow change presented in Chapter 3. This concept is given by Eqs (4.5) and (4.6):

$$\frac{\Delta G}{G} = \frac{\Delta P}{P} \geq 0.01 \quad \text{fast change} \quad (4.5)$$

$$\frac{\Delta G}{G} = \frac{\Delta P}{P} < 0.01 \quad \text{slow change} \quad (4.6)$$

where  $\Delta P$  is the historical change in PV power and  $P$  is the previous iteration for PV power. If the value of  $P$  is changed due to a solar irradiance change, the value of  $\Delta P$  also changes in the same direction. Consequently, the value of  $\frac{\Delta P}{P}$  is almost constant during varying weather conditions. In addition, this value is positive when the operation point is on the drift issue, as mentioned in Chapter 3. The value is used in the fuzzy rules to detect the drift problem early. Defining the input and output of membership functions is considered an important step in the fuzzy logic design [137] and those for the proposed system are selected as following Eqs (4.7) and (4.8):

$$\frac{\Delta P}{\Delta V} = \frac{P_{(k)} - P_{(k-1)}}{V_{(k)} - V_{(k-1)}} \quad (4.7)$$

$$\frac{\Delta P}{P} = \frac{P_{(k)} - P_{(k-1)}}{P_{(k-1)}} \quad (4.8)$$

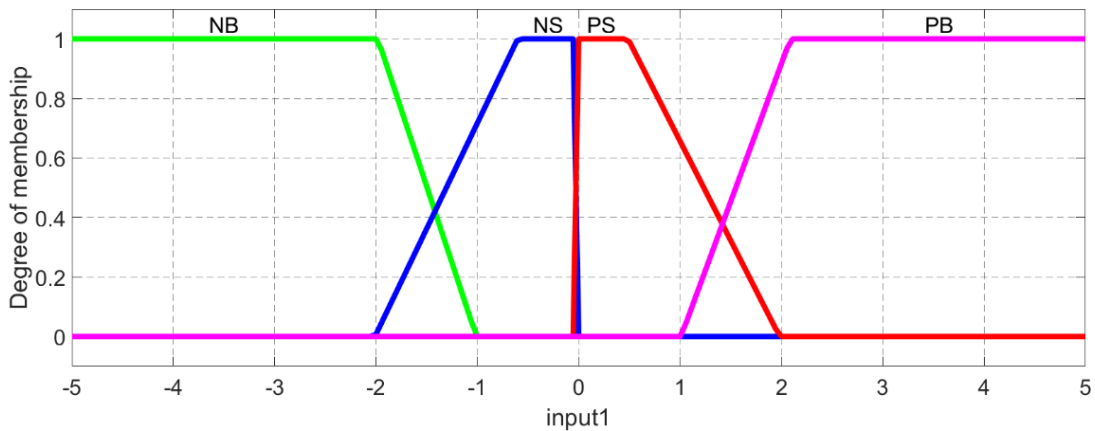
where Eq. (4.7) represents the historical change in PV power relative to the historical change in PV voltage, whilst Eq. (4.8) pertains to the historical change in PV power relative to the previous iteration for it and the output of proposed fuzzy system is determined as in Eq. (4.4). The principle work of this proposal is to examine the first input. If this value is greater than zero the incremental change of the duty cycle increases until the MPP is reached, whilst if it is less

than zero the opposite occurs also until the optimal value is reached. While the second input is then used to address the drift problem. The variable inputs and output are divided into four fuzzy subsets: positive big (PB), positive small (PS), negative big (NB), and negative small (NS), as shown in Figure 4.7. The variable second input ( $\Delta P/P$ ) is adjusted according to Eqs. (4.5) and (4.6). The fuzzy rules of the proposed system are based on the P&O-MPPT algorithm, with there being a total of 16. If the value of ( $\Delta P/\Delta V$ ) is NB and ( $\Delta P/P$ ) is also NB, then so too is the duty cycle is NB. The process is continued until the optimal MPP is reached. To avoid the drift problem associated with positive fast change in solar irradiance, the fuzzy rules are changed in a reverse direction when ( $\Delta P/P$ ) > 0.01, which is equal to the PB in the second input. All the fuzzy rules of the proposed MPPT method, as well as its 3D surface are provided in Table 4.2, and Figure 4.8, respectively.

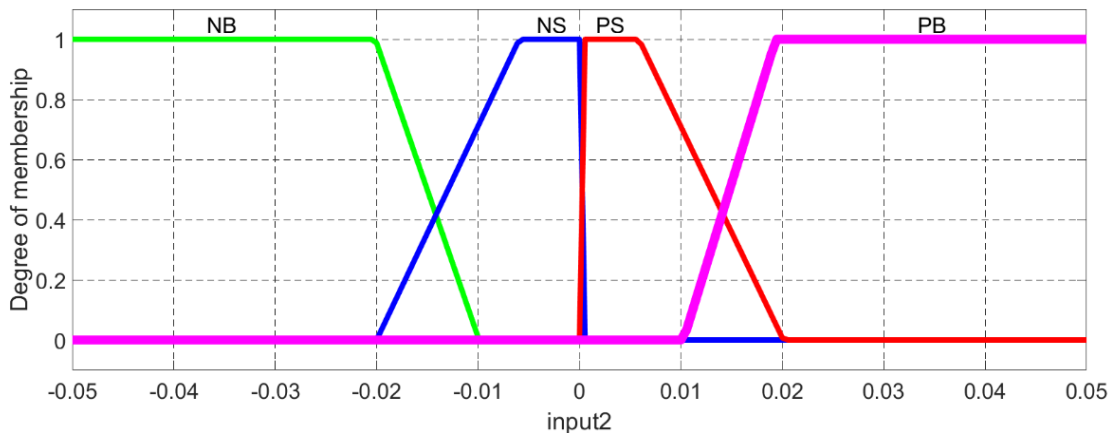
The output of proposed system is the variable duty cycle  $\Delta D$ , which is added to the previous iteration for the duty cycle, as show in Eq. (4.4). As a result, the step size of the duty cycle is large when the operational point is far from the MPP, and it automatically becomes tiny, when the operational point closes in on it. Consequently, the proposed system increases the speed of MPPT tracking when the weather conditions change rapidly. In addition, it reduces the oscillation around the MPP for steady-state conditions. Moreover, what is proposed is more accurate for addressing the new MPP when the irradiance changes owing to the adaptive rules of the fuzzy system according to weather conditions. Furthermore, the proposed system provides a lesser complex implementation, minimum processing time and more delivery when compared with the conventional FLC-MPPT method, because of its lesser number of fuzzy rules.

**Table 4.2. The fuzzy rules that are used in the proposed method.**

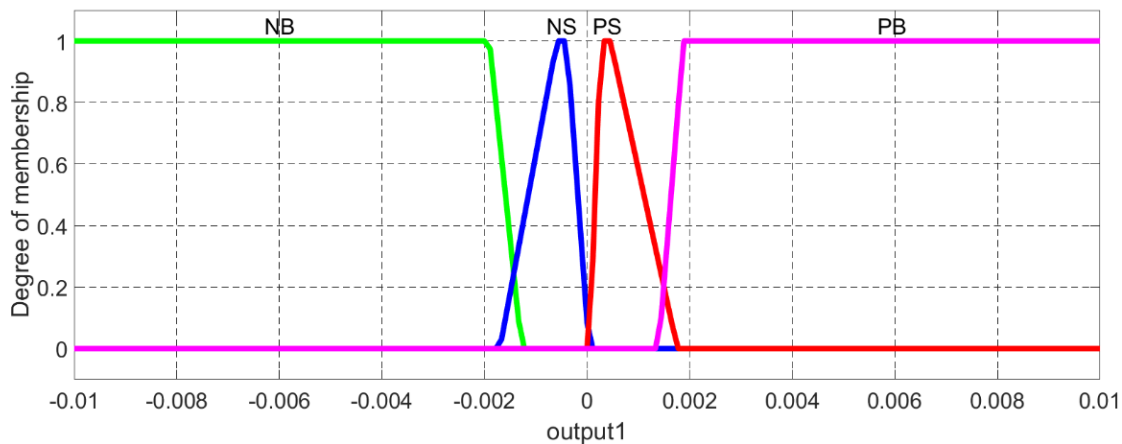
$\Delta P/P$	$\Delta P/\Delta V$			
	NB	NS	PS	PB
NB	NB	NS	PS	PB
NS	NB	NS	PS	PB
PS	NB	NS	PS	PB
PB	PB	PS	NS	NB



(a)



(b)



(c)

Figure 4.7. The designed membership functions of the proposal: (a) input1  $\frac{\Delta P}{\Delta V}$ ; (b) input 2  $\frac{\Delta P}{P}$ ; and (c) output  $\Delta D$ .

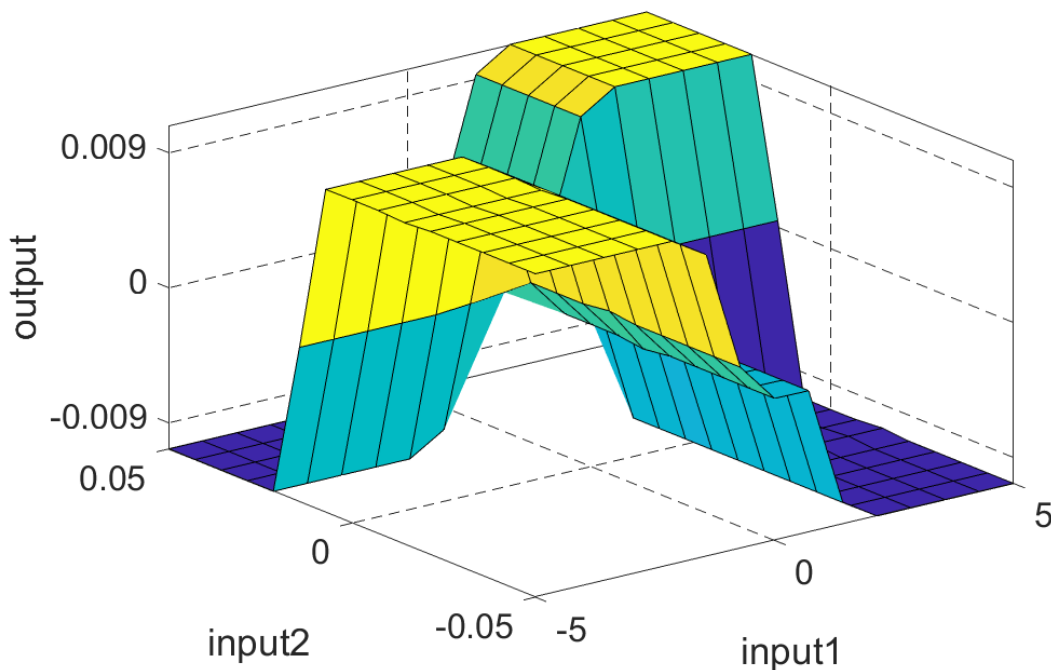


Figure 4.8. A 3D surface between input1 ( $dp/dv$ ) and input2 ( $dp/p$ ) verse output ( $\Delta D$ ).

#### 4.5 Simulation Results

To test the performance of the proposed FLC method, a MATLAB-SIMULINK model for the PV system has been developed. The PV system used in this simulation consists of a PV array, DC–DC boost converter with the MPPT controller, DC-AC inverter and utility grid. The parameters of this PV system are calculated and given in Chapter 3. The simulation was divided into two scenarios. First, the proposed method and conventional P&O were simulated. The input solar irradiance on the PV array was rapidly increased from 400 to 1000 W/m<sup>2</sup> from 1 to 2 s, as shown in Figure 4.9. This reference signal is dissimilar to that presented in Chapter 3, which was rapidly decreased and then, increased. This is because the drift problem was found to happen most clearly when the weather conditions surrounding the PV array increase rapidly. This is the main problem raised and addressed in this Chapter.

As shown in Figure 4.10(a), the power tracking of the proposed FLC method addresses the right direction of the input irradiance, whilst that of the conventional P&O algorithm was lost when the solar irradiance changed rapidly. As a result, the latter method takes a longer time than the proposed one to address the phenomenon of the drift problem, as shown in Figure 4.10(b). In addition, the duty cycle of the proposed method is more accurate in finding the new MPP after solar irradiance changes, and it has a smooth oscillation around this value for steady-

state conditions when compared with the conventional P&O-MPPT, as shown in the zoomed area in Figure 4.10(c). Consequently, the output power of conventional P&O-MPPT method and the proposed FLC method at the steady-state condition, after they reach to the MPP, are 100.722 kW and 100.724 kW, respectively, as shown in the zoomed area in Figure 4.10(a)

In the second scenario, the proposed method and the conventional FLC-MPPT algorithm were simulated under the same weather conditions as previously. The simulation results again proved that the proposed method avoids the system experiencing the drift problem. In addition, it gives a fast response to finding the new MPP during a high change in solar irradiance, whereas the FLC-MPPT continues to suffer from the drift problem, as shown in Figure 4.11. However, this problem was more effective on the conventional P&O-MPPT than the conventional FLC-MPPT, as shown in Figures 4.10(b) and 4.11(b).

Whilst the fluctuations of the MPPT tracker around the MPP steady-state conditions are higher in the proposed method when compared with the conventional FLC-MPPT, as shown in the zoomed area in Figure 4.11(c), the output PV power of the conventional FLC-MPPT is lower due to it having more membership functions, thus resulting in a longer computation time. Consequently, the lost power is a higher in the conventional FLC-MPPT than the proposed MPPT method. As a result, the outputs under the steady state condition being 100.723 kW and 100.724 kW, respectively, as shown in the zoomed area in Figure 4.11(a).

To validate the accuracy of the proposed MPPT tracker for the grid-connected PV system, DC voltage, injected current and grid voltage, before and after the weather conditions change, were simulated. As shown in the zoomed area in Figure 4.12(a), the output voltage of the DC-DC boost converter is stable even during rapid weather conditions change as the one cycle at 1.1 s. Hence, the injected current and the grid voltage of the grid-connected PV system is stable at all times, as shown in Figures. 4.12(b) and 4.12(c), respectively. As a result, the proposed method is more effective for working with the grid-connected PV system under varying weather conditions.

To assess further the proposed MPPT technique, Table 4.3 compares its properties with the conventional P&O-MPPT and FLC-MPPT. As can be seen, the proposed MPPT method has a medium oscillation around the MPP point under the steady state condition, a smaller number of fuzzy rule subsets, simple implementation and the highest output power. Moreover, according to the simulated results, the proposed technique accurately tracks the MPP and avoids the drift problem.

Notably, whilst the power improvement of the PV system based on the proposed method is only 1W and 2 W under steady state conditions more than with the conventional FLC-MPPT and conventional P&O-MPPT methods, respectively, it will capture a substantial amount energy over the lifespan of the PV system (25 years), as shown in Table 4.4. In addition, this value will be higher given the lower drift correction power of the conventional FLC-MPPT and P&O-MPPT methods under a rapid change of weather conditions.

**Table 4.3. A comparison of the properties of the proposed method, conventional P&O and conventional FLC.**

MPPT	Number of fuzzy rules	Oscillation	Implementation	Output power (kW)
Proposed method	16	Medium	Simple	100.724
Conventional FLC	25	Low	Complex	100.723
Conventional P&O	-	High	Simple	100.722

**Table 4.4. A comparison of the output energies of the proposed method, conventional P&O and conventional FLC.**

MPPT	Power (Kw)	Energy (kWh) over 25 years	The value of the capturing energy
Proposed method	100.724	543909600	10800
Conventional FLC	100.723	543904200	5400
Conventional P&O	100.722	543898800	0

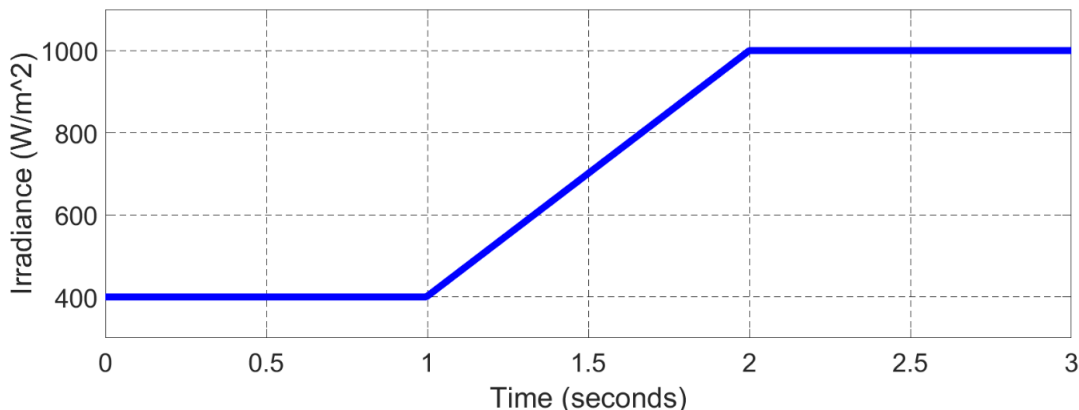
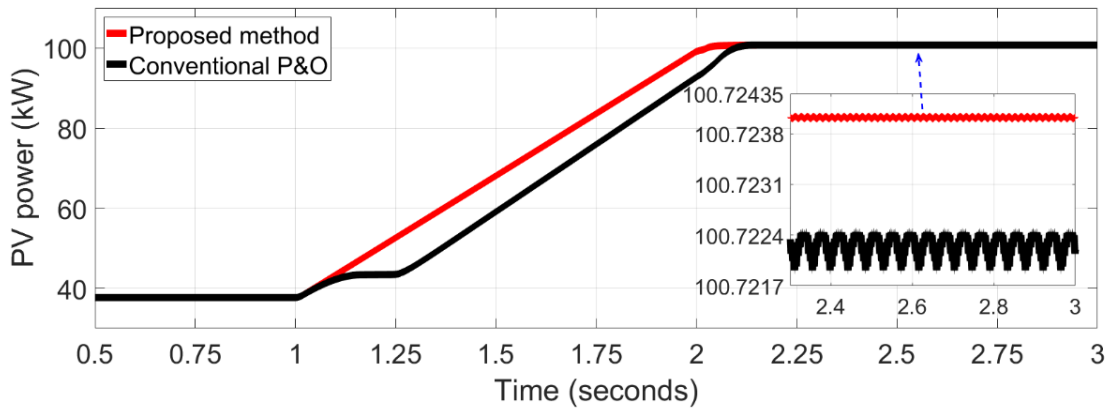
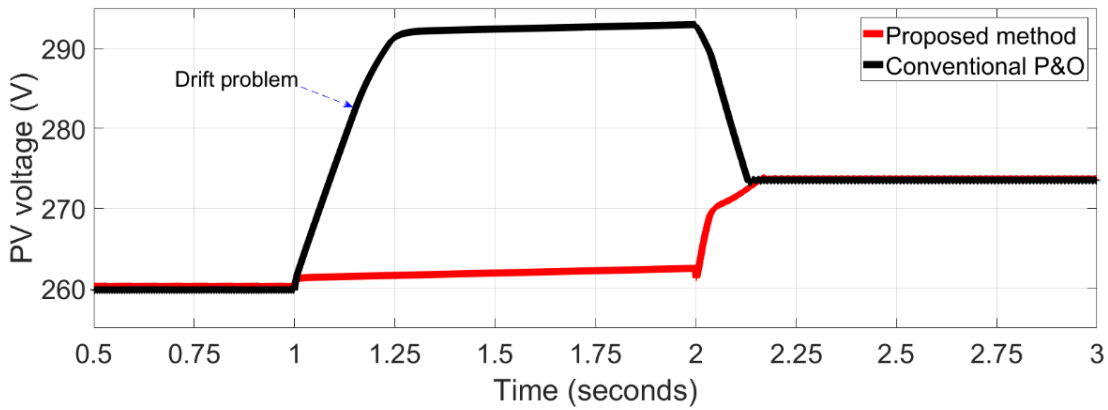


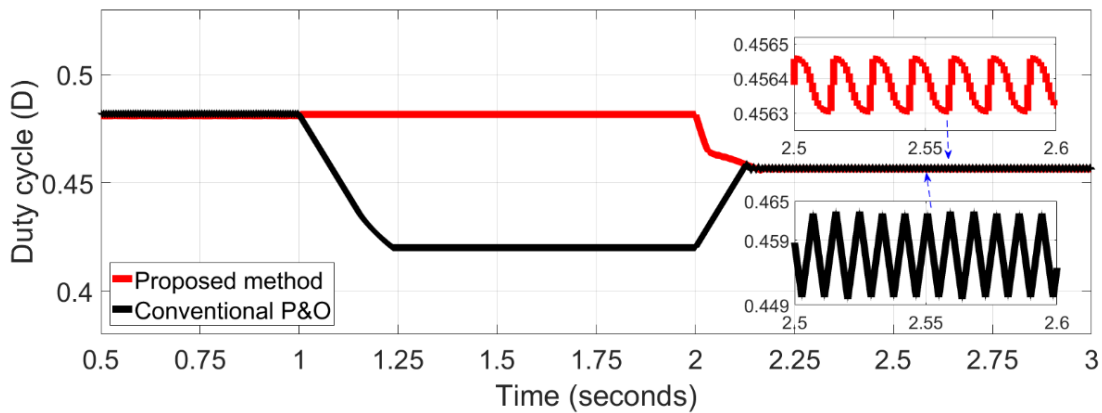
**Figure 4.9. The input solar irradiance based on a rapid changing condition**



(a)

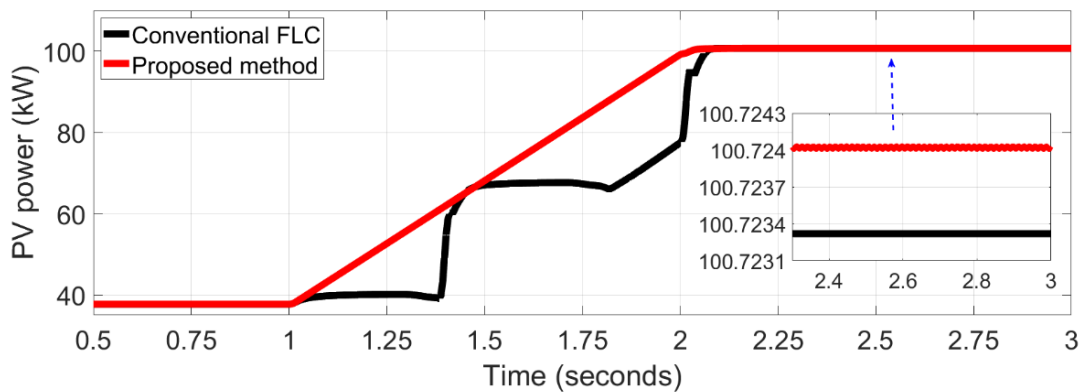


(b)

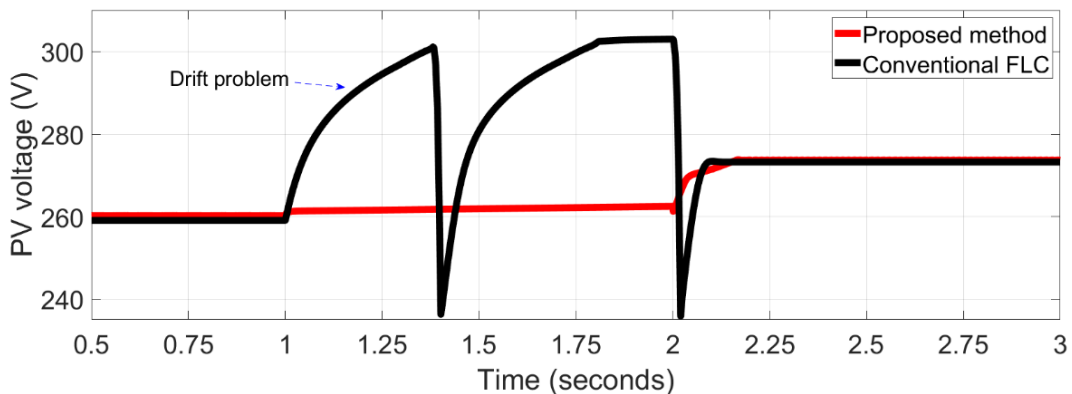


(c)

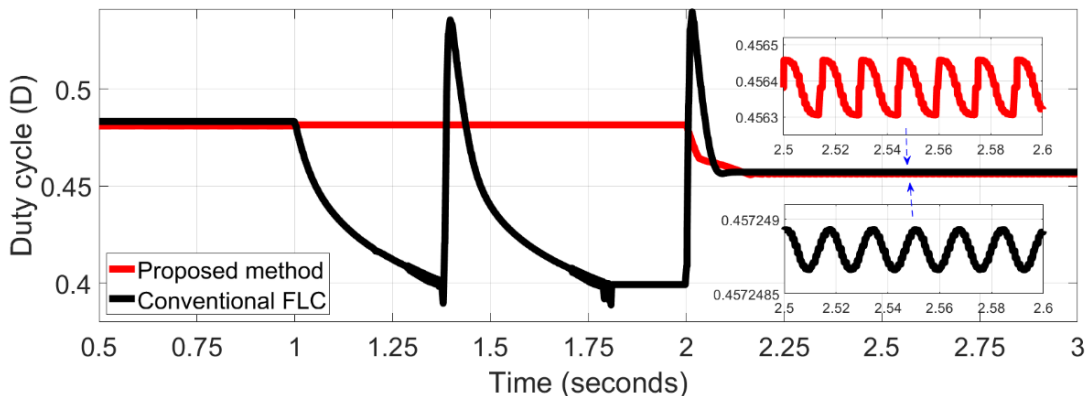
Figure 4.10. PV array system for the proposed method versus conventional P&O under rapidly changing weather conditions: (a) power, (b) voltage, and (c) duty cycle.



(a)

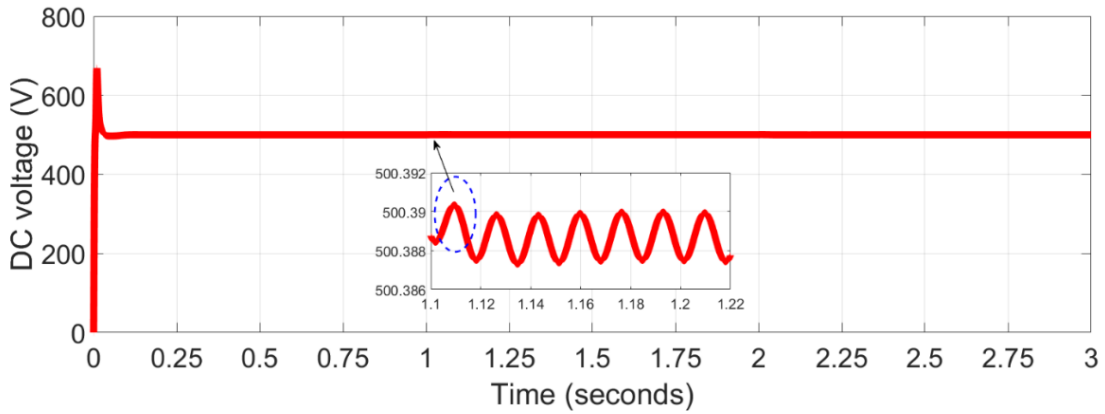


(b)

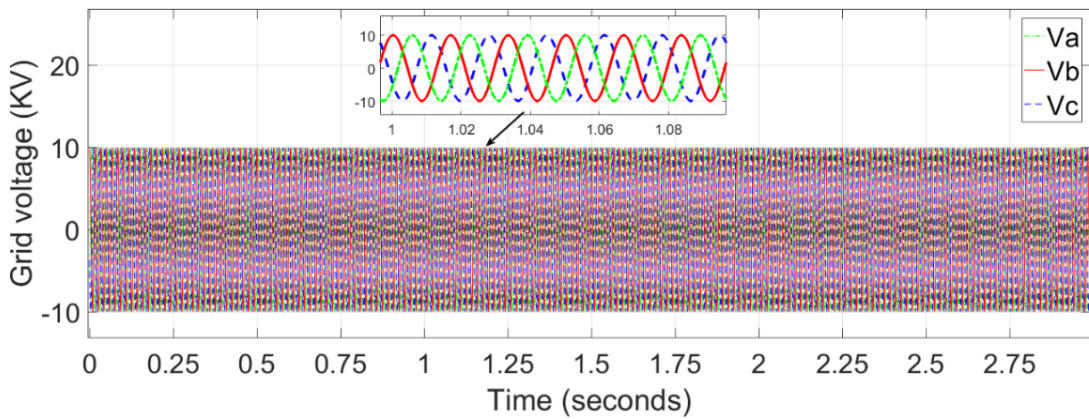


(c)

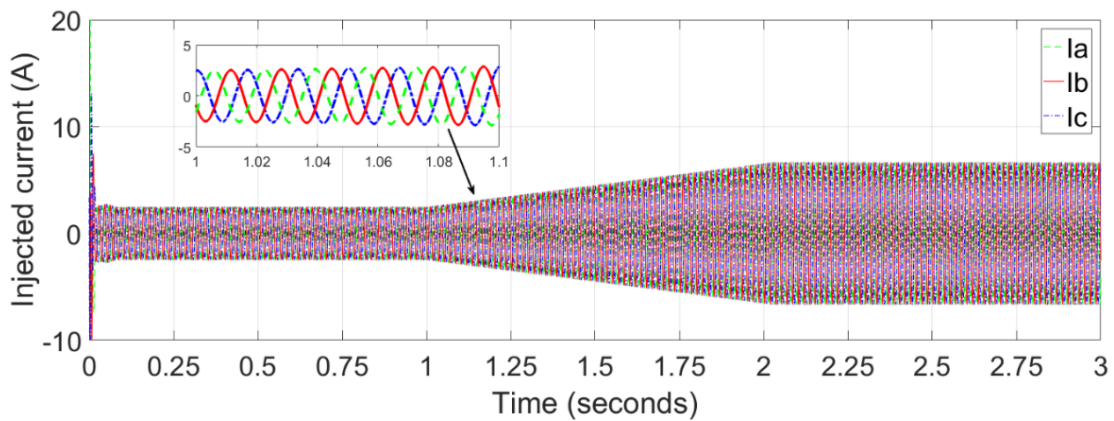
Figure 4.11. PV array system for the proposed method versus conventional FL under rapidly changing weather conditions: (a) power, (b) voltage, and (c) duty cycle.



(a)



(b)



(c)

Figure 4.12. Grid-connected PV system using the proposed MPPT method: (a) the DC voltage, (b) the grid voltage and (c) the injected current to the grid.

#### 4.6 The EN 50530 Standard Test of MPPT Efficiency

To assess the proposed FLC method, EN50530 standard test of MPPT efficiency [138] was used. Basically, it involves supplying triangular waveforms of irradiance sequentially with different ramp gradients. The first sequence is a slow change of irradiance and then, this is gradually increased. In this work, three triangular sequences were applied, slow, fast and very rapid change in solar irradiance about 10, 40 and 80 W/m<sup>2</sup>/s, respectively, as shown in Figure 4.13. The comparison between the proposed method and the conventional P&O method is shown in Figure 4.14(a).

Clearly, the tracking power of the latter avoids the drift problem during a slow change in the solar irradiance ( $\Delta G < 10 \text{ W/m}^2/\text{s}$ ) due to the large and fixed step size of the duty cycle, as show in first sequence, as shown in the zoomed in part of Figure 4.14(a). However, the tracking power of the conventional P&O method drifts away from the right direction when the irradiance increases at a fast pace in second sequence ( $\Delta G > 10 \text{ W/m}^2/\text{s}$ ), as show the second sequence, because the MPPT tracking is unable to address this rapid change in weather conditions. In third sequence, the problem becomes worse, when the irradiance is increased very rapidly ( $\Delta G \gg 10 \text{ W/m}^2/\text{s}$ ), as shown in the zooming in of the third sequence. In case of decreasing irradiance, the tracking power addresses the right direction under different sequences, as shown in the other side of the first sequence.

The comparison between the proposed method and the conventional FLC method is shown in Figure 4.14(b). Whilst the latter method suffers from the drift problem under fast changes in weather conditions (increasing and decreasing the input solar irradiance), as shown in the zoomed in part of Figure 4.14(b)., the problem is minimal when compared to the conventional P&O method. This is because the MPPT tacking of the conventional FLC method can address the problem early. However, the problem became a much worse when the irradiance changes very rapidly. In contrast, the proposed method avoids the drift problem for all three ramp gradients, as shown in Figures 4.14(a) and (b).

To calculate the average tracking efficiency of the MPPT controller, the MPPT efficiency formula is used, as given in Eq. (4.9) [138]:

$$\eta_{.MPPT}(average) \% = \frac{\int P_{out} (t)dt}{\int P_{max} (t)dt} \quad (4.9)$$

where  $P_{out}$  is the output power of the PV array and  $P_{max}$  is its theoretical maximum power. The actual power is calculated using the sensors of the current and voltage of the PV array and then multiplied. The theoretical maximum power is calculated using the general equations of PV array, as given in Eqs (3.1) -(3.4). The tracking time (t) is calculated according to the ability of the power tracking to reach the MPP under same weather condition for the actual power and the theoretical power of the PV array. Then, various tracking times are used to calculate the average tracking efficiency of the MPPT method.

Whilst the MPPT efficiency of the proposed method for  $400 \text{ W/m}^2$  appears to be the lower in the beginning of the signal test, it achieves an average tracking efficiency of 99.6% under all the varying weather condition scenarios, whereas those for the conventional FLC-MPPT and P&O-MPPT methods are 96.4 %, and 93.5%, respectively, as shown in Figure 4.15 and Table 4.5.

**Table 4.5. A Comparative study regarding the average efficiency for the proposed method and the conventional FLC and P&O-MPPT techniques.**

MPPT method	Average efficiencies
Proposed method	99.6%
Conventional FLC	96.4%
Conventional P&O	93.5%

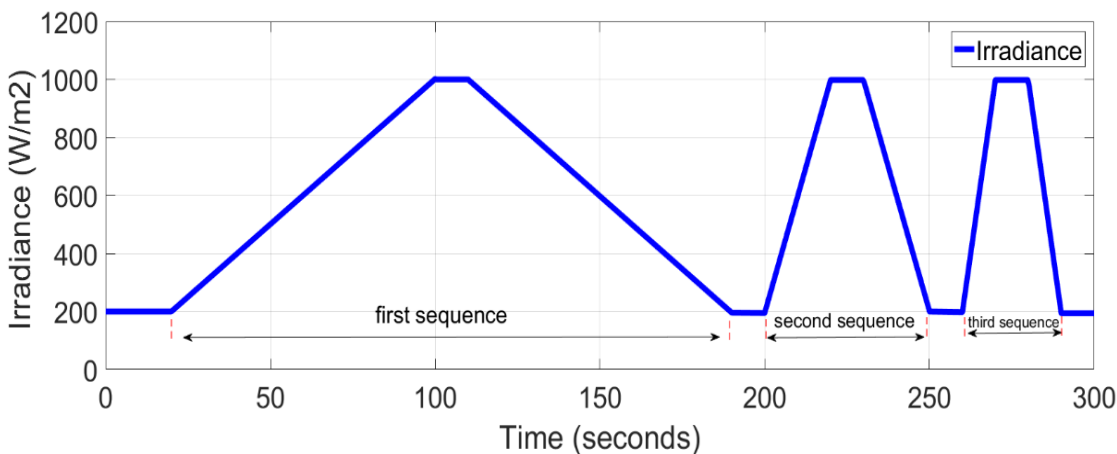


**Figure 4.13. Triangular waveforms of irradiance for the EN50530 standard test of MPPT efficiency.**

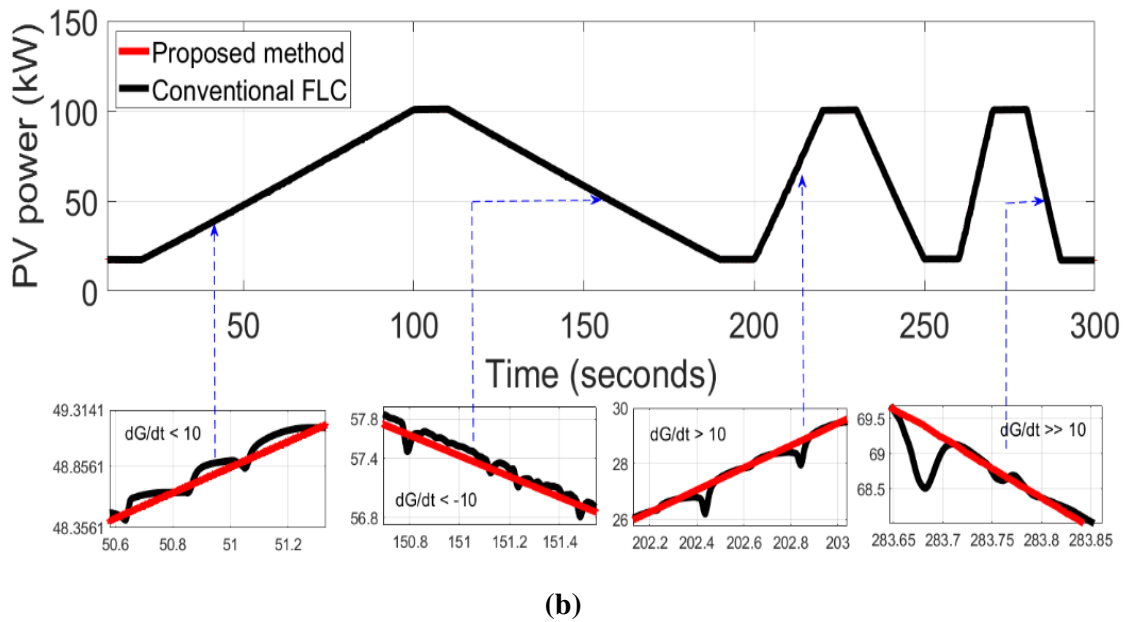
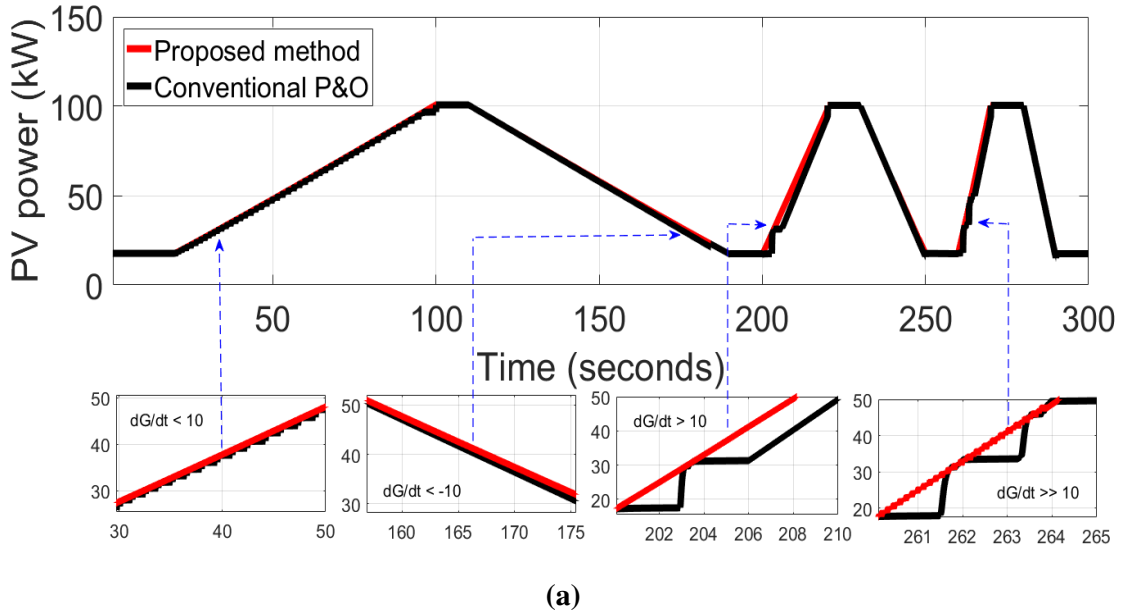
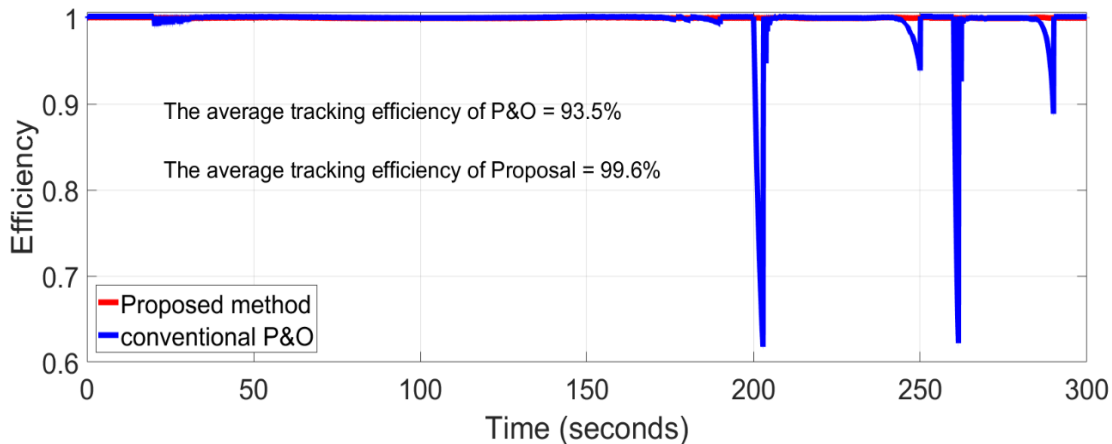
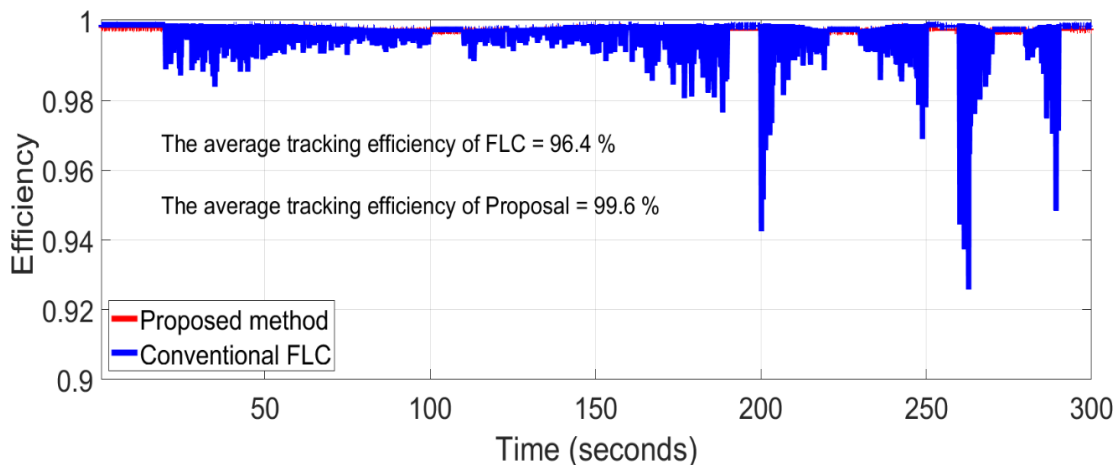


**Figure 4.14.** The PV power for the EN50530 standard test of MPPT efficiency, (a) MPPT power tracking for P&O versus the proposed method, (b) MPPT power tracking for FLC versus the proposed method.



(a)



(b)

**Figure 4.15. The average efficiency of power tracking under the EN50530 standard test for: (a) P&O-MPPT versus the proposed method; and (b) FL-MPPT versus the proposed method.**

### 4.7 Summary

A proposed maximum power point tracking technique based on fuzzy logic control for a grid-connected PV system has been presented, which has the ability to track the MPP when there are big fluctuations of irradiation. The advantages and disadvantages of the FLC-MPPT has been discussed. The designed membership functions of FLC the controller where tuned based on modified a P&O algorithm to incorporate the advantages of the P&O-MPPT and the FLC-MPPT as well as to eliminate their drawbacks. The P&O-MPPT, FLC-MPPT and proposed method were simulated, being then compared, according to their common features. The EN50530 standard test was used to calculate the efficiency of the proposed method under

varying weather conditions. The simulation results have revealed that the proposed technique exhibits a higher output power, and no divergence from the MPP during varying weather conditions regardless of the speed of change. That is, the proposed concept has been shown to be highly effective for working with a grid-connected PV system, achieving efficiencies of around 99.6%. Finally, this modification has been shown to be simple to implement.

## Chapter 5

### Design of an Efficient MPPT based on ANFIS

In this Chapter, an efficient maximum power point tracking technique based on ANFIS using a real photovoltaic system data is designed. Those real data are collected throughout the whole 2018 from experimental tests of a photovoltaic array installed at Brunel University, London, United Kingdom. Normally, data from experimental tests include errors and therefore are analysed using a curve fitting technique to optimize the tuning of ANFIS model. A real measurement test of semi-cloudy day is used to calculate the average efficiency of the proposed method under varying climate conditions.

#### 5.1 Related Works

As mentioned in Chapter 2, the MPPT controller based on artificial intelligence techniques for a PV system has been widely used in recent years. This is because it can solve the significant issues associated with the classical MPPT methods. Moreover, these techniques do not need complex mathematics or accurate parameters when managing the system. In particular, the ANFIS-MPPT is one of the most powerful controllers for a PV system due to experiencing less fluctuation around the optimized MPP point, fast tracking speed and low computation time. However, the main disadvantages are the lack of accurate training data and tuning of the ANFIS model. Hence, several types of ANFIS-MPPTs have been designed using different types of training data. Among them, in [94], Lasheen and Abdel-salam developed an MPPT technique based on adaptive ANFIS and Hill Climbing (HC) techniques to increase the generated energy from a PV system. This proposed technique is a combination of two stages to adjust the property duty cycle of a boost converter for MPP tracking.

In the first stage, the duty cycle is estimated, whilst in the second, the exact duty cycle corresponding to the optimized MPP point is determined. In order to construct the training of

the ANFIS system, the ranges of the ambient temperature and solar irradiance are determined, according to the latitude and longitude of the site of the PV system. With same ideal, Farzaneh et al. [54] presented an intelligent MPPT for PV system using hybrid ANFIS and Particle Swarm Optimization (PSO) technique to reduce the converging time of the MPPT algorithm under partially shaded conditions. The solar irradiation and temperature operation are selected as the input, whilst the optimal duty cycle ( $Dm$ ) is the output, which is optimized using the PSO algorithm. The data of the ANFIS system are collected from different scenarios of the PV operating system under varying partial shading. Whilst these proposals increase the efficiency of the PV system, their implementations become over complex due to an additional step unit.

Hence, Muthuramalingam and Manoharan [95] present a comparative study among P&O-ANFIS, PSO-ANFIS and ANN-MPPTs for a stand-alone PV system under partial shade conditions. The training data of the ANN method are collected from a single operating test of the PV array, while the P&O-ANFIS and PSO-ANFIS are derived from the operational PV system, with the P&O and PSO, respectively. In [101], Abido et al. designed an efficient ANFIS-MPPT method based on a large training dataset for PV systems. The inputs of the proposed ANFIS technique consist of the irradiance and temperature conditions, whilst the output is the optimized PV voltage at the MPP point ( $Vm$ ). The large training dataset is collected from Simulink operation tests of a PV module under a wide range of weather conditions to avoid the system having a high training error.

In [139], Kharb et al. modelled an intelligent MPPT controller based on ANFIS to solve the complexity of the tracking mechanism and non-linear nature of a PV system. The temperature and irradiance of the weather conditions are used as inputs of the training data of proposed method, while the output is the value of maximum power from the PV array at a specific temperature operation and irradiance level ( $Pm$ ). In [140], Abu-Rub et al. designed an intelligent MPPT technique based ANFIS for a solar PV system to reduce converge tracking time under a fast change in weather conditions. The key point of this proposal is that the maximum power of the PV module is adjusted under specific conditions. The proposed ANFIS-MPPT is trained by the solar irradiation level and temperature operation of the Simulink operation of a PV module under varying weather conditions and the output is the maximum power. In [141], Abu-Rub et al. designed an intelligent MPPT controller based on ANFIS to generate the maximum power of a PV system in the standalone operation. The maximum power generation of the load is ensured by an adaptive ANFIS-MPPT with a quasi-Z-source inverter.

The inputs of the proposed ANFIS method consist of the solar irradiance and temperature, while the output gives the optimum voltage at the MPP point of each of the weather conditions. The training data are collected based on a simulation test of a single PV module under various environmental conditions. In [98], Bin-halabi et al. proposed and implemented an intelligent MPPT method using an ANFIS model to enhance the performance of a PV system. The main contribution of this work is eliminating the need for inputting irradiance sensor. The PV voltage, PV current, and temperature operation are selected as the input, whilst the optimal PV voltage at the MPP is the output of the ANFIS model. The data of the ANFIS system are collected from Simulink operation tests of a PV system under varying climate conditions.

In [142], Murdianto et al. designed an intelligent MPPT based on ANFIS for a PV system to generate maximum output power. This work involves utilizing the maximum power for energy storage using a SEPIC converter. The solar irradiance and temperature operation are selected as the input, with the optimal PV current at the MPP ( $I_m$ ) being the output of the ANFIS model. The data of ANFIS system are collected from the curve characteristics the PV array under varying weather conditions. In [96], Aldair et al. designed and implemented an ANFIS-MPPT technique using an FPGA board for standalone photovoltaic systems to demonstrate the usefulness of ANFIS. The solar irradiance and temperature operation are selected as the inputs of the ANFIS model, whilst the optimal current is the output.

The training data are used to define the input membership function of the proposed method by assuming that the PV array is located in the south of Iraq. In [143], an intelligent approach to optimizing the efficiency of a PV system by the ANFIS-MPPT technique is presented. The system consists of a PV array, MPPT controller, DC/DC converter and a DC motor pump. The PV current and PV power are selected as the input, with the duty cycle being the output of the proposed MPPT method. The data of ANFIS system are collected from several experiments performed on a PV array under various values of solar irradiance and a constant temperature at 25°C.

In [144], an intelligent MPPT controller was proposed for a PV system using an ANFIS model to track the MPP point under varying weather conditions. The inputs of the proposed ANFIS method consist of the current and voltage of a PV module, whilst the output gives the propriety duty cycle for a power conversion system. The proposed ANFIS method generates change in the duty cycle based on a historical change of PV power and derivate in this value. In [30], Ounnas et al. design an efficient MPPT technique based ANFIS for PV systems to

determine the MPP point under different weather conditions. The solar irradiance and temperature operation are selected as the inputs of the ANFIS model, whilst the optimal voltage at the MPP is the output. The data of ANFIS model is collected from the power–voltage curve of PV array under different weather conditions.

The results in previous report that the conventional ANFIS-MPPT based on theoretical data increased tracking speed and reduced oscillations. However, they are not achieving a higher efficiency when compared with hybrid methods because of a shortage of accurate training data. Consequently, Khosrojerdi et al. [97] proposed an intelligent MPPT technique based on ANFIS for standalone PV systems using a large real data. The solar irradiation and temperature operation are selected as the input of the ANFIS model, whilst the optimal voltage at the MPP and duty cycle are the outputs. The training data of the proposed ANFIS system are collected from experimental testing of a PV array installed in Ottawa, Canada. With the same idea, Chaouachi et al. [89] presented a novel methodology for maximum power point tracking of a grid-connected photovoltaic system using an experimental data of a PV system installed in Tokyo, Japan. The operating temperature and irradiance level are used as input training data of the proposed ANFIS method, and the output is the reference voltage.

Although those proposed method in [97] and [89] trained using the real data, they are not optimized. Hence, the MPPT tacker are achieving lower efficiency compared with a hybrid algorithm under different weather conditions. In this Chapter, an experimental training data is collected during one year from experimental tests of a PV array installed at Brunel University London, Uxbridge, United Kingdom, as shown in Figure 5.1. Then, they are analysed and optimized using Curve Fitting technique to design an efficient maximum power point tracking technique for photovoltaic system. The installed PV modules characteristics are given in Table 5.1.

The rest of this Chapter is organized as follows. Section 5.2 discusses the MPPT using the ANFIS algorithms. The stand-alone PV system based on the ANFIS-MPPT controller is presented in Section 5.3. The methodology of collected the training data is explained in Section 5.4. While Section 5.5 presents the curve fitting technique. In Section 5.6, the tuning and optimising of proposed ANFIS model are given, whilst the results are provided and discussed in Section 5.7. Real measurement test results of one day are provided in Section 5.8, with Section 5.9 containing the summary of this Chapter.



Figure 5.1. The studied PV array installed at Brunel University London, UK.

Table 5.1. PV module characteristics.

Parameters	Value
Cell number	48
Dimensions	1.318×994×46 mm
Nominal power	185W
Open circuit voltage	30.2 V
Maximum power voltage	24 V
short circuit current	8.54 A
Maximum power current	7.71 A
Temperature Coefficient ( $P_{max}$ )	-0.485%/°C
Temperature Coefficient ( $I_{sc}$ )	+0.053%/°C
Temperature Coefficient ( $V_{oc}$ )	-104 mV/°C
Type of PV cell	Monocrystalline
Type of PV module	Sharp NU-S5E3E 185
Conversion Efficiency	14.1%

## 5.2 ANFIS Technique

ANFIS technique is considered a hybrid method based on the architecture of a neural network and fuzzy logic inference [145]. It is adapted neural network technique based on fuzzy inference system. The principle work of this technique is depended on three concepts:

1. Rule base selects fuzzy rules.
2. Data base identifies the membership functions using the fuzzy rules.
3. Reasoning mechanism inferences the rules with deriving output.

To address and optimise the signal system, a hybrid-learning rule combining back-propagation, gradient-descent and a least-squares are used [146]. The ANFIS structure consists of five layers: fuzzification, rules, normalization, consequent, and addition, as shown in Figure 5.2. In the first layer, every node of the training data is an adaptive node, with the node function using Eqs. (5.1) and (5.2) to generate the defined membership functions:

$$A_{1,i} = \mu x_i(x) \quad \text{for } i = 1,2 \quad (5.1)$$

$$A_{1,i} = \mu y_{i-2}(y) \quad \text{for } i = 3,4 \quad (5.2)$$

where,  $\mu$  is the defined membership functions and  $A_{1,i}$  is the defined membership value for the inputs  $x$  and  $y$ . The subscripted 1 and  $i$  is the layer number and node number of the training data, respectively. The defined membership functions can be any shaped function, such as triangular, trapezoidal or Gaussian. The best membership functions which achieve a less training error. In layer 2, every node is a fixed node based on one the valid fuzzy rule. The output value is given by Eq. (5.3):

$$A_{2,i} = \omega_i = \mu X_i(x) \mu Y_i(y) \quad i = 1,2 \quad (5.3)$$

In layer 3, every node is fixe based on the normalization of each valid fussy rule, using Eq. (5.4):

$$A_{3,1} = \omega_i = \frac{\omega_i}{\omega_1 + \omega_2} \quad (5.4)$$

In layer 4, every node is adapted and calculated based on the rule consequent, as given in Eq. (5.6):

$$A_{4,1} = \omega_i f_i = \omega_i (p_i x + q_i y + r_i) \quad (5.6)$$

where,  $pi$ ,  $qi$  and  $ri$  are consequent parameters, which require being optimized in the training operation. In layer 5, all input nodes are summed together to get the final output signal, as given in Eq. (5.7):

$$A_{5,1} = \sum_i \omega_i f_i = \frac{\sum_i \omega_i f_i}{\sum_i \omega_i} \quad (5.7)$$

where  $\omega_i$  is the minimum number of membership functions and  $f_i$  is the centre value of the output membership function. The training procedure of ANFIS model is depended on a number of epochs. In each epoch, the output nodes are determined in layer 4 while the consequent parameters are determined in layer 5. A back propagation (BP) algorithm or hybrid algorithm are used to learn the process of the ANFIS model.

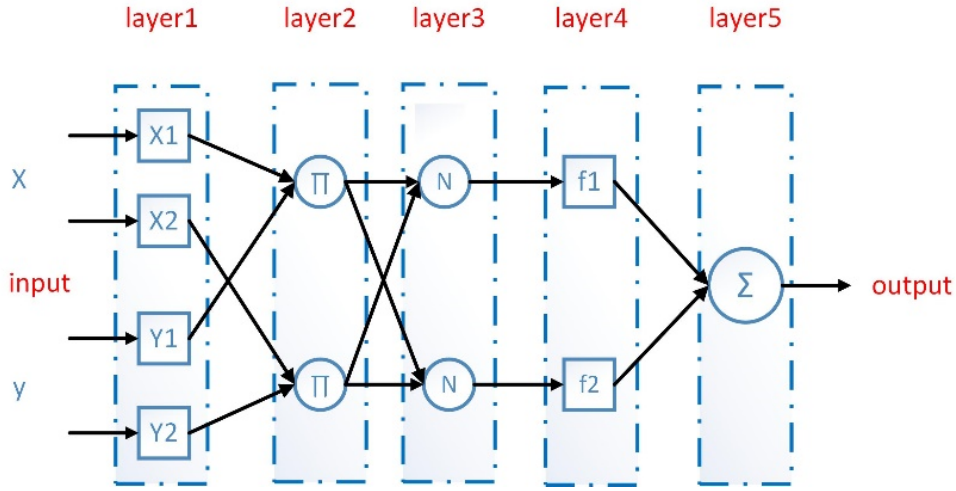


Figure 5.2. A block diagram of the ANFIS model [145].

### 5.3 ANFIS-MPPT Controller

The traditional ANFIS-MPPT method usually has two inputs and one output, as shown in Figure 5.3. The operating temperature ( $T_x$ ) and irradiance level ( $G_x$ ) are usually used as inputs to the training data of the ANFIS method, and the output is the reference power ( $P_{ref}$ ). Under the same weather conditions, the actual PV power ( $P_{act}$ ) is calculated using the sensed voltage and current of the PV operation. These two power readings are compared, and the error ( $e$ ) is given to a Proportional Integral (PI) controller to generate the signal of a DC-DC convertor by a PWM generator, to adjust the operating MPP point of the PV module. The signal control ( $s$ ) of the PI controller is given by Eq. (5.8):

$$D = K_P(P_{act} - P_{ref}) + \frac{K_I}{S}(P_{act} - P_{ref}) \quad (5.8)$$

where,  $K_P$  and  $K_I$  represent the proportional and integral gain of the PI controller, respectively. In general, the MPPT technique based on ANFIS has been designed to solve the limitations of an intelligent system. In addition, it can adjust its parameters to give a faster response and less oscillation under different weather conditions due to less time being consumed in the defuzzification stage. However, getting accurate training data and tuning ANFIS model are big challenges when designing an efficient ANFIS-MPPT. In this Chapter, the proposed ANFIS model is designed using real data collected from experimental PV tests installed at Brunel University London, Uxbridge, United Kingdom.

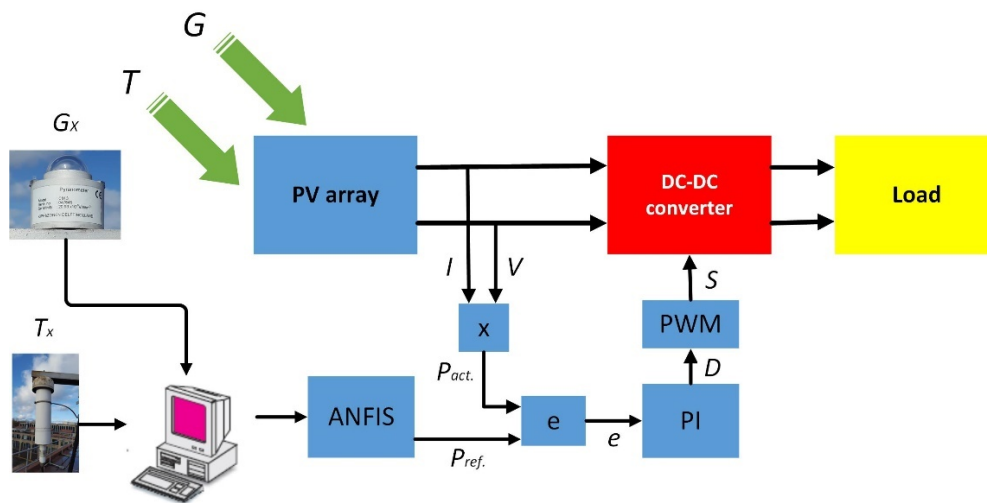


Figure 5.3. The diagram of a PV system using an ANFIS-MPPT.

#### 5.4 Methodology of Collected Data

A micro-grid PV system is installed at Brunel University London, Uxbridge, UK, to collect real training data, as show in Figure 5.4. The PV array consists of five PV modules connected in series. This PV array is connected to the micro-grid through dedicated Sunny Boy Inverter. The main reason to use this DC-AC inverter is that it conforms the regulations concerning small-scale PV generation. In addition, it has inbuilt communication system, anti-islanding unit and voltage protection. To measure and collect the electrical parameters of the PV system, Sunny Boy Controller Pulse is connected to the inverter by RS485 transmission protocols. In addition, a weather station comprising of a Pyrometer, Hydrometer, and Anemometer and wind vane is installed and connected to the Sunny Boy Controller Pulse via RS232 cable for studying and analysing the dependence of weather parameters. Although four parameters of weather conditions (irradiation, temperature, wind speed and humidity) are measured, the solar

irradiation and ambient temperature are selected to design PV-MPPT systems because they are the most effective on PV systems than other parameters according to the general equation of PV cell. The ranges of the ambient temperature and solar irradiance are determined according to the latitude and longitude of Uxbridge, London, UK, which are 51.531 and -0.474, respectively.

A supervisory control and data acquisition system (SCADA) was used to monitor and control the system, linked to the university local area network (LAN) using TCP/IP and SBC Net Port system commination. The Sunny Boy controller read data every 5 minutes periodically in daytime and switched off at night. It then turns on every 15 minutes to exam the weather conditions otherwise it returns to power-save mode. The data were recorded on PC and stored as a Microsoft Excel Sheet. To avoid failure in the commination system, an external modem was installed with the system to send an alarm signal to the system’s operator if any such problems occurred. Throughout whole the year 2018, about 48,500 data readings were collected and recorded comprising the irradiance level and temperature operation of the atmospheric station, with the output being the measured power of the photovoltaic array at the maximum power point.

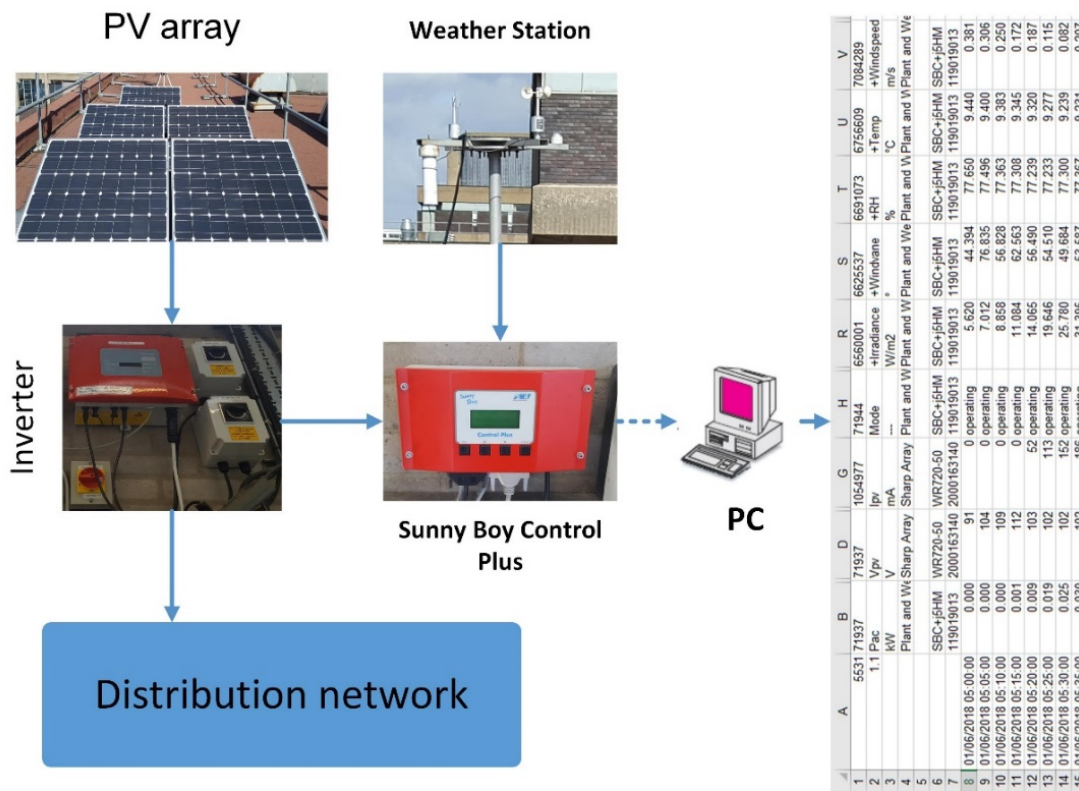


Figure 5.4. The general diagram of a collected data system.

## 5.5 Curve Fitting Technique

It is very common in engineering practice to obtain and record real data from device systems. Engineers use these data to understand underlying properties and solve issues of the system. However, it is not easy or even possible to determine the relationship that describes the behaviour of the system using the real data. Regression analysis of data is a statistical procedure and can be used to identify the relationships among different points. Whilst there are varying methods of the regression analysis, a curve fitting technique is considered as one of the best methods which is utilised in this work [147].

This technique is attempted to find a mathematical function that can describe the measurements of real data as accurate as possible. It is not necessary that the function obtained will pass through all the real data points. However, the smallest possible error of fitting curve should be gotten which defined as Eq. (5.9):

$$p = \sum_{i=1}^n r_i^2 = \sum_{i=1}^n [y_i - (a_1x_i + a_0)]^2 \quad (5.9)$$

where  $r_i$  is the residual vector of each data point,  $y_i$  the value of the straight line evaluated at  $x_i$  point,  $a_i$  and  $a_0$  are the coefficients of curve fitting and  $n$  is the numbers of data. Hence, for exemplify, the equations of curve fitting coefficients for five points are writing as Eqs. (5.10-14):

$$a_1x_1 + a_0 = y_1 \quad (5.10)$$

$$a_1x_2 + a_0 = y_2 \quad (5.11)$$

$$a_1x_3 + a_0 = y_3 \quad (5.12)$$

$$a_1x_4 + a_0 = y_4 \quad (5.13)$$

$$a_1x_5 + a_0 = y_5 \quad (5.14)$$

Now, those above five equations are writing in a more compact method using matrix notation, as defined in Eq. (5.15):

$$Ab = y \quad (5.15)$$

where,

$$A = \begin{bmatrix} x_1 & 1 \\ x_2 & 1 \\ x_3 & 1 \\ x_4 & 1 \\ x_5 & 1 \end{bmatrix}, \quad b = \begin{bmatrix} a_1 \\ a_0 \end{bmatrix}, \quad y = \begin{bmatrix} y_1 \\ y_2 \\ y_3 \\ y_4 \\ y_5 \end{bmatrix}$$

Now, the residual matrix notation is written as Eq. (5.16):

$$r = y - Ab \quad (5.16)$$

Substituting Eq. (5.16) into Eq. (5.9), the following is obtained:

$$p = \sum_{i=1}^n r_i^2 = r^T r = y^T y - 2y^T A b + b^T A^T A b \quad (5.17)$$

where,  $r^T$  is the transposed residual matrix notation. To minimize the value of  $p$ , the derivation process is used. This gives in Eq. (5.18):

$$\frac{\partial p}{\partial b} = 0 = -2y^T A + 2A^T A b \quad (5.18)$$

Now, the coefficients of fitting curve (b) is defined as Eq. (5.19):

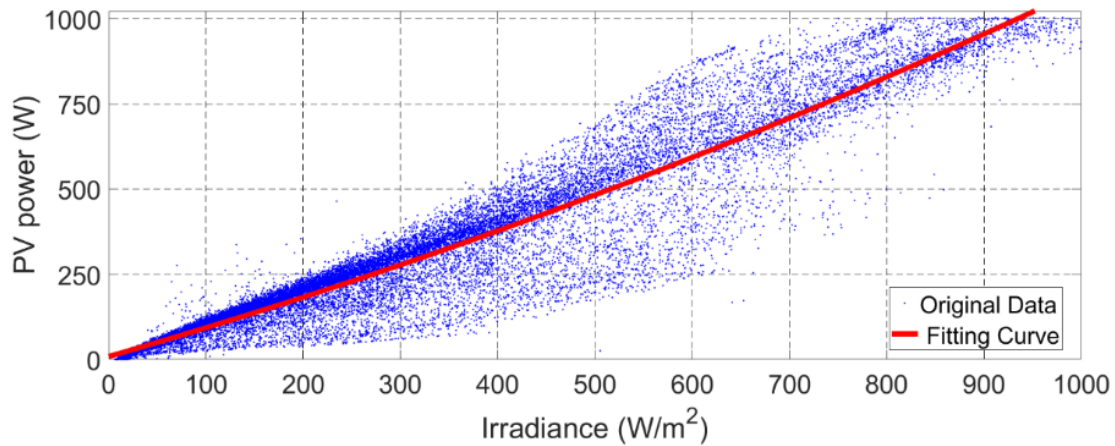
$$b = (A^T A)^{-1} y^T A \quad (5.19)$$

In this application, y-axis is the PV power and x-axis are irradiance and temperature of weather conditions. About 48,500 data sets for one year are used. In addition, the second order polynomial of last squares is utilised to get a best fit as shown in Eqs. (5.20) and (5.21).

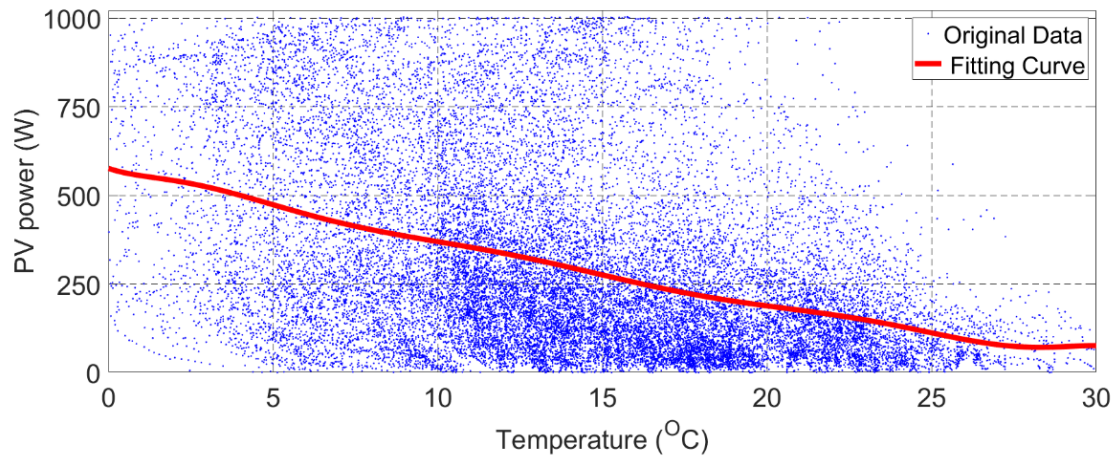
$$y = 3.416 \times 10^{-7} x^2 + 0.0011 x + 0.00115 \quad (5.20)$$

$$y = -1.858 \times 10^{-7} x^2 + 0.015 x + 0.00649 \quad (5.21)$$

To draw those fitting curves, MATLAB code is generated based on Eqs. (5.20) and (5.21). As noticed from Figure 5.5, the power generation of the PV array increases as solar irradiance increases, conversely it is better for low temperature operation than raised one. In addition, the PV generated power almost depends on the irradiance as linearity. In contrast, the operating temperature is less effective on PV power generation as well as non-optimized linearity. Those conceptions will be used in Section 5.6 to adjust the defined membership function of proposed ANFIS model.



(a)



(b)

**Figure 5.5. The fitting curve of (a) PV power - irradiance level, (b) PV power - temperature operation.**

## 5.6 Tuning of Proposed ANFIS Network

Using a MATLAB/Simulink model, an efficient ANFIS-MPPT method based on the large and real data of a PV system is designed to avoid the system from having a high training error. Those data are collected throughout the whole 2018 from experimental tests of a photovoltaic array installed at Brunel University London, Uxbridge, United Kingdom, as described in Section 5.4. The inputs of the proposed ANFIS technique consists of the irradiance level and temperature operation of weather conditions, which are collected by a weather station, and the reference power is measured from the PV installed array, as the output of the ANFIS system.

The estimation accurate PV power depends on the training dataset; therefore, it is very important to select the training data with wide variations of the solar irradiance and the operating temperature [87]. Hence, the measured data for 40 days selected 10 days from each season whose have different variation of weather conditions are used. The ANFIS model based on those data achieves a better performance when compared with the ANFIS model based on total collected data due to its very short training time, lower number of epochs (50) and lower target error (0.08) while the training parameters of the latter model is a very long time, more number of epochs (980) and higher target error (0.14), as shown in Table 5.2.

To select the best membership function of the ANFIS model, different types of membership functions are tested. The linear type for the output membership functions and the triangular type for the input membership functions (trimf) achieve less tolerance of Mean Square Error (MSE) about 0.0706, as shown in Table 5.3 and Figure 5.6. In addition, triangular membership functions have a simple formula and high computational efficiency [96]. As proved in Section 5.4, the PV generated power almost depends on the irradiance as linearity. In contrast, the operating temperature is less effective on PV power generation as well as non-optimized linearity.

According to those conceptions, the numbers of input membership functions (mf) of solar irradiance are selected more than the numbers of input membership functions of operating temperature to able the ANFIS model predicting an accurate power generation of the installed PV array under varying conditions. In addition, the variable second input is adjusted according to the fitting curve of operating temperature by shafting the MF of the second input. Hence, they avoid the state of non-optimized linearity in this second input. Those membership functions for each input are learned by the ANFIS model based on 15 fuzzy rules derived from 8 input defined membership functions as shown in Figure 5.7.

The quantity of membership functions of the input applying irradiance is divided into five values: very low, low, medium, high and very high, while the quantity of membership functions of the surrounding temperature is divided into three values: low, medium, and high. The fuzzy inference system is trained based on the hybrid optimization method by combining the back propagation gradient techniques and the least squares. The surface of training data indicates that the reference power of installed PV array increases smoothly, with an increase in the radiation level and with a decrease in the temperature operation, as shown in Figure 5.8.

**Table 5.2. Simulation ANFIS model based on optimized data VS total data.**

Model	Training time	Number of epochs	Error (%)
Optimized data	Very short	50	8
Total data	Too long	980	14

**Table 5.3. Mean Square Error (MSE) for different input membership functions.**

Purpose	Function	Error
Triangular mf.	Trimf	0.0706
Trapezoidal mf.	Trapmf	0.1085
Generalized bell curve mf.	Gbellmf	0.0787
Gaussian curve mf.	Gaussmf	0.0766
Two-sided Gaussian curve mf.	gauss2mf	0.0894
PI-shaped curve mf.	Pimf	0.1215
Difference of two sigmoid mf.	Dsigmf	0.0808
Product of two sigmoid mf.	Psigmf	0.0819

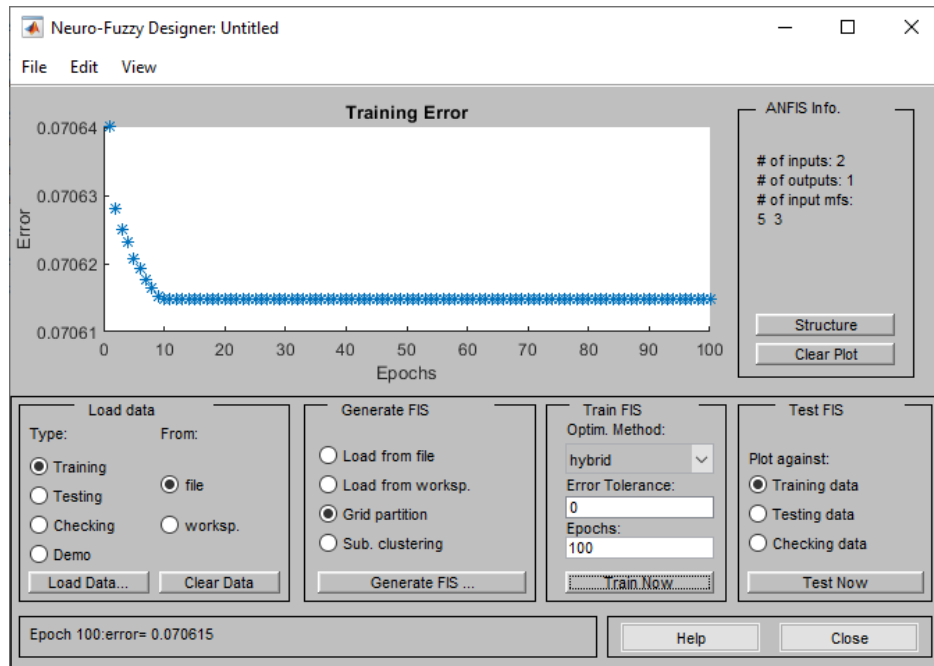
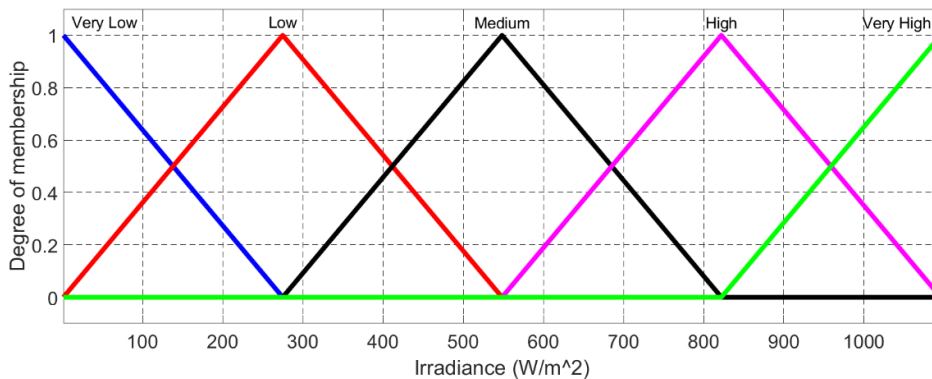
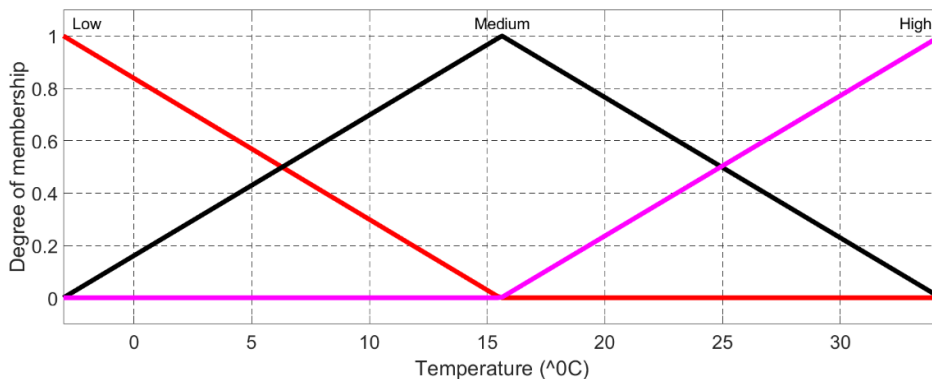


**Figure 5.6. Training data error versus epochs for the ANFIS model.**



(a)



(b)

Figure 5.7. The defined membership function for (a) irradiance, and (b) temperature.

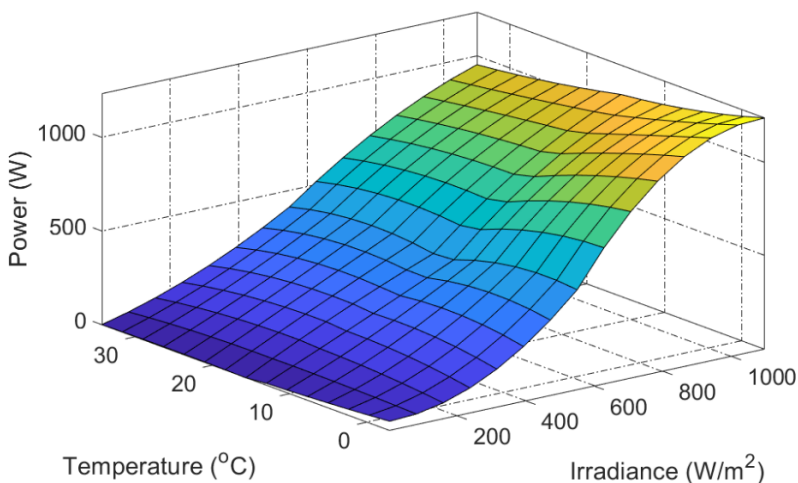


Figure 5.8. A 3D surface between inputs irradiance and temperature verse PV power.

## 5.7 Results and Discussion

In this chapter, a MATLAB-Simulink model for a stand-alone PV system based on ANFIS-MPPT controller is simulated instead of a grid-connected PV system because the training data of ANFIS model are collected from a micro-grid PV system. This PV system consists of a PV array, DC–DC boost converter with an MPPT controller and resistive load. The main parameters of PV model are given in Table. 5.1. The PV array consists of five PV modules connected in series. The parameters of the DC-DC converter are 0.5mH, 65 $\mu$ F and 850 $\mu$ F which are determined using Eqs. (3.13), (3.14) and (3.15). While the resistive load, switching frequency, current diode and updating time are selected at 15 $\Omega$ , 5kHz, 10A and 500 $\mu$ s, respectively. To assess the performance, the optimal ANFIS-MPPT, conventional P&O-MPPT, conventional FLC-MPPT and conventional ANFIS-MPPT methods are simulated under similar conditions.

The simulation was divided into two scenarios; fixed input solar irradiation and variation input solar irradiation. The input irradiation and temperature of the first scenario is fixed at 1000 W/m<sup>2</sup> and 25°C, respectively. As shown in in the zoomed area in Figure 5. 9 (a), the converging time of the power tracker for the optimal ANFIS-MPPT method is the lowest when compared to the conventional ANFIS-MPPT, conventional FLC-MPPT and conventional P&O-MPPT methods, being about 0.07 s, 0.08, 0.11 s and 0.13 s, respectively.

Moreover, it has the lowest fluctuation around the MPP point for steady-state, thus resulting in less computation time, as shown in the zoom in of Figures. 5.9 (b) and (c). Furthermore, it is more accurate for addressing the optimised MPP point when compared with the conventional ANFIS-MPPT, conventional FLC-MPPTs, as shown in the zoomed area in Figure 5.9 (b), due to the large and accurate training dataset. As a result, the PV voltage at the MPP point for the optimal ANFIS-MPPT is in the middle of the optimized voltage of the conventional P&O-MPPT, while the PV voltage at the MPP point for the conventional ANFIS-MPPT and conventional FLC-MPPTs are to the right and left of the optimized voltage of P&O-MPPT with low and medium oscillations, respectively. However, the fluctuation problem is the highest in the conventional P&O-MPPT owing to the continuous perturbation of the P&O tracker for reaching the optimized MPP point, as explained in Chapter 4.

Therefore, the lost power in the optimal ANFIS-MPPT is less than for the conventional FLC-MPPT and conventional P&O-MPPTs. As a result, the output power of the optimal ANFIS-MPPT, conventional ANFIS-MPPT, conventional FLC-MPPT and conventional P&O-

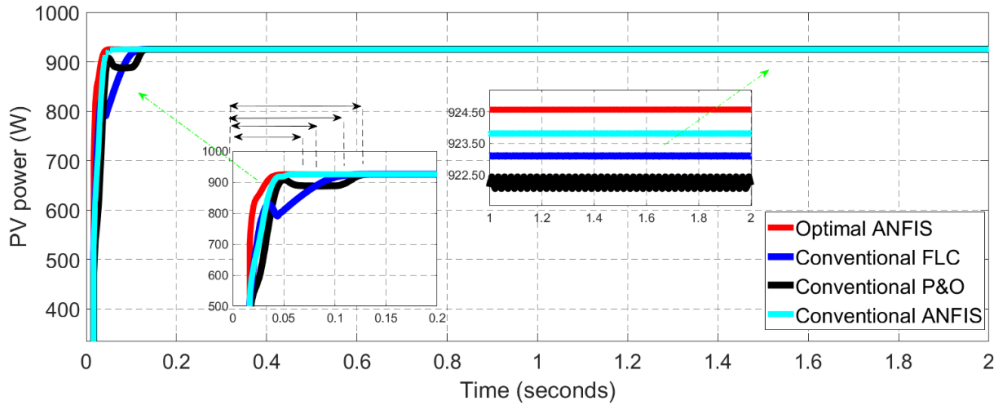
MPPTs, after they have reach the optimised MPP point, are about 924.50 W, 923.75 W, 923.25 W and 922.5 W, respectively, as shown in the zoomed area in Figure 5.9(a).

In the second scenario, the input irradiation level is rapidly increased from 200 to 1000 W/m<sup>2</sup> at 1 to 2 s, and the temperature operation is kept at 25 °C. As shown in Figure 5.10(a), the power tracker of the optimal ANFIS-MPPT addresses the right direction of the input solar irradiance when it changed rapidly owing to its large training and optimized tuning of the proposed model, whilst the tracking power of conventional ANFIS-MPPT, conventional FLC-MPPT and conventional P&O-MPPTs do not address the right direction when the input irradiation changed suddenly. Notably, the conventional P&O-MPPT was the mostly effected by the drift problem and the conventional ANFIS-MPPT was the least effective by this issue.

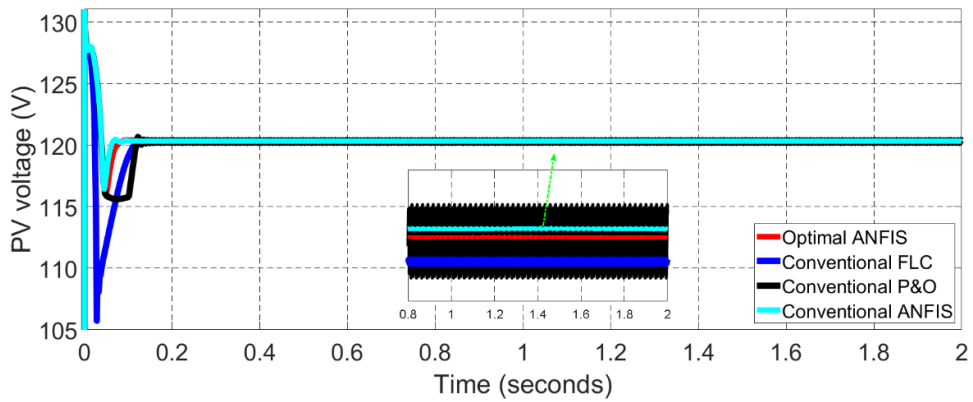
As a result, they take a longer time than MPPT based on the optimal ANFIS to address the drift issue phenomenon, as shown in Figure 5.10. In addition, it is a more robust in addressing the right direction during a rapid change in solar irradiance. On another words, this issue was more effective on the conventional P&O-MPPT then the conventional FLC-MPPT. To assess the optimal ANFIS-MPPT further, Table 5.4 compares its properties with the conventional ANFIS-MPPT, conventional FLC-MPPT and conventional P&O-MPPTs. As can be seen, the optimal ANFIS-MPPT has the lowest converging time, the least oscillation around the MPP point and the highest output power. Moreover, it is the most accurate in tracking the MPP point and avoiding the drift phenomenon.

**Table 5.4. A comparison of the properties of the ANFIC, P&O and FLC-MPPT.**

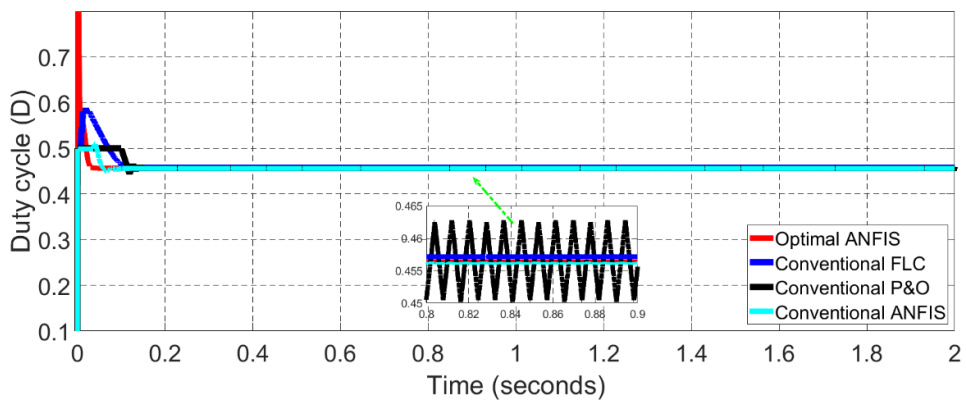
<b>MPPT</b>	<b>Converging time (s)</b>	<b>Oscillation</b>	<b>Drift problem</b>	<b>Output power (W)</b>
Optimal ANFIS	0.07	Low	Avoidance	924.50
Conventional ANFIS	0.08	Low	Suffering	923.75
Conventional FLC	0.11	Medium	Suffering	923.25
Conventional P&O	0.13	High	Suffering	922.50



(a)

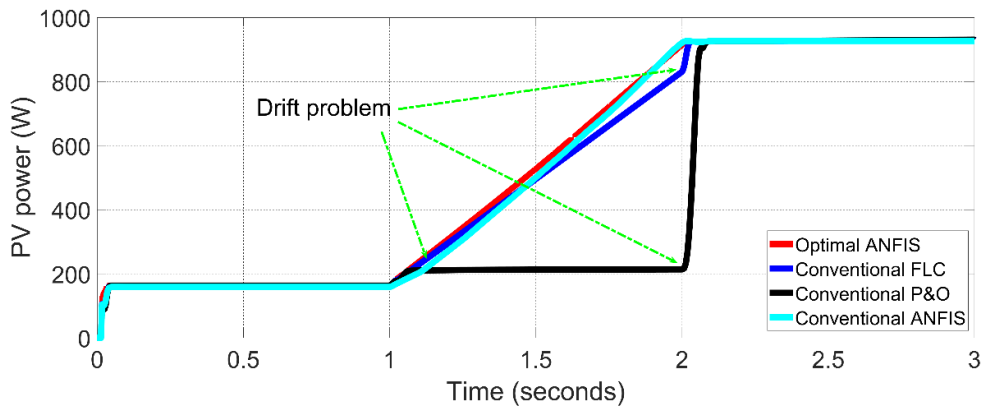


(b)

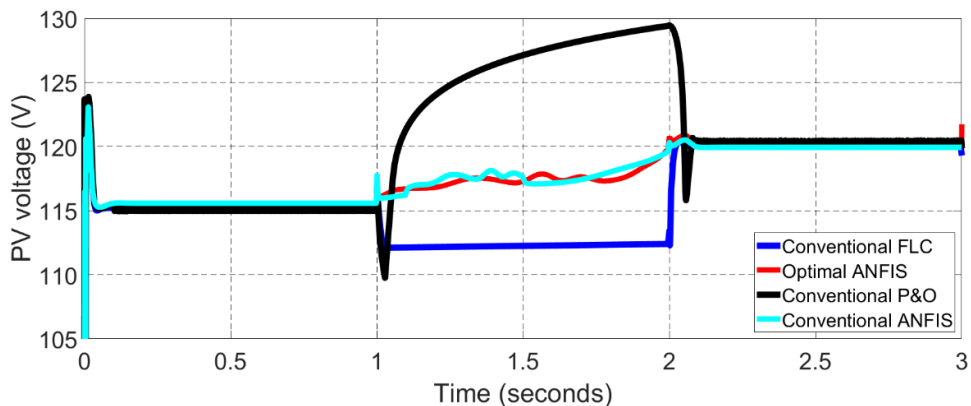


(c)

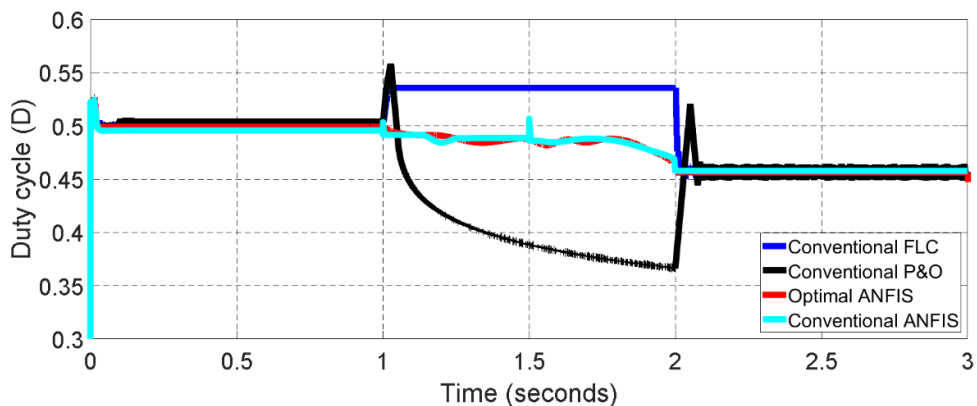
Figure 5.9. PV array system for the ANFIS method versus P&O and FLC methods under a fixed irradiation condition: (a) power, (b) voltage, and (c) duty cycle.



(a)



(b)



(c)

**Figure 5.10. PV array system for the optimal ANFIS versus conventional ANFIS, conventional P&O and conventional FLC methods under a rapid change in weather conditions: (a) power, (b) voltage, and (c) duty cycle.**

## 5.8 Real Measurement Test

To assess the proposed method, the four previous techniques have been compared based on real measurement of the input solar irradiance and temperature for one day on 10<sup>th</sup> June 2018 (05.00 – 20.00), as shown in Figures 5.11 (a) and (b). Those data were collected as mentioned and explained in Section 5.3. Notably, the EN50530 test was used to calculate the average tracking efficiency of the FLC-MPPT method, while experimental testing was utilised to calculate the average tracking efficiency of the ANFIS-MPPT method. This is because, the EN50530 test was designed to calculate the tracking efficiency of MPPT methods under a rapid change in weather conditions, when a drift problem can occur, which is the major issue of the FLC-MPPT method presented in chapter 4. While the experimental test is proposed to calculate the tracking efficiency of MPPT methods under varying weather conditions, in this state, the inaccurate tracker justifies clearly, which is the major issue of the ANFIS-MPPT method explained in this chapter.

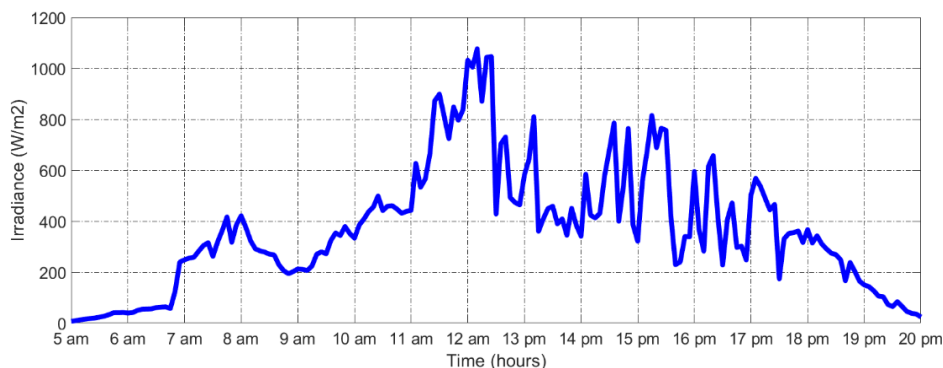
The comparison between an optimal ANFIS-MPPT and conventional P&O-MPPT is shown in Figure 5.13(a). Clearly, the power tracker of the latter method addresses the right direction during a slow change in the weather conditions owing to the large and constant step size of the incremental duty cycle. However, the power of the conventional P&O-MPPT drifts away from the correct direction when the solar irradiation and ambient temperature increases rapidly, because it is not able to cope with the rapid change in the input irradiation, as mentioned and explained in Chapter 4. That is, the issue becomes worse when the solar irradiation is changed suddenly. However, the tracking power of the P&O-MPPT addresses the right direction under the different case of decreasing irradiation, as shown in the zoomed area in Figure 5.12(a).

The comparison between the optimal ANFIS-MPPT and a conventional FLC-MPPT is shown in Figure 5.12(b). Whilst the latter method suffers from the drift problem under rapid changes in weather conditions (increasing and decreasing the weather conditions), as shown in the zoomed area in Figure 5.12(b), the problem can be seen as being minimal when compared to the conventional P&O-MPPT. As mentioned in Chapter 4, this is because the MPPT tracking of the conventional FLC enables it to address the problem early. The comparison between the optimal ANFIS-MPPT and a conventional ANFIS-MPPT is shown in Figure 5.12 (c). Although the latter method almost avoids the deviation under different weather conditions, it is not accurate to address the MPP. In contrast, the tracking power of ANFIS-MPPT based on the

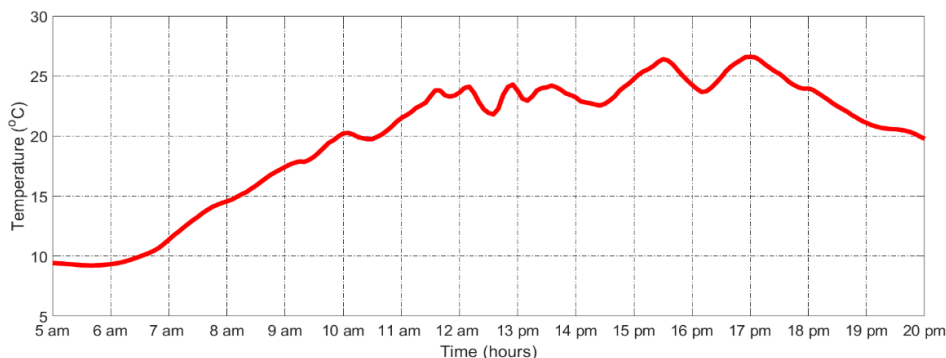
large and real training data avoids the problem under different weather conditions. To calculate the tracking efficiency of the MPPT controller, the average MPPT efficiency formula is used, as given in Eq. (4.9), explained in Chapter 4. Whilst the efficiency of ANFIS-MPPT method for a beginning day appears to be the lowest, it achieves an average efficiency of 99.3% under all the different climate conditions, whereas those for the conventional ANFIS, conventional FLC and conventional P&O-MPPTs are 97.9%, 96.8 %, and 92.6%, respectively, as shown in the zoomed area in Figures 5.13 (a), (b) and (c), as well as Table 5.5.

**Table 5.5. Comparative study regarding the average efficiency for the optimal ANFIS, conventional ANFIS, conventional FLC and P&O-MPPT techniques.**

MPPT method	Average efficiencies
Optimal ANFIS	99.3%
Conventional ANFIS	97.9%
Conventional FLC	96.8%
Conventional P&O	92.6%

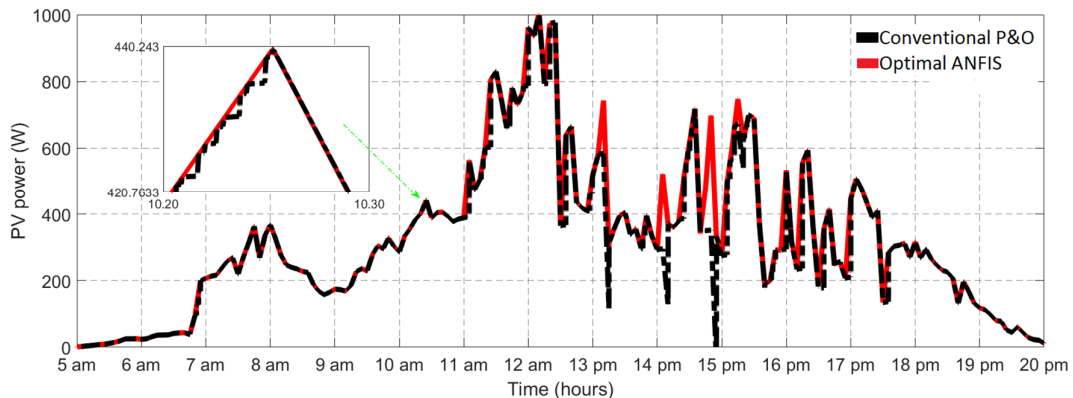


(a)

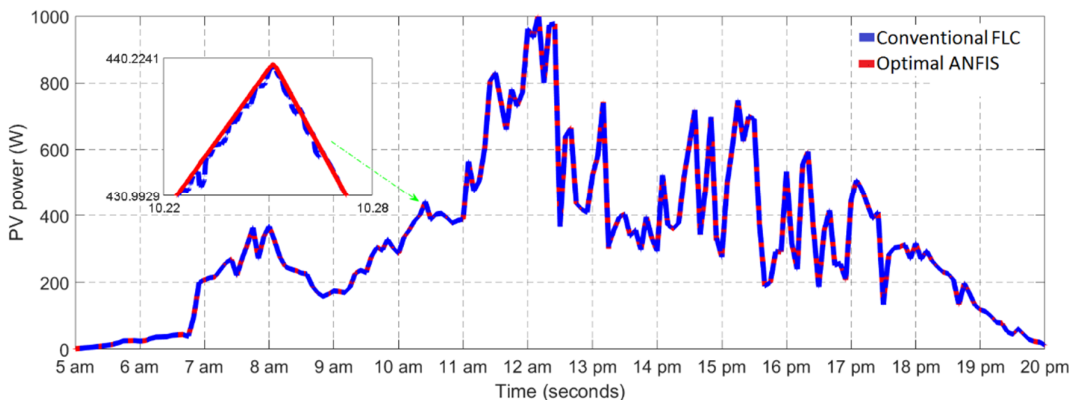


(b)

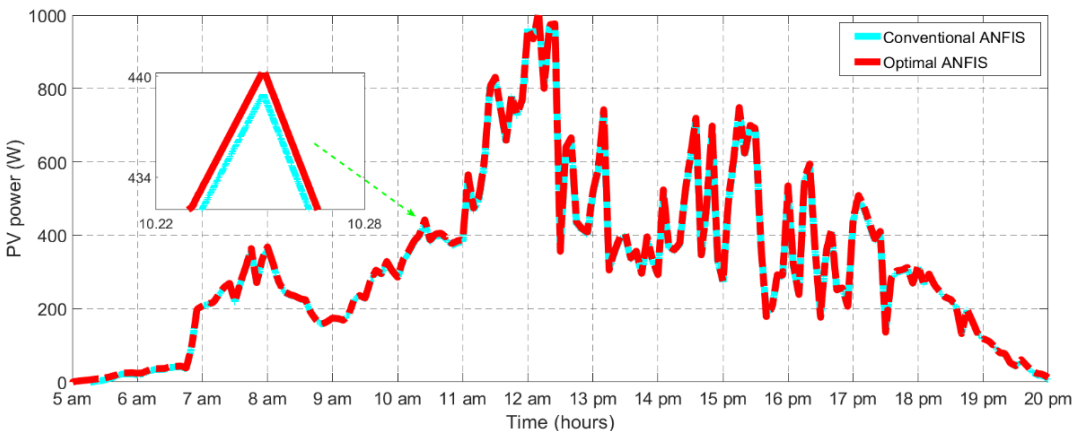
**Figure 5.11. Real measurement test of one day of: (a) irradiance, and (b) temperature.**



(a)

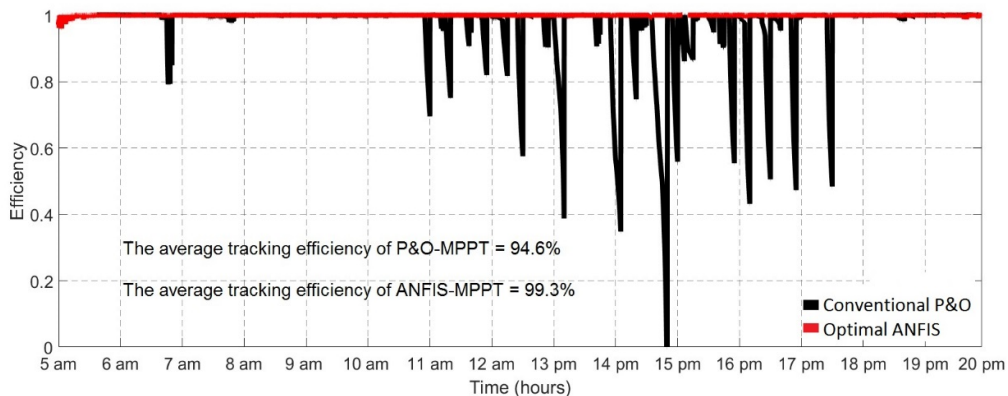


(b)

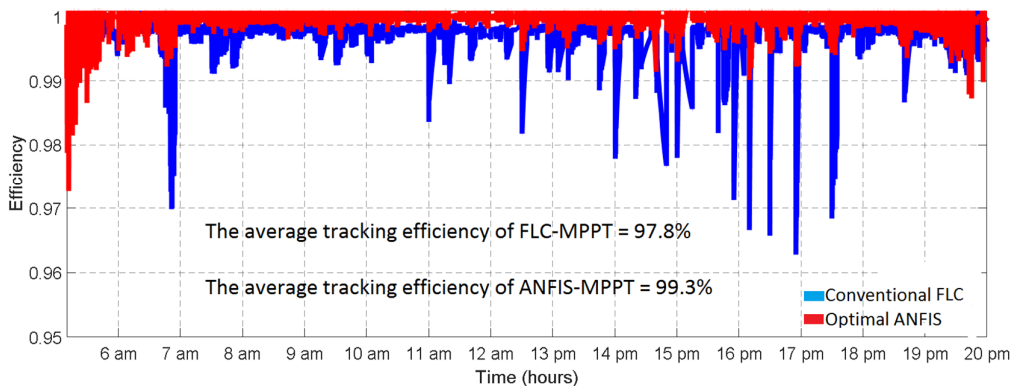


(c)

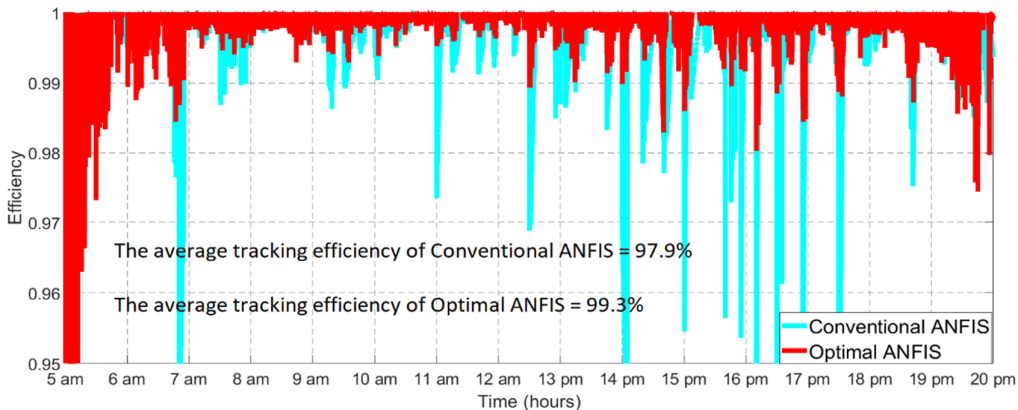
**Figure 5.12. MPPT power for: (a) P&O versus the optimal ANFIS, (b) FLC versus the optimal ANFIS and (c) conventional ANFIS versus the optimal ANFIS.**



(a)



(b)



(c)

**Figure 5.13. The average efficiency of the generated power of PV array under the real measurement test for: (a) P&O versus optimal ANFIS; and (b) FLC versus optimal ANFIS and (c) conventional ANFIS versus optimal ANFIS.**

## 5.9 Summary

An efficient maximum power point tracking technique based on ANFIS using a real photovoltaic system data has been designed in this Chapter. The large training dataset was collected during one year from the experimental testing of a PV array installed at Brunel University, London, UK, and then, they are analysed and optimised using a fitting curve technique to avoid the system from having a high training error. The solar irradiation and ambient temperature are selected as the input, whilst the maximum available power from the PV array is the output of what is termed the ANFIS model. Under the same weather conditions, actual PV power is measured using a sensed voltage and the current of a PV Simulink operation. These two power outputs are compared, and the error is given to PI controller to generate the signal of a DC-DC converter by the PWM generator, to adjust the operating MPP point of the PV array.

To sum up, a literature review on ANFIS-MPPT for a PV system has been presented. The methodologies of collected and optimized data and the tuning of proposed ANFIS model were explained. The P&O-MPPT, FLC-MPPT and the proposed ANFIS method were simulated, being then compared, regarding their popular features. The real test outcomes for semi-cloudy day were used to calculate the efficiency of the proposed technique under varying weather conditions. The results have demonstrated that the proposed method exhibits higher generated power, and no deviation from the optimized MPP point during different climate conditions than the alternative ones proposed, achieving efficiencies of greater than 99.3%. Finally, the implementation of this proposal can be considered simpler than hybrid methods.

## Chapter 6

### An optimised Neural Network for Predicting the MPP

In this Chapter, a feedforward Artificial Neural Network (ANN) technique using experimental data is designed for predicting the maximum power point of a photovoltaic array. An ANN model training strategy is challenging due to the variations in the training and the operation conditions of a photovoltaic system. In order to improve ANN model accuracy, the Particle Swarm Optimisation (PSO) algorithm is utilised to find the best topology and to calculate the optimum initial weights of the ANN model. Hence, the dilemma between computational time and the best-fitting regression of the ANN model is addressed, as well as the mean squared error being minimised. Experimental data of a sunny and cloudy day are utilised to determine the average tracking efficiency of this proposed method under varying atmospheric conditions.

#### 6.1 State of the Art

The ANN approach is the leading technique used in PV-MPPT applications, because it is able to predict the MPP of PV arrays accurately under various weather conditions [148]. Unfortunately, as aforementioned, the ANN model training strategy is challenging in relation to designing the optimised ANN-MPPT controller for PV systems due to the variations in the training data and operation conditions. In order to improve model accuracy, several researchers have proposed various optimisations, among them Hiyama et al. [87] presented a novel methodology based on a regression analysis method to select effective data for training an ANN-MPPT model. The data set was collected from experimental tests of a PV array installed at Kumamoto University, Kumamoto, Japan, for one year and then, the measured data for two days with a widely varying weather conditions were selected. This proposal gives accurate predictions when compared with an ANN-MPPT based on the total data. Afin and Akkaya [88]

used a genetic algorithm (GA) to select automatically the effective data among all those collected, resulting in a smaller mean squared error of the ANN training network. Simulation and experimental results confirmed that this proposed conception is effective for working with PV systems.

In [89], Chaouachi et al. classified the real data of a PV system installed in Tokyo, Japan, into three multi-layers based on a fuzzy rules-based before they fed them into an ANN for offline training. The results of this proposed method reveal that it achieves the highest efficiency when compared to the conventional ANN and P&O algorithms under different climatic conditions. With the same idea, Fathabadi [149] used the Lambert W function with a feed foreword ANN technique to calculate the characteristics of silicon and plastic PV cells. The major contribution of this method is that it enhances the performance of the ANN model in predicting the PV curve.

In [150], Akkaya et al. used the GA to optimise the size of the hidden layer of an ANN model using an evolutionary hybrid algorithm, which resulted in minimising the mean squared error of the ANN training. The experimental results prove that the proposed method is efficient for controlling PV systems under varying atmospheric conditions. Similarly, Af et al. [151] used the GA to find the optimal numbers of neuron nodes for a multi-layer neural network. The results demonstrated that the proposed technique is valid in that comparison between the practical and simulation results showed good agreement. In the same vein, Zhang and Bai [152] adapted the GA to find the optimal number of a radial basis function ANN for modelling PV arrays. The results proved that the proposed method can accurately predict optimised PV power under various conditions. Hamdi et al. [153] the authors used a particle swarm optimisation (PSO) algorithm instead of the GA one to find the main parameters of the radial basic function of an ANN network using a novel adaptive strategy. The results provided evidence that the proposed method enhances the efficiency of MPPT tracking.

However, the selecting the effective training data and determining the topology of ANN model whose report in previous proposals are considered basic criteria to enhance their performance. Hence, Duman et al. [61] used a hybrid PSO gravitational search algorithm (GSA) to calculate a suitable activation function of ANN layers, resulting in the achievement of an accurate power prediction. Unfortunately, this modification is classified as a complex method. There are novel optimisations based on the Grey Wolf and Bee Colony algorithm that have been proposed in recent years, which have been used to enhance the performance of AI techniques such as [154]–[156]. In this work, PSO is utilised to improve the accuracy of ANN

model due to its sampling technique and fast optimisation delivery. The rest of this Chapter is organised as follows: Sections 6.2 presents a schematic diagram of PV system based on optimised ANN-MPPT controller. Sections 6.3 and Section 6.4 cover the principles the feedforward ANN technique and PSO algorithm, respectively. Section 6.5 explains the training of proposed ANN model. In Section 6.6, the results are provided. Experimental measurement test results for sunny and cloudy days are provided and discussed in Section 6.7, whilst Section 6.8 presents the comparative study based on the properties of the proposed methods in this thesis. Finally, Section 6.9 contains the summary of this Chapter.

### 6.2 Optimised ANN-MPPT Method

In this Chapter, a feedforward ANN technique is employed to predict the maximum power point (MPP) of a PV array using a large real training dataset, as shown in Figure 6.1. Those data are collected from experimental tests on a PV array installed at Brunel University London, Uxbridge, United Kingdom, as mentioned in Chapter 5. To optimise the training strategy of the ANN model, the PSO algorithm is utilised. This strategy is divided into two parts: determining the right topology and then, optimising the initial weights of the feedforward ANN model. That is, the issue between the computational time and the best-fitting regression of the distribution of the ANN nodes is solved in the first part, while the global minimum training error of the ANN model is addressed in the second. Consequently, the predicting function of the proposed ANN method is improved under various weather conditions. The irradiance ( $G_x$ ) and temperature ( $T_x$ ) of the atmospheric conditions are used as the inputs of the proposed ANN model, whilst the predicting power ( $P_{ref.}$ ) is the output.

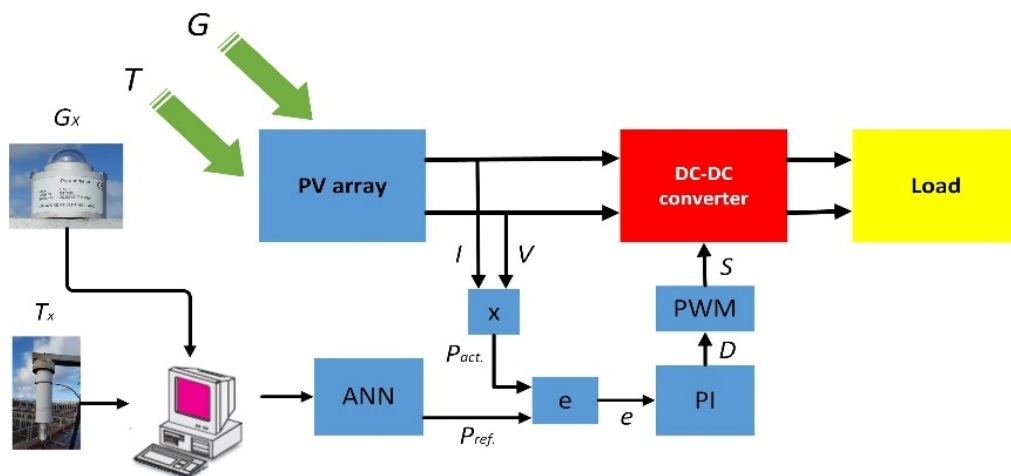


Figure 6.1. General diagram of a stand-alone PV system using an ANN-MPPT method.

This regulates the  $D$  of a DC-DC boost converter after being compared with the PV's actual power ( $P_{act.}$ ) using a proportional-integral (PI) controller. The  $D$  is converted into the signal ( $s$ ) of the DC-DC converter using a pulse-width modulation generator (PMW) to regulate the operating MPP of the PV array. As mentioned in chapter 5, the signal control ( $s$ ) of the PI controller is given by Eq. (5.8).

### 6.3 ANN Algorithm

An ANN technique is a distributed processing technique, which is able to save experimental knowledge of application systems [157]. It does not require a good knowledge when modelling an application system, but it does need accurate data to predict output functions as close to reality. This algorithm converts the training data to a non-linear mapping between inputs and output nodes. ANN topology is classified in to two types: feedforward and feedback networks. The first type is the most commonly deployed due to its usage of less memory in the implementation stage [158]. Furthermore, it has proven to be highly powerful when working with non-linear systems, such as a PV array. The feedforward ANN is also classified into three kinds includes single layer, multilayer and radial basis function nets. The multilayer feedforward ANN is the most popular type because it has a high ability to determine the weighting of hidden layer [159].

In general, the multilayer feedforward ANN has three layers, input, hidden and output, as shown in Figure 6.2. Moreover, the neurons of each layer are connected through the weights of the other neurons and bias terms in the antecedent layers. This distributed processing system is defined mathematically by Eq. (6.1):

$$y = \sum_{i=1}^n w_{ij}x_j + b_j \quad (6.1)$$

where,  $x_j$  is the input training node,  $w_{ij}$  are the connection weights associated with the input, hidden and layer nodes,  $b_j$  is the bias of the hidden and the output layer nodes and  $n$  is the number of input signals. A sigmoid activation function is frequently utilised to determine the hidden layer input and target the hidden layer output. To learn the process of a feedforward ANN system, the back propagation (BP) algorithm is used. It is a complex gradient algorithm deployed for enhancing the performance of the ANN by changing the weights of each node and the bias terms until the output value at the output layer predicts the actual outputs as closely as

possible, thus resulting in a reduction in the training error. The mean squared error (MSE) is usually chosen as the cost function, which is given by Eq. (6.2):

$$MSE = \frac{1}{n} \sum_{i=1}^n \sum_{j=1}^m [Y_j(i) - T_j(i)]^2 \tag{6.2}$$

where,  $n$  is the number of input data,  $m$  is the number of output signals,  $Y_j(i)$  is the real output, and  $T_j(i)$  is the target output. There are two main issues when designing a feedforward ANN: finding the best topology of its structure (the number of hidden layers and units in these); and optimising the initial weights of the training nodes.

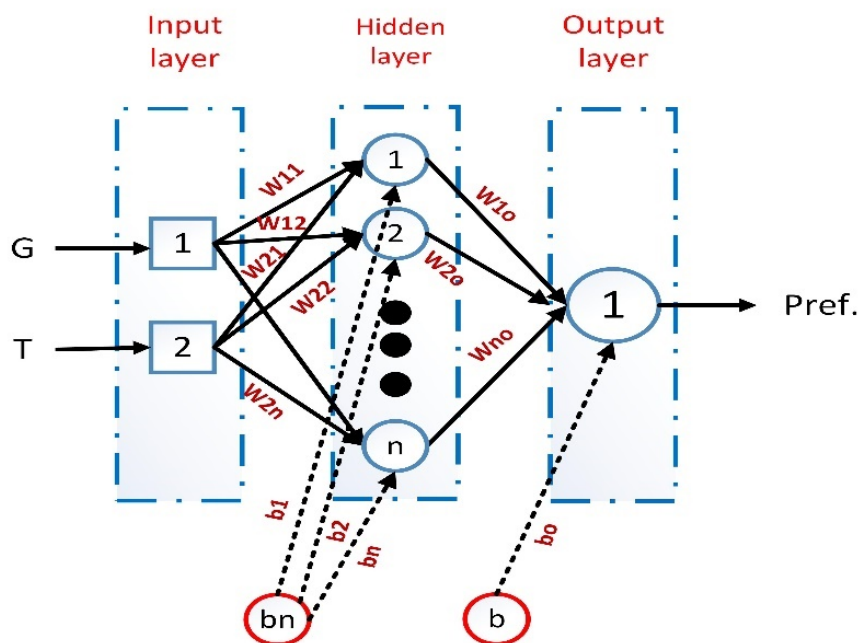


Figure 6.2. Block diagram of an ANN system.

### 6.3.1 Hidden Layer Size

Calculating the optimum number of hidden layers and units in each is an important task for the feedforward ANN design, as this addresses the issue between the computational time and best fitting regression of the distribution of the ANN nodes [150]–[153], [160]. If the ANN model has too many units in the hidden layers, the computational time becomes too long, thus resulting in an over fitting regression. In contrast, if the ANN model has too few units in hidden layers, then it will have low computational time when there is a linear fitting regression. The most common method for finding the hidden layer size is a trial and error technique. However, this technique is inadequate as it requires a very long time.

### 6.3.2 Initial Training Weights

As aforementioned, the BP algorithm is used to learn the process of the feedforward ANN model based on searching an error surface. This processing search is changing as gradient descent regarding to the incremental change in the weight ( $\Delta W$ ), As explained in Eq. (6.3);

$$w_{ji}^l(t) = \eta w_{ji}^l(t-1) + \mu \Delta w_{ji}^l(t) \quad (6.3)$$

where  $w_{ji}^l(t)$  and  $w_{ji}^l(t-1)$  are the current and previous assumed training weights, respectively,  $\eta$  is the learning rate and  $\mu$  is the momentum coefficient. Each iteration in the BP algorithm has two steps: a forward step to produce an updating solution; and a backward step to compute and modify the MSE to new weights based on Eqs. (6.2) and (6.3). This procedure continues until the optimal training weights of the ANN model are determined. Many studies have pointed out that this method will be failed to find the optimised training weights, because it mostly depends on the size of  $\Delta W$  [160]–[162]. If  $\Delta W$  is large, this can lead to accelerate training and large fluctuating research on the error surface, thus resulting in a non-converged optimising solution. Conversely, if  $\Delta W$  is small, this can lead to slower training and smooth fluctuating research on the error surface, which could mean that the training process is stopped before the global minimum error is found. Regarding this concept, the assumed initial weights play a crucial role in designing an accurate ANN model.

### 6.4 PSO Algorithm

The PSO algorithm is considered a high-quality search tool in engineering applications[163]. The principle idea of this algorithm is that it tries to find an optimised area, where each space has a degree of possibility for a candidate solution [164]. The movement of the PSO algorithm is inspired from the behaviour of birds flocking, which depends on the individual and neighbouring experiences of the PSO optimiser during each particle step. The procedure of the PSO algorithm is divided into four steps, as shown in Figure 6.3. In the first, the PSO optimiser starts the search within a random particle value. This particle value is selected based on the degree of possibility of solution spaces regarding several varying optimisations. In the second step, it compares the previous and next best fitness values ( $P_{bi}$ ) and ( $P_{li}$ ), respectively, to search for optimised solutions in the same space. In the third step, the best and global best positions ( $G_{bi}$ ) are compared to select the global fitness value. During this step, these positions are adapted and recorded for the next step mathematically, as defined by Eqs. (6.4) and (6.5):

$$V_i^{k+1} = w \times V_i^k + r_1 \times c_1 \times (P_{bi} - X_i^k) + r_2 \times c_2 \times (G_{bi} - X_i^k) \quad (6.4)$$

$$X_i^{k+1} = X_i^k + V_i^k \quad (6.5)$$

where,  $X_i$  is the current position of each particle,  $V_i$  is the speed of the search space,  $i$  is the optimisation vector,  $k$  is the number of iterations.  $w$  represents the inertia weight factor of the speed,  $c_1$  is the cognitive coefficient of the single particles,  $c_2$  is the social coefficient of all the particles and  $r_1$  and  $r_2$  are the random velocity values of the search space in the range 0 to 1. In the fourth step, the best particle in terms of the fitness evaluation is determined and saved to enhance the particle movement steps in each iteration. Those steps continue to work until a stopping condition is achieved or the number of iterations has ended. The stopping condition and the number of iterations are proposed based on the required accuracy of the system and control processing time.

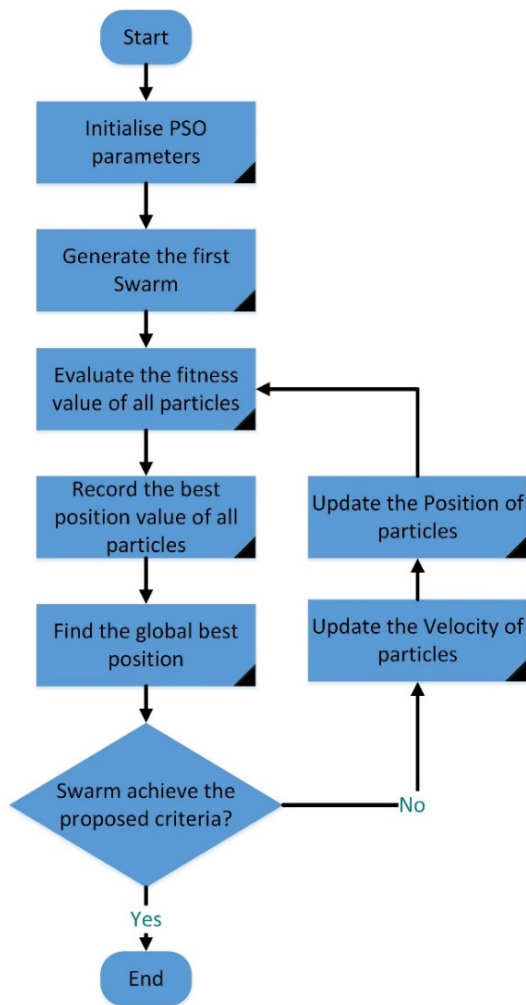


Figure 6.3. The Flowchart of a PSO algorithm.

### 6.5 Training of ANN Model

Using a MATLAB-Simulink model, an intelligent ANN-MPPT technique based on a large and real data set of a PV system is proposed. These data are collected from the PV system installed at Brunel University London, as explained in Chapter 5. The inputs of the ANN method consist of the G level and T operation of climatic conditions, while the maximum power measurement of the PV installed array at the MPP is the output. As mentioned earlier, the accurate prediction of PV power using the ANN technique mostly depends on the training strategy of ANN network. This starts with selecting the topology of the ANN model and then, optimising its initial weight values. To address this strategy, two algorithms are developed in the form of a hybrid PSO-ANN technique. The parameters of the PSO optimiser are set as having the following values:  $c1 = 1.49618$ ,  $c2 = 1.49618$ ,  $w = 0.7298$ ,  $k = 50$  and the swarm size = 20. In addition, the transfer function is utilised as object function of the PSO algorithm. A schematic diagram of the training methodology of the PSO-ANN algorithm is presented in Figure 6.4.

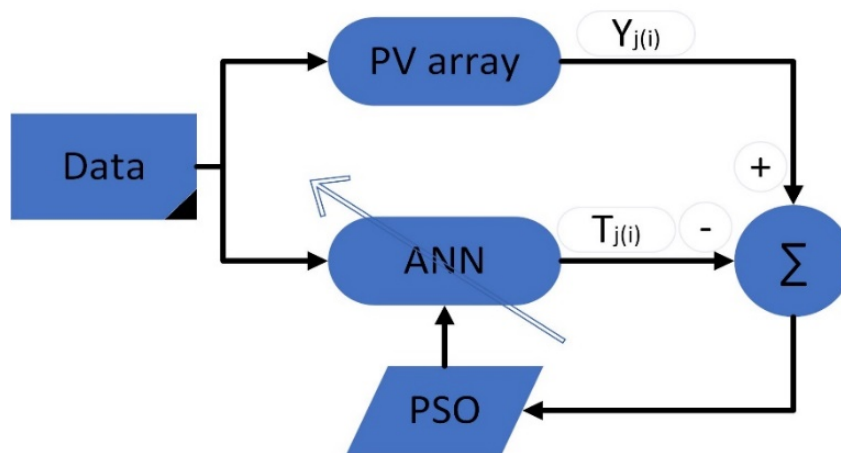


Figure 6.4. Schematic diagram of the training methodology.

#### 6.5.1 PSO-ANN algorithm - selected as the best topology of an ANN network

In the first part of this modification, the PSO algorithm is employed with the ANN model to find the best topology of the feedforward ANN network. Hence, a hybrid algorithm is used to test progressively increase the number of neurons in hidden layer without requiring the user to preselect the number, which may be inaccurate. The main steps of this are provided in Table 6.1. The lower and upper boundaries of the neuron numbers in this algorithm are 10 to 20. In

this work, one hidden layer with two inputs and one output of the neural network is achieved with minimum training error, while the optimised number of neurons in it is 18 neurons. This topology will be used in the second modification to find the optimal initial weights of the ANN model.

**Table 6.1. The main steps of the first proposed algorithm to find the optimised topology of the ANN.**

Step	Command
1	Load data;
2	Set the number of the hidden layer;
3	Set the main parameters of the PSO algorithm
4	Initialise the random number for the neurons of the hidden layer;
5	Generate (for loop) to calculate the MSE for each particle using “netff”, “train” and “net” commands and Eq. (6.2);
6	Update the MSE value for each particle;
7	Compare the $P_{ji}$ with the $P_{bi}$ of the PSO algorithm for each particle;
8	Compare the $P_{bi}$ with the $G_{pi}$ of the PSO algorithm for each particle;
9	Update the velocity and position values of the PSO algorithm by Eqs. (6.4) and (6.5);
10	If the maximum iterations are reached or the stopping condition is achieved, print the result (the number of neurons of the hidden layer), otherwise return to step 5.

### 6.5.2 PSO-ANN algorithm - determining the initial weights of the ANN model

Once the topology of ANN network has been selected, a hybrid algorithm based on the PSO and ANN method is designed to find the optimised initial weights of the ANN model. These are determined to improve the output prediction of the model when the assumed initial weight values are correcting. To this end, the PSO algorithm is utilised with the ANN technique. The main steps of the hybrid algorithm are described in Table 6.2. The lower and upper boundaries of the weight values in this algorithm are - 0.9 to 0.9. As a result of running this hybrid algorithm the optimised initial weights are obtained. The search history of the algorithm is presented in Figure 6.5. Then, the optimal initial weights are used to train the ANN model using the “nntool” command of MATLAB. Next, the optimised initial weights are replaced

with the standard training weights in a field of the initial weights of the “nntool” box. Consequently, the performance of the ANN model based on the optimised training strategy using the real data achieves better prediction than with a conventional ANN. This is because of its MSE and lesser number of epochs, about 0.00068 and 17 respectively, while those of the non-optimal ANN are about 0.0079 and 68, respectively, as shown in Figure 6.6. Table 6.3 presents the rudimentary statistical analysis of the proposed algorithm. Notably, this proposal is simpler to design, because it does not need an extra unit in the implementation stage to improve its accuracy.

**Table 6.2. The major steps of the second proposed algorithm to find the initial weights of the ANN.**

Step	Command
1	Load data;
2	Set the testing and training samples,
3	Select the number of neurons in the hidden layer regarding to the first modification;
4	Set the number of initial weights of the ANN;
5	Set the main parameters of the PSO algorithm;
6	Generate (for loop) to calculate the random weights of the ANN using “netff”
7	Generate (for loop) to determine the optimised initial weights after training the ANN using the “neural_model” “findfitness”, “train” and “net” commends.
8	Calculate the MSE value based on Eq. (6.2) for each particle;
9	Update the MSE value for each particle;
10	Compare the $P_{ji}$ with the $P_{bi}$ of the PSO algorithm for each particle;
11	Compare the $P_{bi}$ with the $G_{pi}$ of the PSO algorithm for each particle;
12	Update the velocity and position values of the PSO algorithm by Eqs. (6.4) and (6.5);
13	If the maximum iterations are reached or the stopping condition is achieved, print the result (the optimal initial weights of the ANN), otherwise return to step 7.

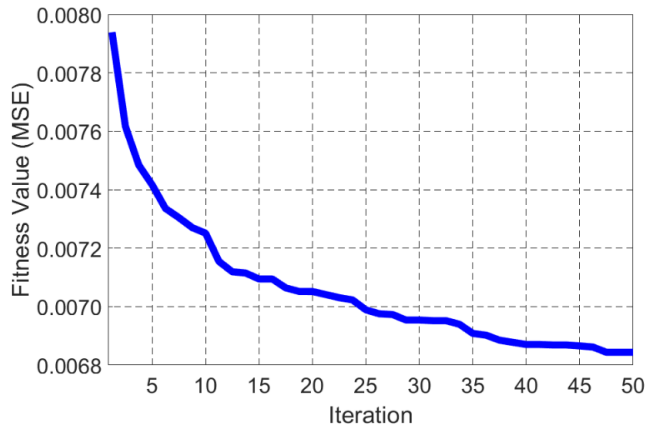
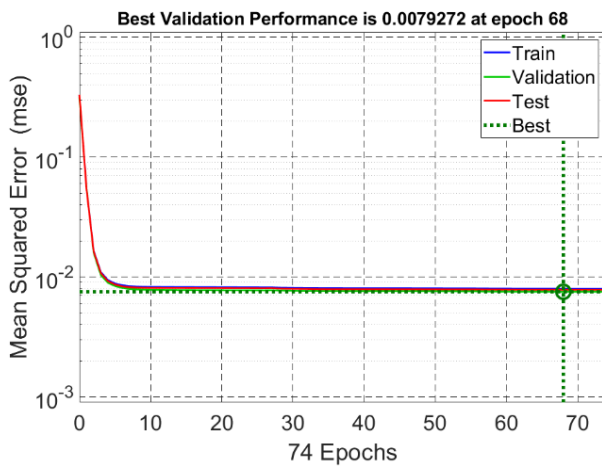
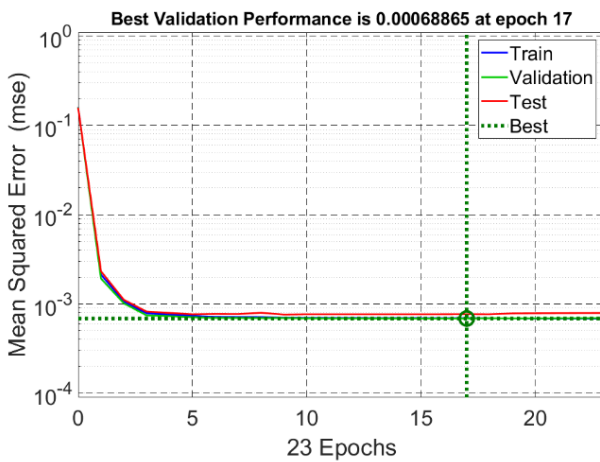


Figure 6.5. The search history of the PSO-ANN algorithm.



(a)



(b)

Figure 6.6. The best validation performance of (a) the conventional ANN and (b) the optimised ANN.

**Table 6.3. The rudimentary statistical analysis of the proposed algorithm.**

<b>Training no.</b>	<b>ANN Topology</b>	<b>The number of weights and biases</b>	<b>Average +Standard deviation of MSE</b>
1	2:10:1	41	$0.00795 \pm 1.2 \times 10^{-3}$
2	2:12:1	49	$0.00781 \pm 1.8 \times 10^{-4}$
3	2:20:1	81	$0.00678 \pm 1.4 \times 10^{-4}$
4	2:17:1	67	$0.000769 \pm 3.22 \times 10^{-5}$
5	2:18:1	73	$0.000689 \pm 1.03 \times 10^{-5}$

## 6.6 Results and Discussion

To assess the performance, a MATLAB/Simulink model for the studied PV system is designed for three popular methods, namely, conventional P&O, FLC and ANN-MPPT as well as the proposed ANN-MPPT method. This PV system consists of a PV array, DC-DC boost converter with the MPPT controller and resistive load, whilst the array consists of five PV modules connected in series. The parameters of this PV system are determined and given in Chapter 5. The solar irradiance, which used in this simulation, is rapidly decreased from 1000 to 200 W/m<sup>2</sup> at 1 to 2 s and then, it is increased from 200 to 1000 W/m<sup>2</sup> at 3 to 4 s, as shown in Figure 6.7, whilst the temperature is kept constant at 25 °C.

As presented in Figure 6.8(a), the predictive power of the proposed ANN method addresses the right direction of input solar irradiance during varying atmospheric conditions owing to its optimised training strategy. In addition, it is a more robust in delivering the optimal MPP under increasing and decreasing radiation. Whereas the conventional methods for the ANN, FLC and P&O techniques drifts away from the right direction when the input irradiance rapidly changed, as presented in Figure 6.8(b). Notably, although this phenomenon is very effective on the conventional P&O-MPPT method by comparison with the conventional ANN and FLC-MPPTs, it almost avoids the problem when the input irradiance decreases rapidly.

Another advantage of this proposed controller is that its converging time to reach the tracking power from the transient state into steady state conditions is the fastest when compared with the conventional ANN, FLC and P&O-MPPT methods, being about 0.06s, 0.08 s, 0.11 s and 0.13 s, respectively, as shown in the zoomed in part of Figure 6.8(a). Moreover, the fluctuation around the MPP for the steady-state conditions of the proposed ANN method is the lowest by comparison with the other methods, thus resulting in less consumption time, as shown in the zoomed in part of Figures. 6.8(a) and (c). Furthermore, it is more precise at

predicting the MPP under steady-state conditions, because the optimal MPP duty cycle of the proposed method is more centred than those of the conventional methods.

Whilst the MPP duty cycle of the conventional ANN and FLC-MPPT methods are to the left and right of the optimal MPP duty cycle of the conventional P&O-MPPT method, respectively. Consequently, the dissipated power in the proposed ANN-MPPT method is the lowest when compared with the conventional ANN, FLC and P&O-MPPT methods. Hence, the tracking power of the proposed ANN-MPPT method along with those of the conventional ANN, FLC and P&O-MPPT methods, after they have reached the MPP, is about 924.60, 924.00 W, 923.25 W and 922.50 W, respectively, as shown in the zoomed in part of Figure 6.8(a). Table 6.4 reports a comparative study covering the main properties of the conventional ANN, FLC and P&O-MPPT methods as well as the optimised ANN-MPPT. Regarding this Table, the converging time and tracking power of the proposed method are the fastest and highest, when compared with the conventional ANN, FLC and P&O methods. In addition, the fluctuation around the MPP is the least of all the methods. Moreover, the predicting power of the optimised ANN avoids the drift problem under instability conditions.

**Table 6.4. A comparative study covering the main properties of the conventional ANN, FLC and P&O-MPPT method as well as the optimised ANN-MPPT.**

MPPT	Tracking time (s)	Oscillation	Power (W)	Drift Problem
Optimised ANN	0.06	Low	924.60	Avoidance
Conventional ANN	0.08	Low	924.00	Suffering
Conventional FLC	0.11	Medium	923.25	Suffering
Conventional P&O	0.13	High	922.50	Suffering

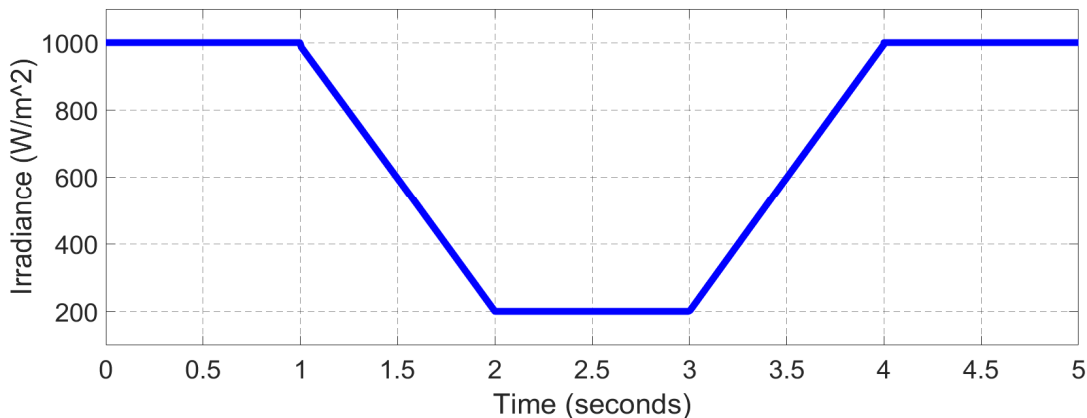
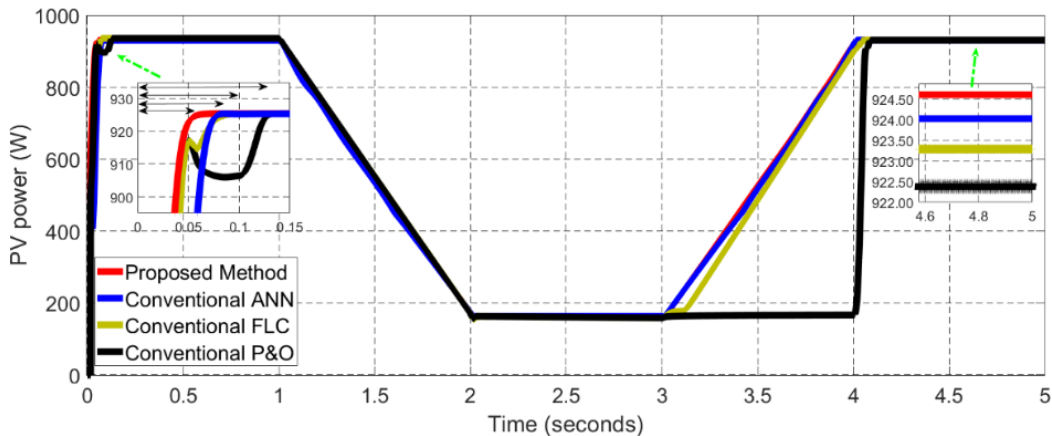
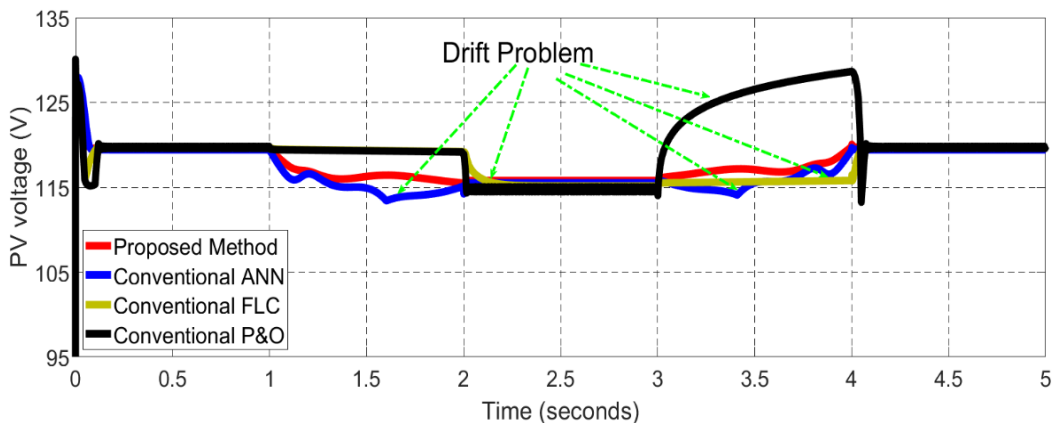


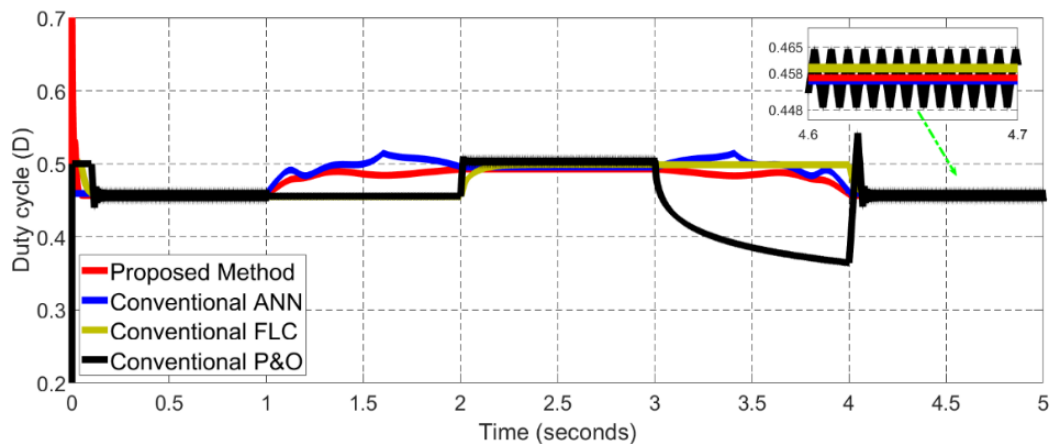
**Figure 6.7. The irradiance level of weather conditions.**



(a)



(b)



(c)

Figure 6.8. PV array system for the proposed method versus the P&O, FLC and ANN methods under theoretical climate conditions: (a) power, (b) voltage, and (c) duty cycle.

## 6.7 Experimental Measurement Tests

To assess the prediction of the proposed ANN method under different climatic conditions, experimental measurement tests of a sunny and a cloudy day on 5<sup>th</sup> July 2018 (06.00 - 19.00) and 30<sup>th</sup> July 2018 (06.00 -19.00), respectively, have been used. The irradiance and temperature of those days are presented in Figures. 6.9(a) and (b). Then, these are applied to the studied PV system with the conventional P&O, ANN and FLC-MPPTs as well as the optimised ANN method, as shown in Figures 6.10 and 6.11.

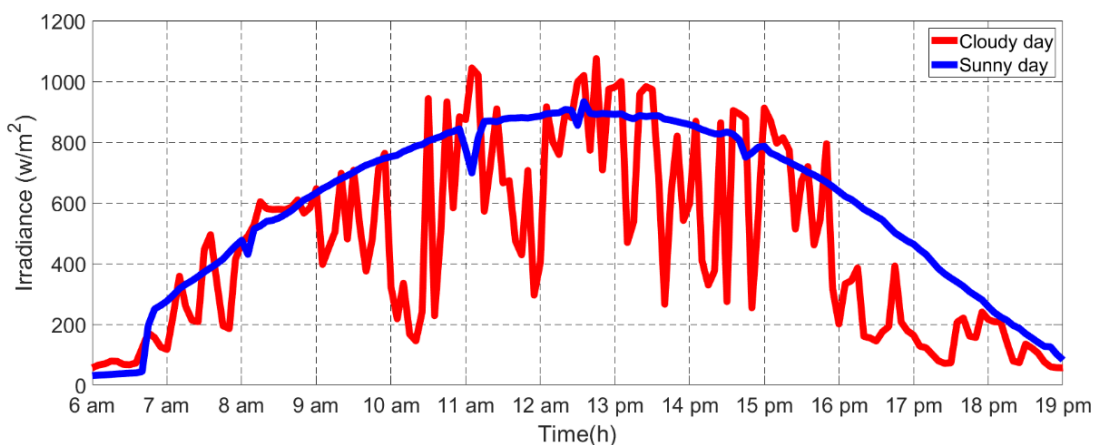
In the first case, the predictive power of the conventional P&O method finds the right direction of the input weather conditions on the sunny day; however, it drifts away from the right prediction on the cloudy day, as presented in the zoomed in parts of Figures. 6.10(a). The issue becomes worse regarding the power of the conventional P&O method, when the solar G of the cloudy day is rapidly changed, as shown in Figure 6.11(a). In the second case, when comparing the proposed ANN method with the conventional FLC one, the predicting power of the latter method suffers from the deviation on both the sunny and cloudy days, as shown in the zoomed in part of Figures. 6.10(b) and 6.11(b). However, the problem can be seen as having a minimum effect when compared with the conventional P&O method.

In the third case, whilst the drift problem seems to have very little effect on the power prediction of the conventional ANN method on both days, it is inaccurate to track the MPP, as shown in the zoomed in part of Figures. 6.10(c) and 6.11(c). Notably, the prediction function of the conventional ANN on the cloudy day has a higher deviation when compared with that on the sunny day. In contrast, the power prediction of the proposed ANN method is as close to the reality during both sunny and cloudy days due to its optimised training strategy.

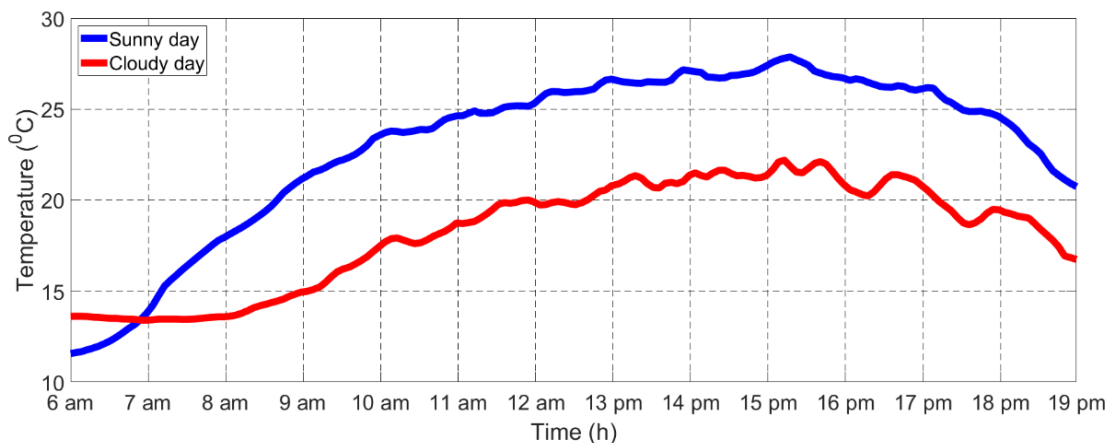
To determine the tracking efficiency of the MPPT methods, the average MPPT efficiency formula based on tracking time is usually used, as given in Eq. (4.9). However, a sample time has been used in this chapter instead of the tracking time. This is because the average MPPT efficiency formula based on the sample time can present the comparative results of several MPPT methods clearly, especially in the case of various experimental tests. The actual and theoretical output power of MPPT method are divided into 12 samples for each hour to calculate the prediction efficiency of the MPPT methods under varying atmospheric conditions. As presented in Figures. 6.12(a), and (b), as well as Table 6.5, the hourly average efficiency of the proposed method achieved the highest efficiency on both sunny and cloudy days by comparison with the conventional ANN, FLC and P&O-MPPT techniques.

**Table 6.5. Comparative study regarding the hourly average efficiency for the proposed method and the conventional ANN, FLC and P&O-MPPT techniques.**

Atmospheric	Average efficiencies			
	Proposed method	Conventional ANN	Conventional FLC	Conventional P&O
Sunny day	99.68%	99.17%	98.90%	98.18%
Cloudy day	99.30%	97.43%	94.69%	88.21%

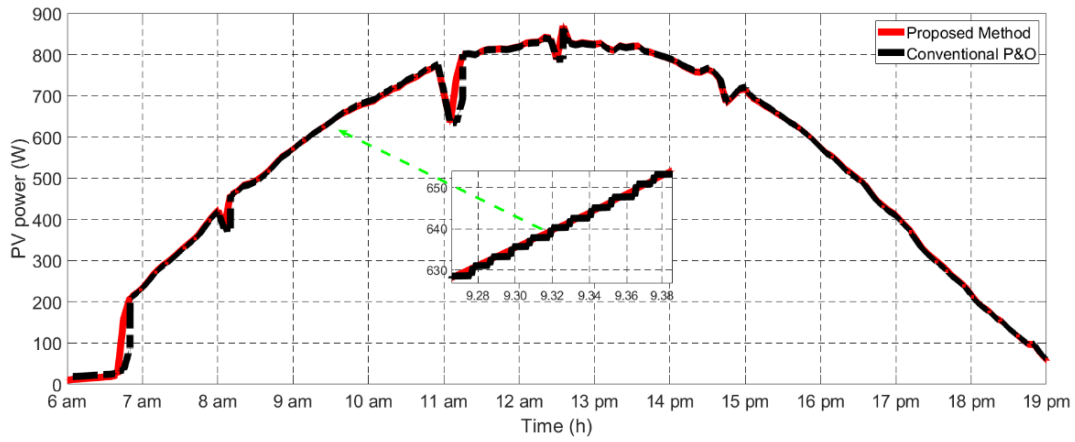


(a)

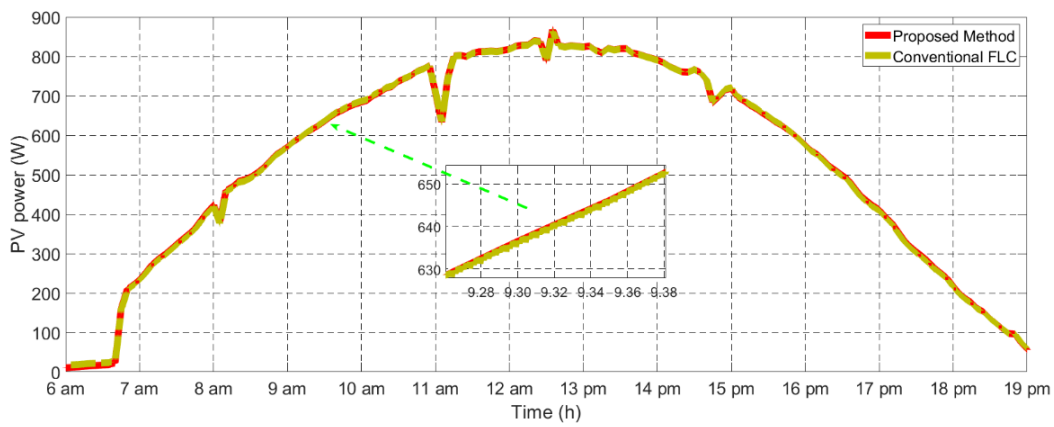


(b)

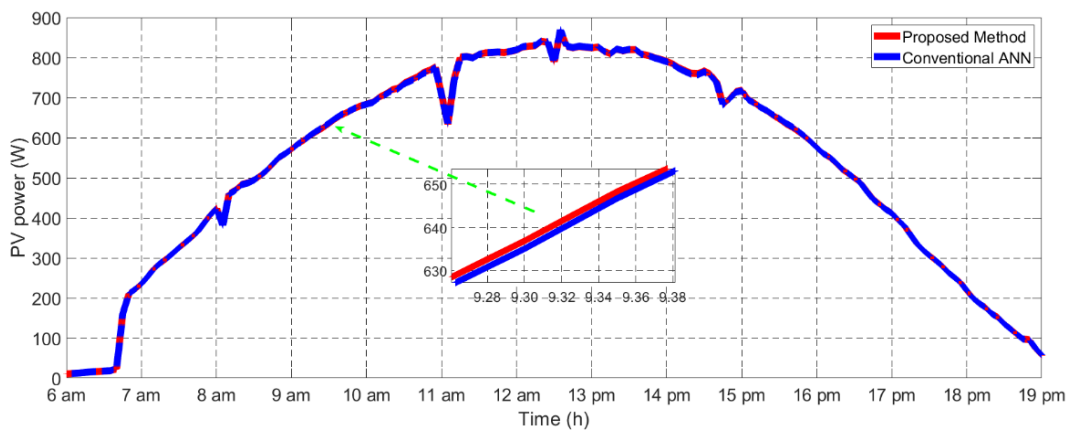
**Figure 6.9. Experimental measurement tests for a sunny and a cloudy day of: (a) irradiation; and (b) temperature.**



(a)



(b)



(c)

**Figure 6.10. MPPT predicting power on a sunny day using the proposed method versus: (a) the conventional P&O method; (b) conventional FLC method; and (c) the conventional ANN method.**

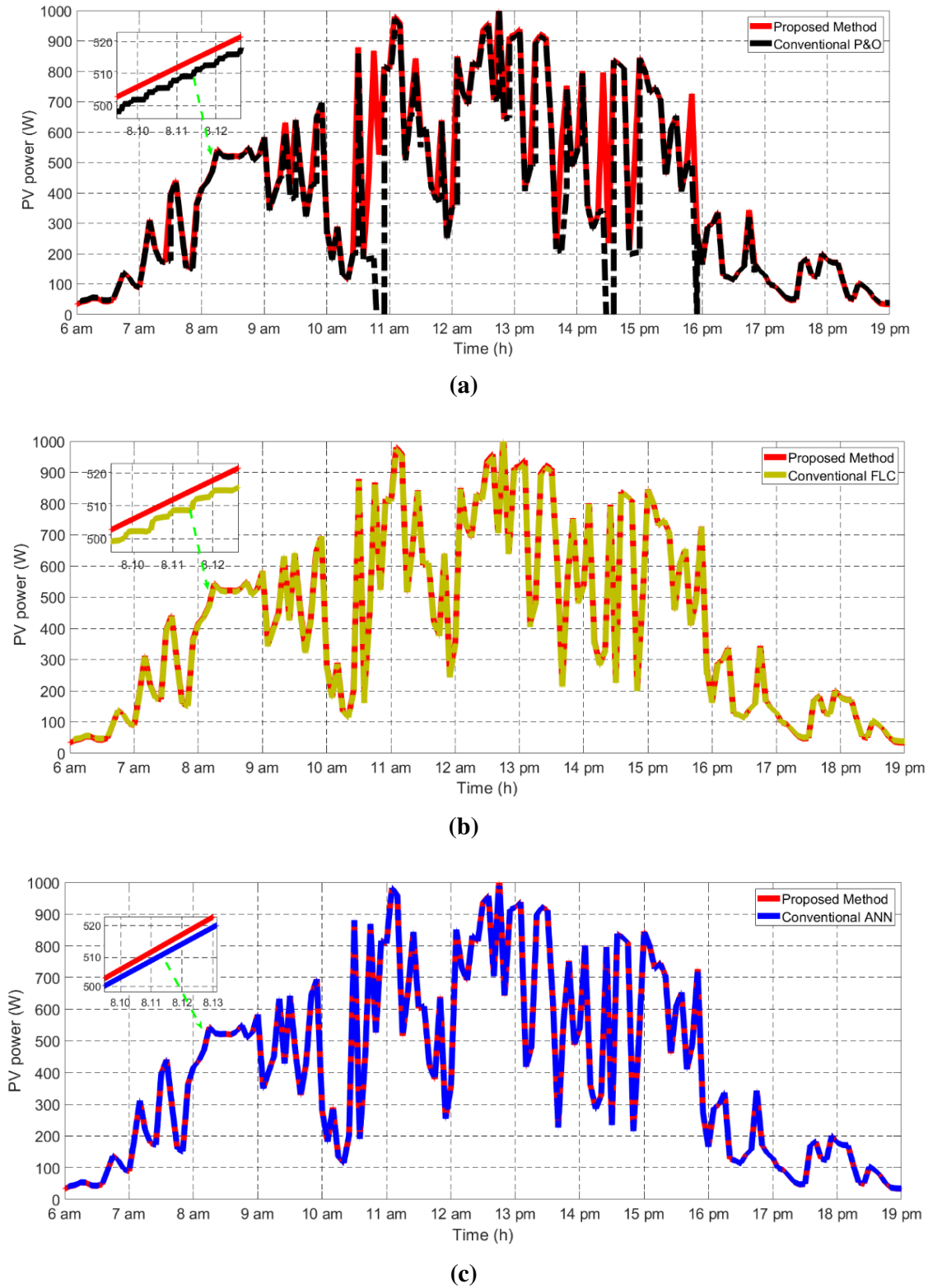
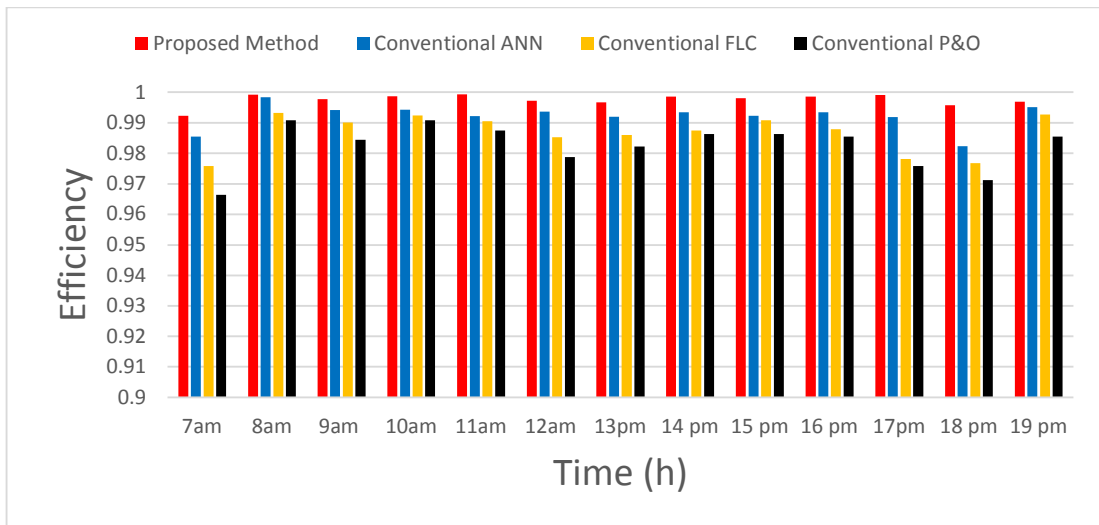
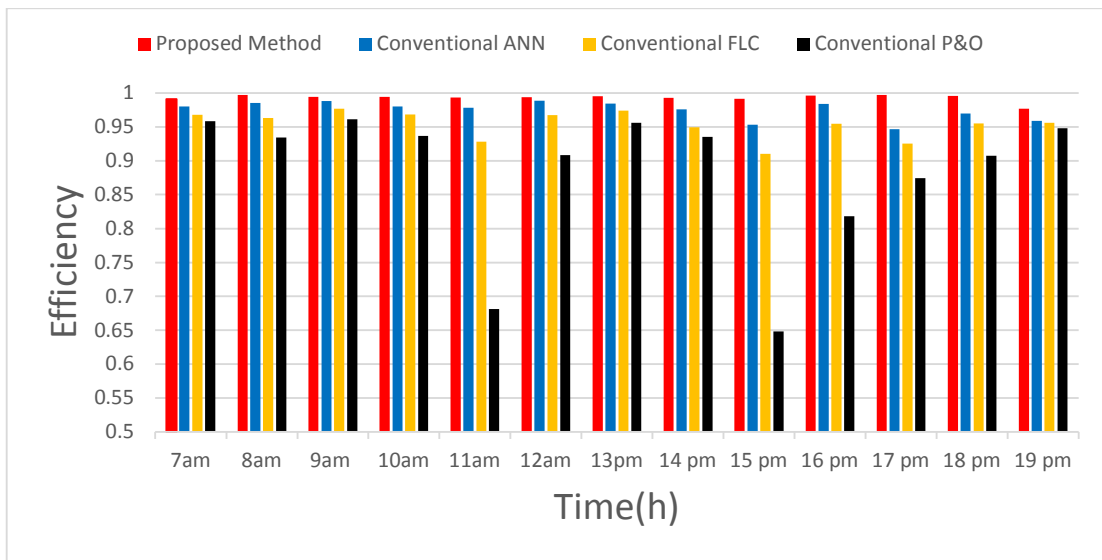


**Figure 6.11. MPPT power prediction on a cloudy day using the proposed method versus: (a) the conventional P&O method, (b) conventional FLC method; and (c) the conventional ANN method.**



(a)



(b)

**Figure 6.12.** The average efficiency of the predicting power for the conventional P&O, FLC and ANN as well as the proposed method on a (a) sunny day and (b) cloudy day.

### 6.8 Overview of the Proposed Methods

According to the results of the proposed methods in this research, the better MPPT controller for PV applications is the optimised training ANN technique using the particle swarm optimisation when compared with the optimal tuning ANFIS technique based on the

curve fitting technique, if the installed PV system data is available. This is because it achieves a higher tracking efficiency about 99.67 % and 99.30 % under the sunny and cloudy day, respectively, while the optimal tuning ANFIS technique achieves about 99.30 % under semi-cloudy day, as well as the tracking time being minimised about 0.01s. This is because of its training error is 0.00068, while the optimal ANFIS is 0.0706.

On other hands, the novel MPPT technique based on the FLC and P&O algorithm is an appropriate method to enhance the PV electrical generation when the very well knowledge of the PV systems is familiar for MPPT designers to design the fuzzy rules of proposed FLC-MPPT owing to its ability to track the MPP when there are big fluctuations of irradiation. Furthermore, it is the lowest complex implementation and least part units when compared with the other intelligent MPPT controllers. Consequently, it achieves the highest tracking efficiency under the EN 50530 standard test around 99.6 %. While the modified P&O-MPPT method has been designed for low-cost PV systems because it is a lower complex modification. As well as, it does not eliminate the oscillation nor avoid the drift problem completely.

### 6.9 Summary

An optimised feedforward artificial neural network technique based on the Particle Swarm Optimisation algorithm using real data has been utilised for modelling a current-voltage characteristic and predicting the maximum power point of photovoltaic arrays. This optimisation was divided into two parts: selecting the best topology and then, optimising the initial weights of the feedforward ANN model. Accordingly, the problem between the computational time and best-fitting regression of the distribution of ANN nodes was solved in the first part, whilst the mean squared error of the ANN model was reduced in the second optimisation. Consequently, the predicting power of the ANN-MPPT controller has been improved under various weather conditions when compared with the conventional ANN, FLC, and P&O methods.

In addition, the converging speed of the proposed method has been enhanced under a transient state. As a result, hourly efficiencies of more than 99.67% and 99.30% on sunny and cloudy days, respectively, have been achieved. Moreover, this controller also improves the stability and reliability of the PV generation when it connects to a grid. Furthermore, the optimisation has been demonstrated to be simple to design. To sum up, a state of the art of the ANN-MPPT for PV systems is advanced. the principles the feedforward ANN technique and PSO algorithm are covered, following by a schematic diagram of ANN-MPPT controller. The

training of proposed ANN model is designed, following by its results. Then, experimental data of a sunny and cloudy day are used to determine the average tracking efficiency of this proposed method under varying atmospheric conditions. Finally, an overview of results of proposed methods in this research is presented.

# Chapter 7

## Conclusions and Future Work

### 7.1 Conclusions

The efficiency, stability and reliability of a photovoltaic energy are considered major factors for establishing this energy resource on the market. In this research, common maximum power point tracking techniques, including perturb and observe, fuzzy logic control, adaptive neural-fuzzy inference system and artificial neural network have been proposed for a grid-connected PV system to maximise the output power of a PV array. The aim has also been improving the stability and reliability of a PV power conversion, especially in the context of a rapid change in atmospheric conditions. The following is an overview of the scope, main contributions and conclusions of the study.

- A comprehensive review of various PV-MPPT methods, including the CV, FOCV, P&O, IC, FLC, ANN, ANFIS and PSO techniques, based on their main features, has been presented. In addition, the advantages and disadvantages of each MPPT method has been described and discussed to help researchers understand and thus, be able to choose a suitable MPPT technique for tackling their specific issues. Regarding the outcome of this evaluation, the MPPT controllers using artificial intelligence techniques have more complexity, cost more and are difficult to implement. However, they have higher tracking efficiency, faster tracking speed and less oscillation than the classical MPPT methods.
- The modelling and control of the PV system have been developed by using MATLAB-SIMULINK to test the performance of the various MPPT controllers. The primary results have proven that employing an MPPT controller with the PV system increases the output PV power, reduces the converging time and minimises MPP fluctuations.

Hence, the average tracking efficiency of the PV system is improved as well as the stability and reliability of the PV generation being enhanced when it connects to the grid.

- Four common types of MPPT controllers, including the P&O, FLC, ANFIS and ANN methods for PV electrical generation, have been developed based on simple optimisation strategies to enhance a PV system further under different atmospheric conditions. The main features of each method were discussed to facilitate MPPT designers' understanding and thus, be able to select a suitable technique for their application area of interest. Then, the proposed methods were developed to improve their performance, especially under a rapid change in climatic conditions.
- Whilst several techniques have been designed, the Perturb and Observe algorithm is widely used for MPPT due to its low cost and simple implementation. However, the main drawbacks of this method are a long converging time, large oscillation around the maximum power point, and the drift problem associated with rapidly changing irradiance. Hence, the modified P&O-MPPT based on Pythagorean theorem and constant voltage algorithm was proposed to address the main issues of the conventional P&O algorithm. However, grid-connected PV systems based on the conventional P&O and modified P&O algorithms deliver fluctuating DC voltage during rapidly changing weather conditions. This is because they do not avoid the drift problem and eliminate the oscillation about the MPP completely.
- A novel maximum power point tracking technique based on fuzzy logic control for a grid-connected PV system has been presented, which has the ability to track the MPP when there are big fluctuations of irradiation. This proposed method incorporates the advantages of the P&O-MPPT to account for slow and fast changes in solar irradiance. There are reduced processing times for the FLC-MPPT for addressing complex engineering problems when the membership functions are few. The simulation results have revealed that the proposed technique exhibits higher output power, and no divergence from the MPP during varying weather conditions regardless of the speed of such change. That is, the proposed concept has been shown to be highly effective for working with a grid-connected PV system, achieving efficiencies of around 99.6% under The EN 50530 standard test.

- An efficient maximum power point tracking technique based on the Adaptive Neural-Fuzzy Inference System (ANFIS) using a real photovoltaic dataset has been designed. A curve fitting technique was used to analysis the input experimental data and optimise the tuning of ANFIS model, thus resulting in avoiding the system from experiencing a high training error. The results have demonstrated that this proposed method exhibits higher generated power, and no deviation from the optimised MPP point during different climate conditions, than the alternative ones, achieving efficiencies of greater than 99.3% under a semi-cloudy day test.
- An optimised feedforward Artificial Neural Network (ANN) technique using real data has been utilised for modelling current-voltage characteristics and predicting the maximum power point of the photovoltaic array. In order to improve the ANN model's accuracy, the particle swarm optimisation (PSO) algorithm was deployed. Accordingly, the predicting power of the ANN-MPPT controller has been enhance under varying weather conditions. In addition, the converging speed of the proposed method has been enhanced under a transient state. As a result, hourly efficiencies of more than 99.67% and 99.30% on a sunny and cloudy day, respectively, have been achieved.
- The optimised training ANN technique based on the PSO algorithm is a preferable method for designing a PV-MPPT controller compared with the optimal tuning ANFIS method based on the curve fitting technique. This is because it achieves a higher tracking efficiency and faster tracking speed under the experimental measurement tests.
- The proposed MPPT technique based on the FLC and P&O algorithm is the most suitable method for enhancing PV electrical generation due to its ability to track the MPP when there are big fluctuations of irradiation. Hence, it achieves the highest tracking efficiency under the EN 50530 standard test. While the modified P&O-MPPT method has been designed for low-cost PV systems system.

### 7.2 Future Work

In this research, various MPPT controllers have been developed to improve the average tracking efficiency, increase the stability and enhance the reliability of a grid-connected PV system, especially under a rapid change in weather conditions. However, there are other challenges that need further solutions, if investing in this type of energy resource is to become more attractive, some suggestions being as follows.

### **Partial Shading Condition**

Enhanced tracking efficiency of a PV system under rapidly changing atmospheric conditions has been demonstrated in this current work. It would prove beneficial to improve the PV system performance under a partial shading condition. This condition happens when there is a shading, which can be caused by tree shadow or dust, i.e. on part of the PV array. In this case, the PV array will generate several MPPs. Hence, the total generating efficiency of the installed PV array decreases. To solve this issue, an MPPT controller based on the PSO algorithm could be used.

### **Fault Ride Through**

A fault situation is considered one of the major challenges facing large-scale PV systems when connected to the grid. This issue can cause a dynamic stability problem with voltage rise. However, disconnection of faulty units could cause the system to malfunction. To address this issue, advanced active control and advanced reactive control would need to be employed.

### **Frequency Response State**

The problem of frequency response happens when the power generation unit or load demand change rapidly, leading to a large frequency deviation. Whilst this issue is very common for classical power grid due to increased power load, it is considered a huge challenge in the case of a grid-connected PV system, because its power generation changes rapidly. To solve this issue, three approaches put forward are: employing an MPPT controller, installing a storage unit and adding a dump load.

### **Economic Dispatch Challenge**

Economic dispatch is a major feature for power generation units when they are connected with a utility grid. The principle idea of this challenge is to deliver optimal generation from each unit in the power plant for a given demand at the lowest possible cost. In classical generation, the economic dispatch challenge is determined according to the relationship between the burning of fossil fuel and the optimal power generation of a traditional plant. While the economic dispatch challenge of a PV system is calculated based on the factor of the capital cost and the optimal power generation of a solar power plant. This issue has three categories of problems that need to be addressed: generation dispatch, reserve strategy, and instability.

## Bibliography

- [1] R. Luna-Rubio, M. Trejo-Perea, D. Vargas-Vázquez, and G. J. Ríos-Moreno, “Optimal sizing of renewable hybrids energy systems: A review of methodologies,” *Sol. Energy*, vol. 86, no. 4, pp. 1077–1088, 2012.
- [2] R. Quadrelli and S. Peterson, “The energy-climate challenge: Recent trends in CO<sub>2</sub> emissions from fuel combustion,” *Energy Policy*, vol. 35, no. 11, pp. 5938–5952, 2007.
- [3] R. Shah, N. Mithulananthan, R. C. Bansal, and V. K. Ramachandaramurthy, “A review of key power system stability challenges for large-scale PV integration,” *Renew. Sustain. Energy Rev.*, vol. 41, pp. 1423–1436, 2015.
- [4] M. A. Laughton, "*Renewable Energy Sources - Report Number 22*" Essex, England: Elsevier applied science, 2003.
- [5] A. Labouret and M. Viloz, "*Solar photovoltaic energy*" London: Institution of Engineering and Technology, 2010.
- [6] V. Verma, A. Kane, and B. Singh, “Complementary performance enhancement of PV energy system through thermoelectric generation,” *Renew. Sustain. Energy Rev.*, vol. 58, pp. 1017–1026, 2016.
- [7] D. Mulvaney “Solar power innovation, sustainability, and environmental justice” *California: University of California Press*, 2019.
- [8] G. C. Bakos and M. Soursos, “Technical feasibility and economic viability of a grid-connected PV installation for low cost electricity production,” vol. 34, pp. 753–758, 2002.
- [9] G. F. Nemet, “How Solar Energy Became Cheap,” *New York: Routledge*, 2019.
- [10] N. L. Panwar, S. C. Kaushik, and S. Kothari, “Role of renewable energy sources in environmental protection: A review,” *Renew. Sustain. Energy Rev.*, vol. 15, no. 3, pp. 1513–1524, 2011.
- [11] G. Masson and M. Brunisholz, “2015 Snapshot of global photovoltaic markets,” *Iea Pvps T1-292016*, pp. 1–19, 2016.
- [12] M. Rekinge and F. Thies, “Global Market Outlook for Solar Power 2015-2019,” *Glob. Mark. Outlook*, p. 32, 2015.
- [13] E. Rakhshani, K. Rouzbehi, J. S. Adolfo, and A. C. Tobar, “Integration of Large Scale PV-Based Generation into,” *Energies*, vol. 12, no. 1425, 2019.

- [14] C. S. Lai, Y. Jia, L. L. Lai, Z. Xu, M. D. McCulloch, and K. P. Wong, "A comprehensive review on large-scale photovoltaic system with applications of electrical energy storage," *Renew. Sustain. Energy Rev.*, vol. 78, no. January, pp. 439–451, 2017.
- [15] G. Masson and I. Kaizuka, "The 23rd international survey report on Trends in Photovoltaic (PV) Applications" IEA International Energy Agency, 2018. Accessed: 6 April 2020. [http://www.comitesolar.cl/wp-content/uploads/2018/12/IEA\\_PVPS\\_Trends\\_2018\\_in\\_Photovoltaic\\_Applications\\_03.pdf](http://www.comitesolar.cl/wp-content/uploads/2018/12/IEA_PVPS_Trends_2018_in_Photovoltaic_Applications_03.pdf)
- [16] S. D. Al-majidi, M. F. Abbod, and H. S. Al-Raweshidy, "Design of an Efficient Maximum Power Point Tracker Based on ANFIS Using an Experimental Photovoltaic," *Electronics*, vol.8, no. 8, pp. 585, 2019.
- [17] I. H. Altas and A. M. Sharaf, "Solar energy and PV systems," *Int. J. Photoenergy*, vol. 2014, 2014.
- [18] G. Notton, V. Lazarov, and L. Stoyanov, "Optimal sizing of a grid-connected PV system for various PV module technologies and inclinations, inverter efficiency characteristics and locations," *Renew. Energy*, vol. 35, no. 2, pp. 541–554, 2010.
- [19] J. M. Pacas, M. G. Molina, and E. C. Dos Santos, "Design of a robust and efficient power electronic interface for the grid integration of solar photovoltaic generation systems," *Int. J. Hydrogen Energy*, vol. 37, no. 13, pp. 10076–10082, 2012.
- [20] V. V Tyagi, N. A. A. Rahim, N. A. Rahim, and J. A. L. Selvaraj, "Progress in solar PV technology : Research and achievement," *Renew. Sustain. Energy Rev.*, vol. 20, pp. 443–461, 2013.
- [21] M. Mani and R. Pillai, "Impact of dust on solar photovoltaic (PV) performance: Research status, challenges and recommendations," *Renew. Sustain. Energy Rev.*, vol. 14, no. 9, pp. 3124–3131, 2010.
- [22] F. H. M. Rafi, M. J. Hossain, and J. Lu, "Hierarchical controls selection based on PV penetrations for voltage rise mitigation in a LV distribution network," *Int. J. Electr. Power Energy Syst.*, vol. 81, pp. 123–139, 2016.
- [23] M.A. Munoz et al., "Early degradation of silicon PV modules and guaranty conditions" *Sol. Energy*, vol:85, no:9, pp. 2264-2274, 2011.
- [24] Y. Yoldaş, A. Önen, S. M. Muyeen, A. V. Vasilakos, and İ. Alan, "Enhancing smart grid with microgrids: Challenges and opportunities," *Renew. Sustain. Energy Rev.*, vol. 72, no. January, pp. 205–214, 2017.

- [25] P. Siano, "Demand response and smart grids - A survey," *Renew. Sustain. Energy Rev.*, vol. 30, pp. 461–478, 2014.
- [26] G. Petrone, G. Spagnuolo, R. Teodorescu, M. Veerachary, and M. Vitelli, "Reliability issues in photovoltaic power processing systems," *IEEE Trans. Ind. Electron.*, vol. 55, no. 7, pp. 2569–2580, 2008.
- [27] V. Devabhaktuni, M. Alam, S. Shekara Sreenadh Reddy Depuru, R. C. Green, D. Nims, and C. Near, "Solar energy: Trends and enabling technologies," *Renew. Sustain. Energy Rev.*, vol. 19, pp. 555–564, 2013.
- [28] A. Sayed, M. El-Shimy, M. El-Metwally, and M. Elshahed, "Reliability, availability and maintainability analysis for grid-connected solar photovoltaic systems," *Energies*, vol. 12, no. 7, 2019.
- [29] O. Deveci and C. Kasnakoğlu, "Performance improvement of a photovoltaic system using a controller redesign based on numerical modeling," *Int. J. Hydrogen Energy*, vol. 41, no. 29, pp. 12634–12649, 2016.
- [30] D. Ounnas, M. Ramdani, S. Chenikher, and T. Bouktir, "An Efficient Maximum Power Point Tracking Controller for Photovoltaic Systems Using Takagi–Sugeno Fuzzy Models," *Arab. J. Sci. Eng.*, vol. 42, no. 12, pp. 4971–4982, 2017.
- [31] A. M. A. Haidar and N. Julai, "An improved scheme for enhancing the ride-through capability of grid-connected photovoltaic systems towards meeting the recent grid codes requirements," *Energy Sustain. Dev.*, vol. 50, pp. 38–49, 2019.
- [32] M. Birane, C. Larbes, and A. Cheknane, "Comparative study and performance evaluation of central and distributed topologies of photovoltaic system," *Int. J. Hydrogen Energy*, vol. 42, no. 13, pp. 8703–8711, 2017.
- [33] N. Karami, N. Moubayed, and R. Outbib, "General review and classification of different MPPT Techniques," *Renew. Sustain. Energy Rev.*, vol. 68, no. July 2016, pp. 1–18, 2017.
- [34] T. M. Razykov, C. S. Ferekides, D. Morel, E. Stefanakos, and H. S. Ullal, "Solar photovoltaic electricity : Current status and future prospects," *Sol. Energy*, vol. 85, no. 8, pp. 1580–1608, 2011.
- [35] M. A. Green, "The Path to 25 % Silicon Solar Cell Efficiency : History of Silicon Cell Evolution," pp. 183–189, 2009.
- [36] G. K. Singh, "Solar power generation by PV ( photovoltaic ) technology : A review," *Energy*, vol. 53, pp. 1–13, 2013.

- [37] G. Verbong, F. W. Geels, and R. Raven, "Multi-niche analysis of dynamics and policies in Dutch renewable energy innovation journeys (1970-2006): Hype-cycles, closed networks and technology-focused learning," *Technol. Anal. Strateg. Manag.*, vol. 20, no. 5, pp. 555–573, 2008.
- [38] D. Version, "Design and Control of an Inverter for Photovoltaic Applications(Thesis)" *Aalborg University: Institute for Energy*, ISBN: 87-89179-53-6,2005.
- [39] B. Kumar, "A study on global solar PV energy developments and policies with special focus on the top ten solar PV power producing countries," *Renew. Sustain. Energy Rev.*, vol. 43, pp. 621–634, 2015.
- [40] F. Obeidat, "A comprehensive review of future photovoltaic systems," *Sol. Energy*, vol. 163, no. October 2017, pp. 545–551, 2018.
- [41] T. Grau, M. Huo, and K. Neuhoff, "Survey of photovoltaic industry and policy in Germany and China," *Energy Policy*, vol. 51, pp. 20–37, 2012.
- [42] S. T. A. van den Heuvel and J. C. J. M. van den Bergh, "Multilevel assessment of diversity, innovation and selection in the solar photovoltaic industry," *Struct. Chang. Econ. Dyn.*, vol. 20, no. 1, pp. 50–60, 2009.
- [43] Z. Shahan "13 Charts On Solar Panel Cost & Growth Trends " *clean technica*, 4 Sep. 2014. <https://cleantechnica.com/2014/09/04/solar-panel-cost-trends-10-charts/>.
- [44] W. Tian et al. "Effect of urban climate on building integrated photovoltaics performance." *Energy Conversion and Management*, vol. 48, no. 1, pp. 1–8, 2007.
- [45] K. Hara, T. Horiguchi, T. Kinoshita, K. Sayama, H. Sugihara, and H. Arakawa, "Highly efficient photon-to-electron conversion with mercurochrome-sensitized nanoporous oxide semiconductor solar cells," *Sol. Energy Mater. Sol. Cells*, vol. 64, no. 2, pp. 115–134, 2000.
- [46] Y. T. Tan, D. S. Kirschen, and N. Jenkins, "A model of PV generation suitable for stability analysis," *IEEE Trans. Energy Convers.*, vol. 19, no. 4, pp. 748–755, 2004.
- [47] K. Ishaque and Z. Salam, "A deterministic particle swarm optimization maximum power point tracker for photovoltaic system under partial shading condition," *IEEE Trans. Ind. Electron.*, vol. 60, no. 8, pp. 3195–3206, 2013.
- [48] J. P. Ram, T. S. Babu, and N. Rajasekar, "A comprehensive review on solar PV maximum power point tracking techniques," *Renew. Sustain. Energy Rev.*, vol. 67, pp. 826–847, 2017.

- [49] S. D. Al-Majidi, M. F. Abbod, and H. S. Al-Raweshidy, "A novel maximum power point tracking technique based on fuzzy logic for photovoltaic systems," *Int. J. Hydrogen Energy*, vol. 43, no. 31, pp. 14158–14171, 2018.
- [50] A. Orioli and A. Di Gangi, "Load mismatch of grid-connected photovoltaic systems: Review of the effects and analysis in an urban context," *Renew. Sustain. Energy Rev.*, vol. 21, pp. 13–28, 2013.
- [51] O. Haillant, "Accelerated weathering testing principles to estimate the service life of organic PV modules," *Sol. Energy Mater. Sol. Cells*, vol. 95, no. 5, pp. 1284–1292, 2011.
- [52] K. Branker, M. J. M. Pathak, and J. M. Pearce, "A review of solar photovoltaic levelized cost of electricity," *Renew. Sustain. Energy Rev.*, vol. 15, no. 9, pp. 4470–4482, 2011.
- [53] S. Saravanan and N. Ramesh Babu, "Maximum power point tracking algorithms for photovoltaic system - A review," *Renew. Sustain. Energy Rev.*, vol. 57, pp. 192–204, 2016.
- [54] J. Farzaneh, R. Keypour, and A. Karsaz, "A novel fast maximum power point tracking for a PV system using hybrid PSO-ANFIS algorithm under partial shading conditions," *Int. J. of Indus. Electr., Cont. and Optimiz.*, vol. 2, no. 1, pp. 47–58, 2019.
- [55] N. Patcharaprakiti and S. Premrudeepreechacharn, "Maximum power point tracking using adaptive fuzzy logic control for grid-connected photovoltaic system," vol. 30, *Renewable Energy*, pp. 1771–1788, 2005.
- [56] M. Birane, C. Larbes, A. Cheknane, and S. Mat, "Comparative study and performance evaluation of central and distributed topologies of photovoltaic system," *Int. J. Hydrogen Energy*, vol. 42, no. 13, pp. 8703–8711, 2016.
- [57] R. Faranda, S. Leva, P. Milano, and P. Leonardo, "Energy comparison of MPPT techniques for PV Systems Department of Energy," *Wseas Trans. on Power Systems*, vol. 3, no. 6, pp. 446–455, 2008.
- [58] S. D. Al-Majidi, M. F. Abbod, and H. S. Al-Raweshidy. "Design of an Intelligent ANN-MPPT Controller using Real Photovoltaic System Data" 54rd International Universities Power Engineering Conference (UPEC), Bucharest, Romania, 2019.
- [59] M. A. Elgendy, B. Zahawi, S. Member, and D. J. Atkinson, "Assessment of the Incremental Conductance Maximum Power Point Tracking Algorithm," *IEEE Trans. Sustain. Energy*, vol. 4, no. 1, pp. 108–117, 2013.

- [60] L. Bhukya and S. Nandiraju, "A novel photovoltaic maximum power point tracking technique based on grasshopper optimized fuzzy logic approach" *Int. J. Hydrogen Energy*, vol. 45, no. 16, pp. 9416-9427, 2020.
- [61] S. Duman, N. Yorukeren, and I. H. Altas, "A novel MPPT algorithm based on optimized artificial neural network by using FPSOGSA for standalone photovoltaic energy systems," *Neural Comput. Appl.*, vol. 29, no. 1, pp. 257–278, 2018.
- [62] S. D. Al-Majidi, M. F. Abbod, and H. S. Al-Raweshidy. "A Modified P&O-MPPT based on Pythagorean Theorem and CV-MPPT for PV Systems" 53rd International Universities Power Engineering Conference (UPEC), Glasgow, UK, 2018.
- [63] N. S. D. Souza, L. A. C. Lopes, and X. Liu, "Comparative study of variable size perturbation and observation maximum power point trackers for PV systems," *Electric Power Systems Research*, vol. 80, pp. 296–305, 2010.
- [64] F. Paz, S. Member, and M. Ordonez, "Zero Oscillation and Irradiance Slope Tracking for Photovoltaic MPPT," *IEEE Trans. Ind. Electron.*, vol. 61, no. 11, pp. 6138–6147, 2014.
- [65] M. A. Elgendy, B. Zahawi, S. Member, and D. J. Atkinson, "Assessment of the Incremental Conductance Maximum Power Point Tracking Algorithm," *IEEE Trans. on Sustain. Energy*, vol. 4, no. 1, pp. 108–117, 2013.
- [66] J. Ramos-hernanz and J. M. Lopez-guede, "Novel control algorithm for MPPT with Boost converters in photovoltaic systems," *Int. J. Hydrogen Energy*, vol. 42, no. 28, pp. 17831–17855, 2017.
- [67] A. Loukriz, M. Haddadi, and S. Messalti, "Simulation and experimental design of a new advanced variable step size Incremental Conductance MPPT algorithm for PV systems," *ISA Trans.*, vol. 62, pp. 30–38, 2016.
- [68] W. Xiao and W. G. Dunford, "A modified adaptive hill climbing MPPT method for photovoltaic power systems," *PESC Rec. - IEEE Annu. Power Electron. Spec. Conf.*, vol. 3, pp. 1957–1963, 2004.
- [69] M. Killi and S. Samanta, "Modified Perturb and Observe MPPT Algorithm for Drift Avoidance in Photovoltaic Systems," *IEEE Trans. Ind. Electron.*, vol. 62, no. 9, pp. 5549–5559, 2015.
- [70] S. K. Kollimalla and M. K. Mishra, "Variable Perturbation Size Adaptive P&O MPPT Algorithm for Sudden Changes in Irradiance," *IEEE Trans. Sustain. Energy*, vol. 5, no. 3, pp. 718–728, 2014.

- [71] J. Ahmed, S. Member, and Z. Salam, "A Modified P & O Maximum Power Point Tracking Method With Reduced Steady-State Oscillation and Improved Tracking Efficiency," *IEEE Trans. Sustain. Energy*, vol. 7, no. 4, pp. 1506–1515, 2016.
- [72] A. Harrag and H. Bahri, "Novel neural network IC-based variable step size fuel cell MPPT controller Performance, efficiency and lifetime improvement," *Int. J. Hydrogen Energy*, vol. 42, no. 5, pp. 3549–3563, 2016.
- [73] V. K. Devi, K. Premkumar, A. B. Beevi, and S. Ramaiyer, "A modified Perturb & Observe MPPT technique to tackle steady state and rapidly varying atmospheric conditions," *Sol. Energy*, vol. 157, no. September, pp. 419–426, 2017.
- [74] L. Piegari and R. Rizzo, "Adaptive perturb and observe algorithm for photovoltaic maximum power point tracking," *IET Renew. Power Gener.*, vol. 4, no. 4, p. 317, 2010.
- [75] M. Kermadi and E. M. Berkouk, "Artificial intelligence-based maximum power point tracking controllers for Photovoltaic systems: Comparative study," *Renew. Sustain. Energy Rev.*, vol. 69, no. June 2015, pp. 369–386, 2017.
- [76] C. Ben Salah and M. Ouali, "Comparison of fuzzy logic and neural network in maximum power point tracker for PV systems," *Electr. Power Syst. Res.*, vol. 81, no. 1, pp. 43–50, 2011.
- [77] M. Bahrami *et al.*, "Hybrid maximum power point tracking algorithm with improved dynamic performance," *Renew. Energy*, vol. 130, pp. 982–991, 2019.
- [78] P.-C. Cheng, B.-R. Peng, Y.-H. Liu, Y.-S. Cheng, and J.-W. Huang, "Optimization of a Fuzzy-Logic-Control-Based MPPT Algorithm Using the Particle Swarm Optimization Technique," *Energies*, vol. 8, no. 6, pp. 5338–5360, 2015.
- [79] N. Gupta and R. Garg, "Tuning of asymmetrical fuzzy logic control algorithm for SPV system connected to grid," *Int. J. Hydrogen Energy*, vol. 42, no. 26, pp. 16375–16385, 2017.
- [80] Y. Soufi, M. Bechouat, and S. Kahla, "Fuzzy-PSO controller design for maximum power point tracking in photovoltaic system," *Int. J. Hydrogen Energy*, vol. 42, no. 13, pp. 8680–8688, 2016.
- [81] O. Guenounou, B. Dahhou, and F. Chabour, "Adaptive fuzzy controller based MPPT for photovoltaic systems," *Energy Convers. Manag.*, vol. 78, pp. 843–850, 2014.
- [82] T. Obeidi, A. Zerguerras, C. Larbes, and S. M. Al, "Genetic algorithms optimized fuzzy logic control for the maximum power point tracking in photovoltaic system,"

- Renew. Energy*, vol. 34, no. 10, pp. 2093–2100, 2009.
- [83] S. ali Blaifi, S. Moulahoum, R. Benkercha, B. Taghezouit, and A. Saim, “M5P model tree based fast fuzzy maximum power point tracker,” *Sol. Energy*, vol. 163, no. August 2017, pp. 405–424, 2018.
- [84] S. Subiyanto, A. Mohamed, and M. A. Hannan, “Intelligent maximum power point tracking for PV system using Hopfield neural network optimized fuzzy logic controller,” *Energy Build.*, vol. 51, pp. 29–38, 2012.
- [85] M. Nabipour, M. Razaz, S. G. Seifossadat, and S. S. Mortazavi, “A new MPPT scheme based on a novel fuzzy approach,” *Renew. Sustain. Energy Rev.*, vol. 74, no. October 2016, pp. 1147–1169, 2017.
- [86] L. L. Jiang, D. R. Nayanisiri, D. L. Maskell, and D. M. Vilathgamuwa, “A hybrid maximum power point tracking for partially shaded photovoltaic systems in the tropics,” *Renew. Energy*, vol. 76, pp. 53–65, 2015.
- [87] T. Hiyama, S. M. Ieee, and K. Kitabayashi, “Neural Network Based Estimation of Maximum Power Generation from PV Module Using Environmental Information” *IEEE Trans. on Energy Conv.*, vol. 12, no. 3, 1997.
- [88] A. Afşin, and R. Akkaya, “Training data optimization for ANNs using genetic algorithms to enhance MPPT efficiency of a stand-alone PV system,” *Turkish Journal of Electrical Engineering & Computer Sciences*. vol. 20, no. 2, pp. 241–254, 2012.
- [89] A. Chaouachi, R. M. Kamel, and K. Nagasaka, “A novel multi-model neuro-fuzzy-based MPPT for three-phase grid-connected photovoltaic system,” *Sol. Energy*, vol. 84, no. 12, pp. 2219–2229, 2010.
- [90] B. Bendib, F. Krim, H. Belmili, M. F. Almi, and S. Bolouma, “An intelligent MPPT approach based on neural-network voltage estimator and fuzzy controller, applied to a stand-alone PV system,” *IEEE Int. Symp. Ind. Electron.*, no. 1, pp. 404–409, 2014.
- [91] N. Priyadarshi, S. Padmanaban, L. Mihet-Popa, F. Blaabjerg, and F. Azam, “Maximum power point tracking for brushless DC motor-driven photovoltaic pumping systems using a hybrid ANFIS-FLOWER pollination optimization algorithm,” *Energies*, vol. 11, no. 5, 2018.
- [92] A. Arora and P. Gaur, “Comparison of ANN and ANFIS based MPPT Controller for grid connected PV systems,” *12th IEEE Int. Conf. Electron. Energy, Environ. Commun. Comput. Control (E3-C3), INDICON 2015*, pp. 1–6, 2016.
- [93] M. A. Enany, M. A. Farahat, and A. Nasr, “Modeling and evaluation of main

- maximum power point tracking algorithms for photovoltaics systems,” *Renew. Sustain. Energy Rev.*, vol. 58, pp. 1578–1586, 2016.
- [94] M. Lasheen and M. Abdel-salam, “A novel hybrid Maximum Power Point Tracking Technique using Hill Climbing and ANFIS Techniques for PV Applications,” *Renew. Sustain. Energy Rev.*, vol. 171, no. March, pp. 1–31, 2017.
- [95] M. Muthuramalingam and P. S. Manoharan, “Comparative analysis of distributed MPPT controllers for partially shaded standalone photovoltaic systems,” *Energy Convers. Manag.*, vol. 86, pp. 286–299, 2014.
- [96] A. A. Aldair, A. A. Obed, and A. F. Halihal, “Design and implementation of ANFIS-reference model controller based MPPT using FPGA for photovoltaic system,” *Renew. Sustain. Energy Rev.*, vol. 82, no. August 2017, pp. 2202–2217, 2018.
- [97] F. Khosrojerdi, S. Taheri, and A. Cretu, “An Adaptive Neuro-Fuzzy Inference System-based MPPT Controller for Photovoltaic Arrays,” *IEEE Electrical Power and Energy Conference (EPEC)*, Ottawa, Canada, 12–14 October 2016.
- [98] A. Bin-halabi, A. Abdennour, and H. Mashaly, “An Accurate ANFIS-based MPPT for Solar PV System,” *Int. J. Adv. Comput. Res.*, vol. 4, no. 15, pp. 588–595, 2014.
- [99] N. Khaehintung, P. Sirisuk, and W. Kurutach, “A Novel ANFIS Controller for Maximum Power Point Tracking in Photovoltaic Systems,” *Power Electron. Drive Syst. 2003. PEDS 2003. Fifth Int. Conf.*, no. 1, pp. 833–836, 2003.
- [100] S. Vafaei, M. Gandomkar, A. Rezvani, and M. Izadbakhsh, “Enhancement of grid-connected photovoltaic system using ANFIS-GA under different circumstances,” *Front. Energy*, vol. 9, no. 3, pp. 322–334, 2015.
- [101] M. A. Abido, M. S. Khalid, and M. Y. Worku, “An Efficient ANFIS-Based PI Controller for Maximum Power Point Tracking of PV Systems,” *Arab. J. Sci. Eng.*, vol. 40, no. 9, pp. 2641–2651, 2015.
- [102] G. Ciulla, V. Lo Brano, V. Di Dio, and G. Cipriani, “A comparison of different one-diode models for the representation of I-V characteristic of a PV cell,” *Renew. Sustain. Energy Rev.*, vol. 32, pp. 684–696, 2014.
- [103] A. I. M. Ali, M. A. Sayed, and E. E. M. Mohamed, “Modified efficient perturb and observe maximum power point tracking technique for grid-tied PV system,” *Int. J. Electr. Power Energy Syst.*, vol. 99, no. June 2017, pp. 192–202, 2018.
- [104] R. C. Dorf, “The Electrical Engineering Handbook,” *Electr. Eng.*, vol. London, no. 3, p. 0, 1997.

- [105] R. Kadri, H. Andrei, J. Gaubert, T. Ivanovici, G. Champenois, and P. Andrei, "Modeling of the photovoltaic cell circuit parameters for optimum connection model and real-time emulator with partial shadow conditions," *Energy*, vol. 42, no. 1, pp. 57–67, 2012.
- [106] M. Balato, L. Costanzo, and M. Vitelli, "Series-Parallel PV array re-configuration: Maximization of the extraction of energy and much more," *Appl. Energy*, vol. 159, pp. 145–160, 2015.
- [107] H. Fathabadi, "Novel high efficiency DC / DC boost converter for using in photovoltaic systems," *Sol. Energy*, vol. 125, pp. 22–31, 2016.
- [108] D. Meneses, F. Blaabjerg, O. Garcia, and J. a. Cobos, "Review and Comparison of Step-Up Transformerless," *IEEE Trans. Power Electron.*, vol. 28, no. 6, pp. 2649–2663, 2013.
- [109] G. Velasco-Quesada, F. Guinjoan-Gispert, R. Piqué-López, M. Román-Lumbreras, and A. Conesa-Roca, "Electrical PV array reconfiguration strategy for energy extraction improvement in grid-connected PV systems," *IEEE Trans. Ind. Electron.*, vol. 56, no. 11, pp. 4319–4331, 2009.
- [110] K. Zeb *et al.*, "A comprehensive review on inverter topologies and control strategies for grid connected photovoltaic system," *Renew. Sustain. Energy Rev.*, vol. 94, no. June, pp. 1120–1141, 2018.
- [111] S. Öztürk, P. Poşpoş, V. Utalay, A. Koç, M. Ermiş, and I. Çadırcı, "Operating principles and practical design aspects of all SiC DC / AC / DC converter for MPPT in grid-connected PV supplies," *Sol. Energy*, vol. 176, no. July, pp. 380–394, 2018.
- [112] W. Li and X. He, "Review of nonisolated high-step-up DC/DC converters in photovoltaic grid-connected applications," *IEEE Trans. Ind. Electron.*, vol. 58, no. 4, pp. 1239–1250, 2011.
- [113] Z. Waradzyn, R. Stala, A. Mondzik, A. Penczek, A. Skala, and S. Pirog, "Efficiency Analysis of MOSFET-Based Air-Choke Resonant DC-DC Step-Up Switched-Capacitor Voltage Multipliers," *IEEE Trans. Ind. Electron.*, vol. 64, no. 11, pp. 8728–8738, 2017.
- [114] M. A. Alqarni, "A High Efficiency Photovoltaic Inverter System Configuration with Maximum Power Point Tracking (Thesis)," *Brunel University London: College of Engineering, Design and Physical Science*, March 2016.
- [115] H. Chung and Y. K. Mok, "Development of a switched-capacitor DC/DC boost

- converter with continuous input current waveform,” *IEEE Trans. Circuits Syst. I Fundam. Theory Appl.*, vol. 46, no. 6, pp. 756–759, 1999.
- [116] H. Fathabadi, “Novel high efficiency DC/DC boost converter for using in photovoltaic systems,” *Sol. Energy*, vol. 125, pp. 22–31, 2016.
- [117] N. Femia, G. Petrone, G. Spagnuolo, and M. Vitelli, “Optimization of Perturb and Observe Maximum Power Point Tracking Method,” *IEEE trans. on power electr.*, vol. 20, no. 4, pp. 963–973, 2005.
- [118] Y. Yang and F. P. Zhao, “Adaptive perturb and observe MPPT technique for grid-connected photovoltaic inverters,” *Procedia Eng.*, vol. 23, pp. 468–473, 2011.
- [119] D. Sera, R. Teodorescu, J. Hantschel, and M. Knoll, “Optimized maximum power point tracker for fast-changing environmental conditions,” *IEEE Trans. Ind. Electron.*, vol. 55, no. 7, pp. 2629–2637, 2008.
- [120] S. K. Kollimalla, S. Member, M. K. Mishra, and S. Member, “Variable Perturbation Size Adaptive P & O MPPT Algorithm for Sudden Changes in Irradiance,” *IEEE Trans. Sustain. Energy*, vol. 5, no. 3, pp. 718–728, 2014.
- [121] J. Ahmad, “A Fractional Open Circuit Voltage Based Maximum Power Point Tracker for Photovoltaic Arrays,” *2nd International Conference on Software Technology and Engineering*, pp. 247–250, 2010.
- [122] M. A. Abdourraziq, M. Maaroufi, and M. Ouassaid, “A new variable step size INC MPPT method for PV systems,” *Int. Conf. Multimed. Comput. Syst. -Proceedings*, vol. 0, no. 7, pp. 1563–1568, 2014.
- [123] S. Ozdemir, N. Altin, and I. Sefa, “Fuzzy logic based MPPT controller for high conversion ratio quadratic boost converter,” *Int. J. Hydrogen Energy*, vol. 42, no. 28, pp. 17748–17759, 2017.
- [124] T. H. Kwan and X. Wu, “Maximum power point tracking using a variable antecedent fuzzy logic controller,” *Sol. Energy*, vol. 137, pp. 189–200, 2016.
- [125] M. Ammirul, A. Mohd, M. Amran, M. Radzi, A. C. Soh, and N. A. Rahim, “Development of adaptive perturb and observe-fuzzy control maximum power point tracking for photovoltaic boost dc – dc converter,” *IET Renewable Power Generation*, vol. 8, no. 2, 2014.
- [126] B. N. Alajmi, K. H. Ahmed, S. J. Finney, and B. W. Williams, “Fuzzy logic controlled approach of a modified hill climbing method for maximum power point in microgrid stand-alone photovoltaic system,” *IEEE Trans. Power Electron.*, vol. 26, no. 4, pp.

- 1022–1030, 2011.
- [127] A. Harrag and S. Messalti, “How fuzzy logic can improve PEM fuel cell MPPT,” *Int. J. Hydrogen Energy*, vol. 3, pp. 1–14, 2017.
- [128] T. L. Kottas, Y. S. Boutalis, and a. D. Karlis, “New Maximum Power Point Tracker for PV Arrays Using Fuzzy Controller in Close Cooperation With Fuzzy Cognitive Networks,” *IEEE Trans. Energy Convers.*, vol. 21, no. 3, pp. 793–803, 2006.
- [129] M. Cirstea et al., “Neural and Fuzzy Logic Control of Drives and Power Systems,” *England, Oxford:Newnes.*, 2002.
- [130] I. Eker and Y. Torun, “Fuzzy logic control to be conventional method,” *Energy Convers. Manag.*, vol. 47, no. 4, pp. 377–394, 2006.
- [131] E. H. Mamdani and S. Assilian, “An experiment in linguistic synthesis with a fuzzy logic controller,” *Int. J. Man. Mach. Stud.*, vol. 7, no. 1, pp. 1–13, 1975.
- [132] Q. A. TARBOSH et al., “Review and Investigation of Simplified Rules Fuzzy Logic Speed Controller of High-Performance Induction Motor Drives,” *IEEE Access*, vol. 8, pp. 49377 - 49394, 2020.
- [133] J. Zhao and B. K. Bose, “Evaluation of membership functions for fuzzy logic controlled induction motor drive,” *IECON Proc. (Industrial Electron. Conf.)*, vol. 1, pp. 229–234, 2002.
- [134] M. Seyedmahmoudian *et al.*, “State of the art artificial intelligence-based MPPT techniques for mitigating partial shading effects on PV systems – A review,” *Renew. Sustain. Energy Rev.*, vol. 64, pp. 435–455, 2016.
- [135] F. A. O. Aashoor, “Maximum Power Point Tracking Techniques for Solar Water Pumping Systems,” *PhD Thesis: university of Bath*, pp. 1–217, 2015.
- [136] M. Tiar, A. Betka, S. Drid, S. Abdeddaim, M. Becherif, and A. Tabandjat, “Optimal energy control of a PV-fuel cell hybrid system,” *Int. J. Hydrogen Energy*, vol. 42, no. 2, pp. 1456–1465, 2017.
- [137] N. Altin and S. Ozdemir, “Three-phase three-level grid interactive inverter with fuzzy logic based maximum power point tracking controller,” *Energy Convers. Manag.*, vol. 69, pp. 17–26, 2013.
- [138] R. Brundlinger, N. Henze, H. H. Aberlin, B. Burger, A. Bergmann, and F. Aumgartner, “prEN 50530–The New European standard for performance characterisation of PV inverters,” in *Proc. 24th Eur. Photovolt. Solar Energy Conf.*, 2009, pp. 3105–3109.

- [139] R. K. Kharb, S. L. Shimi, S. Chatterji, and M. F. Ansari, "Modeling of solar PV module and maximum power point tracking using ANFIS," *Renew. Sustain. Energy Rev.*, vol. 33, pp. 602–612, 2014.
- [140] H. Abu-Rub, A. Iqbal, and S. M. Ahmed, "Adaptive neuro-fuzzy inference system-based maximum power point tracking of solar PV modules for fast varying solar radiations," *Int. J. Sustain. Energy*, vol. 31, no. 6, pp. 383–398, 2012.
- [141] H. Abu-Rub, A. Iqbal, S. M. Ahmed, F. Z. Peng, Y. Li, and G. Baoming, "Quasi-Z-source inverter-based photovoltaic generation system with maximum power tracking control using ANFIS," *IEEE Trans. Sustain. Energy*, vol. 4, no. 1, pp. 11–20, 2013.
- [142] F. D. Murdianto, O. Penangsang, and A. Priyadi, "Modeling and simulation of MPPT-bidirectional using adaptive neuro fuzzy inference system (ANFIS) in distributed energy generation system," *2015 Int. Semin. Intell. Technol. Its Appl. ISITIA 2015 - Proceeding*, pp. 207–212, 2015.
- [143] F. Mayssa and L. Sbita, "Advanced ANFIS-MPPT control algorithm for sunshine photovoltaic pumping systems," *2012 1st Int. Conf. Renew. Energies Veh. Technol. REVET 2012*, pp. 167–172, 2012.
- [144] B. . Tarek, D. . Said, and M. E. H. . Benbouzid, "Maximum Power Point Tracking Control for Photovoltaic System Using Adaptive Neuro-Fuzzy 'ANFIS,'" *8th Int. Conf. Exhib. Ecol. Veh. Renew. Energies, EVER 2013*, no. 0 I, 2013.
- [145] J. S. R. Jang, "ANFIS : Adap tive-Ne twork-Based Fuzzy Inference System. IEEE Transactions on Systems," *Man Cybern.*, vol. 23, no. 3, pp. 665–685, 1993.
- [146] A. Mellit and S. A. Kalogirou, "ANFIS-based modelling for photovoltaic power supply system: A case study," *Renew. Energy*, vol. 36, no. 1, pp. 250–258, 2011.
- [147] X. Wan, Y. Li, C. Xia, M. Wu, J. Liang, and N. Wang, "A T-wave alternans assessment method based on least squares curve fitting technique," *Meas. J. Int. Meas. Confed.*, vol. 86, pp. 93–100, 2016.
- [148] S. Messalti, A. Harrag, and A. Loukriz, "A new variable step size neural networks MPPT controller: Review, simulation and hardware implementation," *Renew. Sustain. Energy Rev.*, vol. 68, no. October 2016, pp. 221–233, 2017.
- [149] H. Fathabadi, "Novel neural-analytical method for determining silicon/plastic solar cells and modules characteristics," *Energy Convers. Manag.*, vol. 76, pp. 253–259, 2013.
- [150] R. Akkaya et al., "DSP implementation of a PV system with GA-MLP-NN based

- MPPT controller supplying BLDC motor drive,” *Energy Conv, and Mang.*, vol. 48, pp. 210–218, 2007.
- [151] A. Afs et al., “A genetic algorithm optimized ANN-based MPPT algorithm for a stand-alone PV system with induction motor drive,” *Sol. Energy*, vol. 86, pp. 2366–2375, 2012.
- [152] L. Ā. Zhang and Y. F. Bai, “Genetic algorithm-trained radial basis function neural networks for modelling photovoltaic panels,” *Eng. App. of Artif. Intell.*, vol. 18, pp. 833–844, 2005.
- [153] H. Hamdi, C. Ben Regaya, and A. Zaafour, “Real-time study of a photovoltaic system with boost converter using the PSO-RBF neural network algorithms in a MyRio controller,” *Sol. Energy*, vol. 183, no. February, pp. 1–16, 2019.
- [154] P. D’Urso, L. De Giovanni, and R. Massari, “GARCH-based robust clustering of time series,” *Fuzzy Sets Syst.*, vol. 305, pp. 1–28, 2016.
- [155] R. E. Precup, R. C. David, and E. M. Petriu, “Grey Wolf optimizer algorithm-based tuning of fuzzy control systems with reduced parametric sensitivity,” *IEEE Trans. Ind. Electron.*, vol. 64, no. 1, pp. 527–534, 2017.
- [156] W. Hu, Y. Yu, and W. Gu, “Parameter estimation of fractional-order arbitrary dimensional hyperchaotic systems via a hybrid adaptive artificial bee colony algorithm with simulated annealing algorithm,” *Eng. Appl. Artif. Intell.*, vol. 68, no. August 2016, pp. 172–191, 2018.
- [157] Y. Al-dunainawi, M. F. Abbod, and A. Jizany, “A new MIMO ANFIS-PSO based NARMA-L2 controller for nonlinear dynamic systems,” *Eng. Appl. Artif. Intell.*, vol. 62, no. March, pp. 265–275, 2017.
- [158] J. P. S. Rosa, et al., *Overview of Artificial Neural Networks" Cham: Springer*, 2020.
- [159] A. K. Jain, J. Mao, and K. M. Mohiuddin, “Artificial neural networks: A tutorial,” *Computer (Long. Beach. Calif.)*, vol. 29, no. 3, pp. 31–44, 1996.
- [160] I. A. Basheer and M. Hajmeer, “Artificial neural networks: fundamentals , computing , design , and application,” *J. Microbiol. Methods*, vol. 43, pp. 3–31, 2000.
- [161] I. Aljarah, H. Faris, and S. Mirjalili, “Optimizing connection weights in neural networks using the whale optimization algorithm,” *Soft Comput.*, vol. 22, no. 1, pp. 1–15, 2018.
- [162] G. Li, H. Alnuweiri, and Y. Wu, “Acceleration of Back Propagations through Initial Weight Pre-Training with Delta Rule Training a BP Network.” *IEEE International*

*Conference on Neural Networks*, 1993.

- [163] Y. Marinakis, M. Marinaki, and G. Dounias, “A hybrid particle swarm optimization algorithm for the vehicle routing problem,” *Eng. Appl. Artif. Intell.*, vol. 23, no. 4, pp. 463–472, 2010.
- [164] B. Vasumathi and S. Moorthi, “Implementation of hybrid ANN – PSO algorithm on FPGA for harmonic estimation,” *Eng. Appl. Artif. Intell.*, vol. 25, no. 3, pp. 476–483, 2012.

# Appendix A

## Experimental Data Sample

**Table A.1** The data sample which collected from experimental PV test.

<b>Irradiance (w/m<sup>2</sup>)</b>	<b>Temperature (°C)</b>	<b>PV power (kW)</b>
1036.8	32.281	0.8339
1026.3	32.13	0.8323
1018.3	32.988	0.8313
311.888	9.43	0.2429
353.938	9.655	0.2919
238.531	10.223	0.2212
229.232	10.354	0.2296
163.084	10.293	0.1659
160.208	10.176	0.1673
173.966	10.075	0.1925
175.505	9.989	0.1883
238.531	9.963	0.2016
296.242	10.113	0.2079
256.338	10.363	0.1799
187.154	10.646	0.1071
129.188	10.79	0.1281
96.193	10.747	0.0966
127.498	10.669	0.1302
271.126	5.793	0.1855
284.768	6.186	0.2226
239.939	6.335	0.2037
272.399	6.539	0.2457
251.211	6.528	0.2345
325.693	6.641	0.2317
336.763	6.801	0.2268
330.971	7.048	0.2023
345.591	7.213	0.2086
273.216	7.326	0.1891
245.628	7.298	0.2373
156.717	6.647	0.1778
179.805	6.756	0.1953
160.652	6.91	0.1736
187.698	7.071	0.2044
295.686	7.27	0.3094
425.362	7.597	0.3976
313.197	9.268	0.2716
464.033	9.498	0.3787
461.343	9.67	0.3738
396.163	9.969	0.3087
148.614	10.149	0.1239

---

177.127	8.306	0.1806
93.156	8.142	0.0798
40.345	8.011	0.0469
45.949	7.91	0.0595
64.555	7.784	0.0784
95.185	7.574	0.1141
245.388	7.396	0.2261
298.315	7.405	0.2583
283.351	7.687	0.2443
138.354	7.987	0.1372
114.061	8.181	0.1232
92.274	8.19	0.0952
124.953	8.181	0.1337
112.197	8.165	0.1141
265.595	7.67	0.2002
253.948	7.787	0.2114
265.398	7.856	0.1995
293.531	7.942	0.2065
286.715	7.978	0.1925
339.458	8.198	0.2695
270.712	8.279	0.2163
357.453	8.205	0.2709
356.986	8.258	0.2814
371.313	8.519	0.2793
368.285	8.77	0.2947
383.169	8.873	0.2821
368.531	8.89	0.2443
377.697	8.876	0.2527
471.276	9.359	0.3668
415.941	9.519	0.3255
393.354	9.602	0.3143
287.902	9.52	0.2324
333.992	9.426	0.2674
230.119	9.452	0.2107
184.704	9.228	0.1967
229.369	8.962	0.2212
260.087	8.864	0.2282
139.176	9.112	0.1435
114.102	8.681	0.1267
293.297	7.67	0.2835
305.536	7.774	0.2884
232.905	7.88	0.2261
201.298	7.977	0.1897
184.888	8.033	0.1904
186.927	7.983	0.1953
302.878	7.966	0.2772
227.109	7.695	0.2254
379.48	7.78	0.3409

# Appendix B

## Data sheet of Sharp NU-S5E3E 185 PV module



**NUS5E3E / NU185E1**  
**185 W**  
Photovoltaic module monocrystalline



### MONOCRYSTALLINE SILICON PHOTOVOLTAIC MODULE WITH 185 W NOMINAL POWER

Sharp's NUS5E3E / NU185E1 photovoltaic module is designed for large electrical power requirements. Based on the technology of crystal silicon solar cells cultivated for over 40 years, this module has superb durability to withstand rigorous operating conditions and is suitable for grid connected systems.



**Features**

- High-power module (185 W) using 155.5 mm square monocrystalline silicon solar cells with 14.1 % module conversion efficiency.
- Photovoltaic module with bypass diode minimises the power drop caused by shade. Textured cell surface to reduce the reflection of sunlight and BSF (Back Surface Field) structure to improve cell conversion efficiency.
- Using white tempered glass, EVA resin, and a weather-proof film along with an aluminium frame for extended outdoor use.
- Output terminal: Lead wire with waterproof connector.
- NUS5E3E: manufactured in Japan  
NU185E1: manufactured in UK  
Apart from the place of manufacture the models are identical in construction.
- Hail damage resistance tested by TÜV in accordance with IEC61215.

### Specifications NUSSE3E / NU185E1

Cell	Monocrystalline silicon solar cells, 155.5 mm square
No. of cells and connections	48 In series
Maximum system voltage	1,000 V DC
Nominal power	185 W
Dimensions	1,318 x 994 x 46 mm
Weight	16.0 kg
Type of output terminal	Lead wire with connector

### Ambient conditions

Parameters	Rating	Unit
Operating temperature	-40 to +90	°C
Storage temperature	-40 to +90	°C
Storage humidity	up to 90	%

### Temperature coefficients

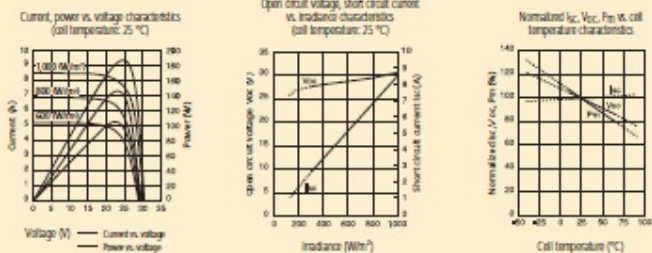
$\alpha P_m$	-0.485% / °C
$\alpha I_{sc}$	+0.053% / °C
$\alpha V_{oc}$	-104 mV / °C

### Electrical data

Parameters	Symbol	Min.	Typ.	Unit
Open circuit voltage	$V_{oc}$	-	30.2	V
Maximum power voltage	$V_{pm}$	-	24.0	V
Short circuit current	$I_{sc}$	-	8.54	A
Maximum power current	$I_{pm}$	-	7.71	A
Nominal power	$P_m$	175.8	185.0	W
Module efficiency	$\eta_m$	-	14.1	%

The electrical data applies under Standard Test Conditions (STC): Radiation 1,000 W/m<sup>2</sup> with a spectrum of AM 1.5 and at a cell temperature of 25 °C.

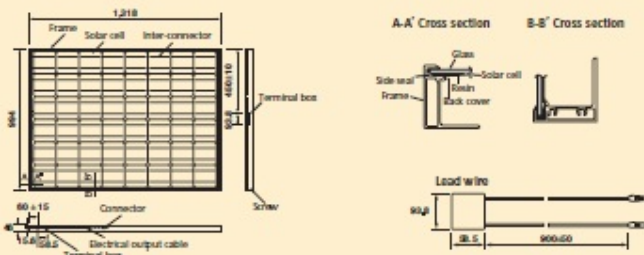
### Characteristics



### Application options

- Grid connected residential systems
- Office buildings
- Solar power stations
- Solar villages
- Villas, mountain cottages
- Lighting equipment
- Traffic signs
- Radio relay stations
- Beacons
- Telemeter systems
- Telecommunication systems

### Outline dimensions



This module should not be connected to any direct load.  
 In the absence of confirmation by specification sheets, Sharp takes no responsibility for any defects that may occur in equipment using any Sharp products shown in catalogs, data books, etc. Contact Sharp in order to obtain the latest specification sheets before using any Sharp products.  
 Specifications are subject to change without notice.

# Appendix C

## PSO-ANN Algorithm (S-Function)

```

clear all
close all

%DATA
load data;

%B=regress(Y,X); % B_matlab=Y*(X^-1)
N_par=1;
%PSO
N=20; % we need to justify for 20 particles.
MaxValue=50;
MinValue=1;
V=zeros(N,1);
Xp=round(MinValue+(MaxValue-MinValue)*rand(N,N_par));

%Second Part

PI=Inf(N,1);
PbestValue=Inf;
LbestValue=Inf;
V=zeros(N,N_par);
Xp_particleBest=zeros(N,N_par);

c1 = 1.49618;
c2 = 1.49618;
w = 0.7298;
Nit=50;
for ii=1:Nit
    % for loop to the PI calculate per each Particle
    for i=1:N
        net=newff(input',P',Xp(i));
        net=train(net,input',P');
        D=net(input');
        XB=mse(D-P');
        PI_l(i,1)=XB;
        %update the position value and the PI value per each
particle
        if PI_l(i,1)<PI(i,1)
            PI(i,1)=PI_l(i,1);
            Xp_particleBest(i,:)=Xp(i,:);
        end
    end
    %update the L-best position value

```

```
[LbestValuen,LbestIndexRow]=min (PI) ; %min_fitness,
min_fitness_index
if LbestValuen<LbestValue
    LbestValue=LbestValuen;
    L_best= repmat (Xp (LbestIndexRow, :), N, 1);
end
%update the G-best position value
[PbestValuen,PbestIndexRow]=min (PI) ; %min_fitness,
min_fitness_index
if PbestValuen<PbestValue
    PbestValue=PbestValuen;
    G_best= repmat (Xp (PbestIndexRow, :), N, 1);
end

%PSO equation
V=w*V+c1*rand (1) * (Xp_particleBest-Xp)+c2*rand (1) * (G_best-
Xp); %update speed
Xp=round (Xp+V); %update position
PI_plot (ii)=mean (PI)
end

plot (PI_plot)

min (PI)
G_best (1, :)
```

# Appendix D

## Modified P&O Algorithm (S-Function)

```
function D = P&O (Param, Enabled, V, I)

% D output = Duty cycle of the boost converter
%
% Enabled input = 1 to enable the MPPT controller
% V input = PV array terminal voltage (V)
% I input = PV array current (A)
%
% Param input:
Dinit = Param(1); %Initial value for D output
Dmax = Param(2); %Maximum value for D
Dmin = Param(3); %Minimum value for D
deltaD = Param(4); %Increment value used to increase/decrease

% ( increasing D = decreasing Vref )
%

persistent Vold Pold Dold;

dataType = 'double';

if isempty(Vold)
    Vold=0;
    Pold=0;
    Dold=Dinit;
end
P= V*I;
dV= V - Vold;
dP= P - Pold;

if dP/P > 0.01
    if V < 244
        D = Dold - deltaD;
    else
        D = Dold + deltaD;
    end
else
    if dP < 0
        if dV < 0
            D = Dold - deltaD;
        else
            D = Dold + deltaD;
        end
    end
end
```

```
    else
      if dV < 0
        D = Dold + deltaD;
      else
        D = Dold - deltaD;
      end
    end
  end
end

if D >= Dmax | D<= Dmin
  D=Dold;
end

Dold=D;
Vold=V;
Pold=P;
```

# Appendix E

## The Simulink model of a grid-connected PV system

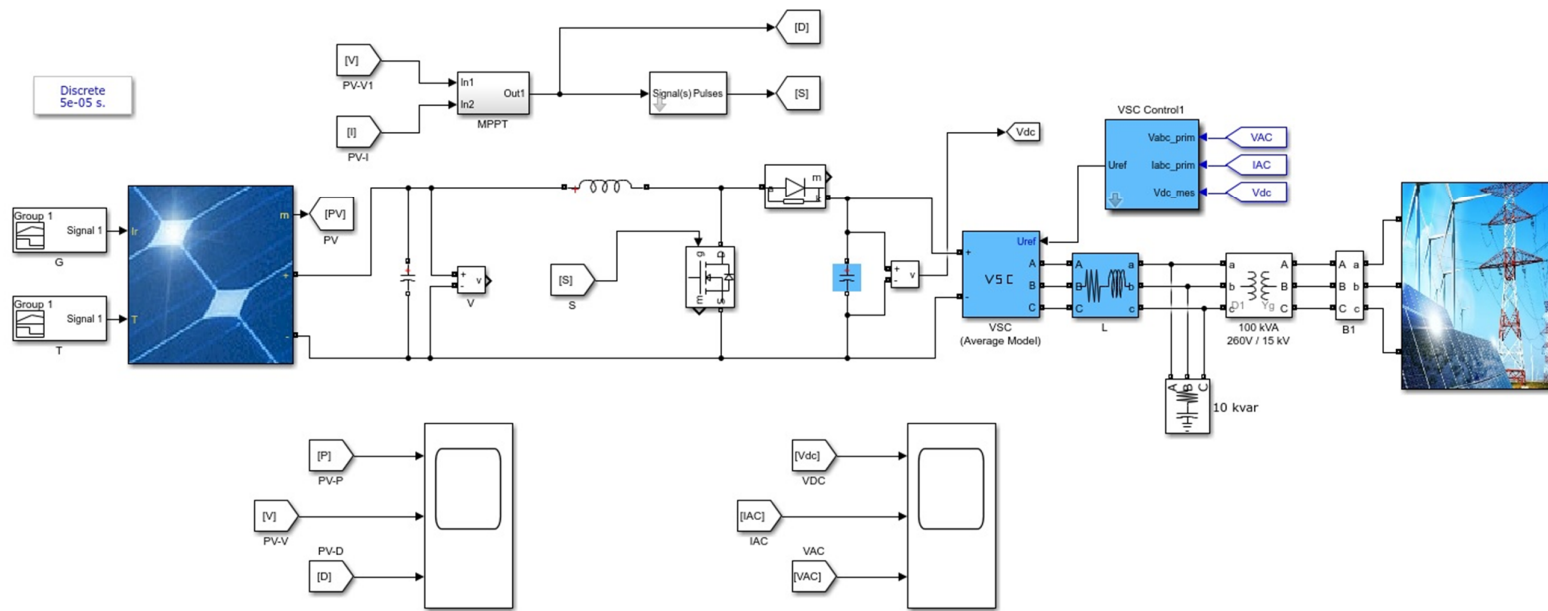


Figure E.1. The Simulink model of a grid-connected PV system based on MATLAB simulation.

# Appendix F

## The graphical rules of a FLC model

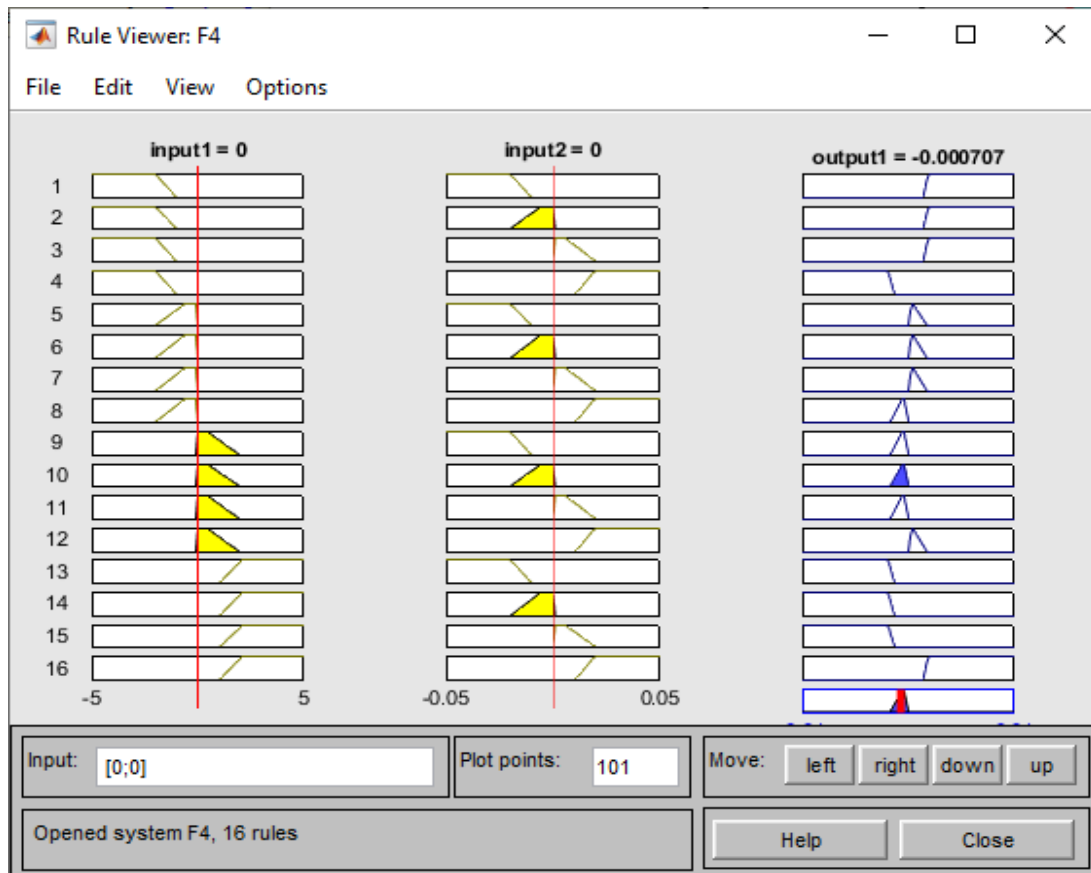


Figure F.1. The graphical rules of a FLC model.

# Appendix G

## The linguistic rules of an ANFIS model

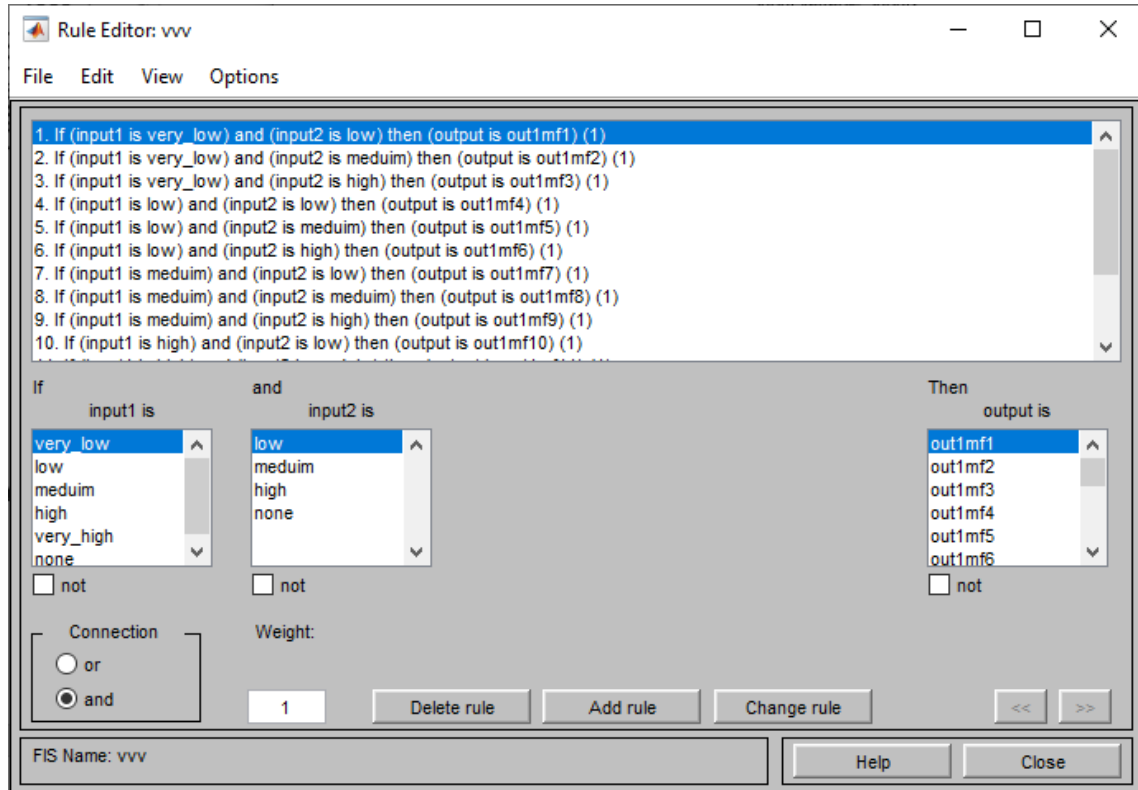


Figure G.1. The linguistic rules of an ANFIS model.

# Appendix H

## Neural Network Training Regression

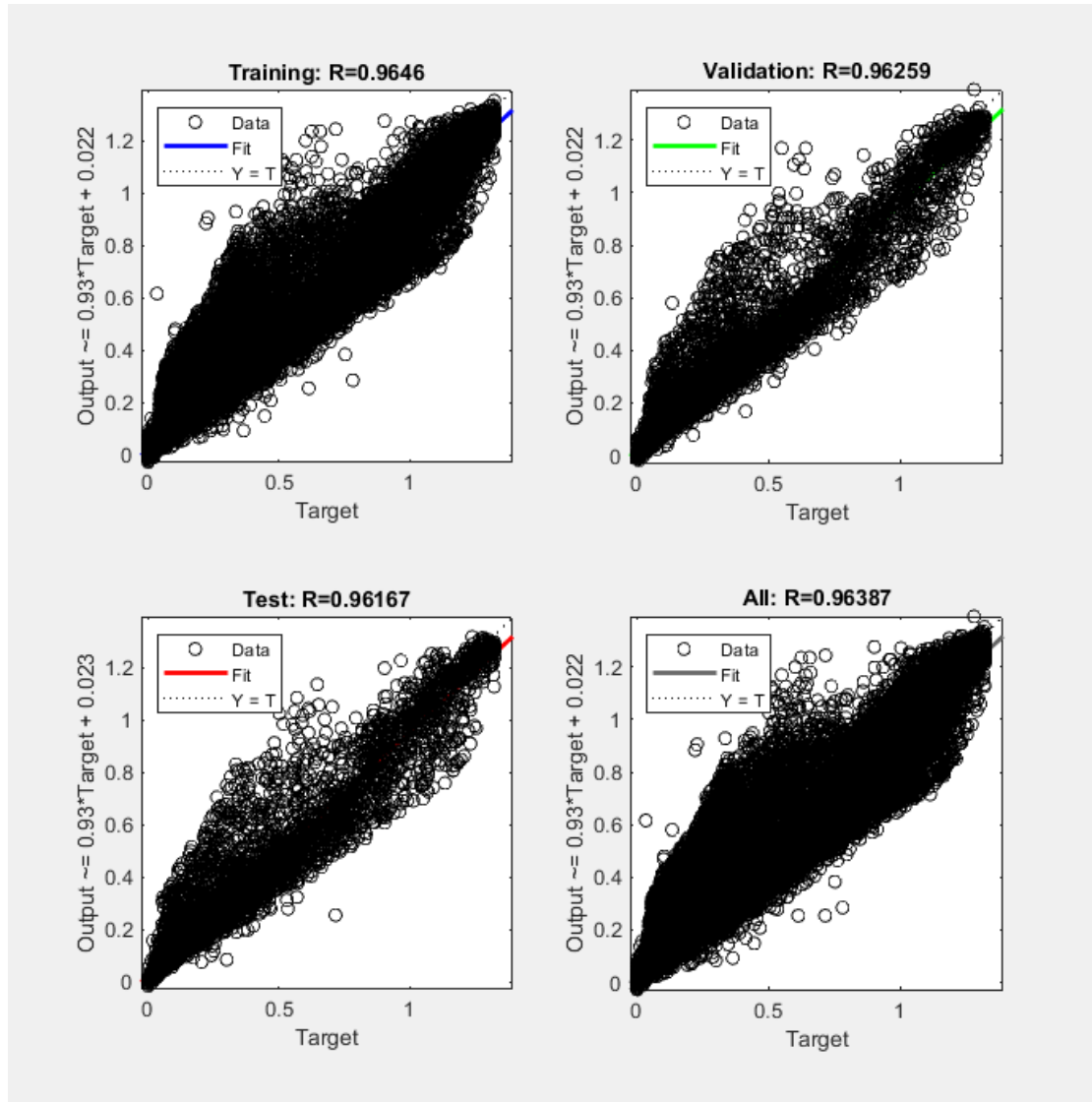


Figure H.1. The training regression of an ANN model